Critical Window in Autism: A Study on Shank3

By

Yuan (Karen) Mei

B.A. Cognitive Neuroscience
Rice University, 2006

SUBMITTED TO THE DEPARTMENT OF BRAIN AND COGNITIVE SCIENCE IN PARTIAL FULFILLMENT OF THE REQUIREMENT FOR THE DEGREE OF

DOCTOR OF PHILOSOPHY IN MOLECULAR AND CELLULAR NEUROSCIENCE
AT THE
MASSACHUSETTS INSTITUTE OF TECHNOLOGY
December 2015 [February 2016]

Signature of Author: Signature redacted

Department of Brain and Cognitive Sciences

Certified by: Signature redacted

Guoping Feng, Professor of Brain and Cognitive Sciences Thesis Advisor

Accepted by: Signature redacted

Matthew A. Wilson, Sherman Fairchild Professor of Neuroscience and Picower Scholar
Director of Graduate Education for Brain and Cognitive Sciences

Dedicated to my family

Acknowledgements:

I would like to thank all of the people who have supported and guided me through my years at MIT. First and foremost, I thank Guoping Feng, who has been a phenomenal Ph.D. advisor who has not only provided critical scientific guidance but also personal guidance. His patient and generous mentorship helped me persevere in my Ph.D. pursuits. I am very grateful to my committee members Troy Littleton, Yingxi Lin, and Kay Tye for sharpening my critical thinking and challenging me to think a little bit harder about each scientific problem. They were always very generous with their time and resources in guiding my intellectual goals.

I also want to thank the entire Feng lab for cultivating a fun and warm environment for doing science. In particular, I'd like to thank Patricia Monteiro, Yang Zhou, Jin-Ah Kim, Xian Gao, Zhanyan Fu, Michael Wells, Congyi Lu, Qian Chen, and Qiangge Zhang for discussing science with me and/or for generously providing their help in completing projects together. I'm also very grateful for the help provided by Triana Dalia, Bailey Clear, and Heather Zaniewski for managing the animal colonies. During my Ph.D., I was lucky to have worked with some very talented and motivated undergraduate students including Alexander Lim, Shijing Feng, Kasey Han, and William Stockton. They contributed significantly to various projects within the lab, and their intellectual curiosity constantly inspired me and reminded me of how exciting the scientific process can be.

I would like to express my gratitude towards my family and friends outside of the lab for their support and encouragement. I could always depend on coffee breaks with Shaiyan Keshvari. His barista skills never failed to turn my frown upside down. Gerald Pho, Annie Chen, and John Liu have been incredible food buddies. They provided such comfort not only through their home-

made food, but also their amazing generosity and genuine spirits. I will never forget the lunch/dinner times with Franny Zhang, Christopher Lam, and Ted Dobie during which they consistently reminded me that there was life beyond Ph.D. I am forever grateful to Robia Pautler, who was the first person to give me the opportunity to work in a lab. Even though I had no prior research experience, she believed in my potential and gave me my first exposure to biological research.

I have always considered myself to be extremely lucky because I have a very supportive family. My parents are my biggest heroes. They overcame such hardships and instilled in me the value of optimism. They are my biggest source of inspiration and my most reliable cheerleaders. I also thank my cousin Hao and his wife Wenzhao, who have been like a brother and sister to me. Finally, I thank Leon Bergen, my partner in life. Being a graduate student is hard, and being the partner of a graduate student is in some ways much harder. Through the last 5.5 years, he had been both. I am constantly in awe of his intelligence and love. Our endless discussions about science and life helped me gain focus and perspective during my Ph.D. I am very excited for the next chapter in our lives.

The following work is based on two manuscripts in collaboration with Patricia Monteiro, Xian Gao, Yang Zhou, Jin-Ah Kim, Zhanyan Fu, and Qiangge Zhang.

Table of Contents

ABSTRACT:

Autism and autism spectrum disorders (ASDs) are clinically defined by the symptoms of social impairment and repetitive behavior, affecting 1 in 68 children in the United States. Because patients with ASDs typically display symptoms before the age of three, the ASDs are classically categorized as developmental disorders. One of the key questions in autism research is whether the pathology is reversible in adults. Many studies of simple sensory systems have reported that there is a distinct critical period for synaptic plasticity. This is most famously supported by the monocular deprivation studies in young kittens, which resulted in irreversible visual impairment in adulthood (Hubel and Wiesel, 1970). However, it is not clear whether this principle extends to more complicated multi-modal behavioral systems.

Here we demonstrate that adult rescue can lead to improvements in selective phenotypes of ASD by generating and using a novel Shank3 conditional knock-in mouse model. Estimated to contribute to about 1% of all ASD cases, Shank3 is one of the most prominent genes associated with autism. It is a master postsynaptic scaffolding protein that mediates synaptic plasticity and remodeling by regulating many neurotransmitter receptors including NMDAR, AMPAR, and numerous actin-binding regulators. Disruptions of Shank3 in mouse models have robustly recapitulated the cardinal phenotypes of autism including anxiety, social interaction deficits, and

compulsive/stereotyped behavior. By specifically expressing Shank3 in adult mice that were initially born as Shank3 knockouts, we show that deficits in the synaptic protein composition and striatal neurotransmission can be fully recovered. We developed a novel neuronal tracing technique to study the dendritic spine density, and found that the dendritic spine number is also significantly increased in the rescue condition after development. In addition, we show that while anxiety and motor coordination are not improved, social interaction and repetitive behavior can be significantly rescued. This suggests that plasticity for certain neural circuits persist into adulthood in the diseased brain, and that the underlying mechanisms for different autistic-like phenotypes have distinct properties.

CHAPTER 1: INTRODUCTION

The Excitatory Synapse

The brain is a complex organ whose proper function depends on regulated communication between billions of neurons wired in intricate circuits. The synapse is the location of information transmission from neuron to neuron, and it is a highly plastic structure that remodels in response to activity. At the excitatory synapse, glutamate is the primary neurotransmitter released from the presynaptic terminal. After the presynaptic neuron fires an action potential and releases glutamate, the neurotransmitter trafficks across the synaptic cleft and binds to a variety of glutamate receptors on the postsynaptic neuron. These receptors are both abundant in number and heterogeneous in class. Upon ligand binding, these diverse receptors activate multiple downstream signaling cascades that eventually lead to molecular, morphological, and electrophysiological responses (Chua et al, 2010; Scannevin and Huganier, 2000).

The site of glutamate binding in most excitatory synapses occurs on mushroom-like projections from dendrites classically known as the dendritic spines. The tips of these spines contain an electron-dense compartment called the postsynaptic density (PSD), which is formed by vast networks of protein. These dense protein clusters serve several critical functions: 1) tether glutamate receptors to the synapse; 2) recruit signaling molecules; 3) couple receptor activity to signaling pathways; and 4) couple these

molecular players to the cytoskeleton (Chua et al, 2010). The ability of the PSD to mediate such complex protein interactions is through several large multi-domain scaffolding proteins at the core of the molecular network. Previous studies have identified three main scaffolding protein families including members from the SAPAP, PSD-95, and Shank families (Chua et al, 2010).

Shank in Autism Spectrum Disorders

ASD as synaptic disorder

Because Shank plays such an important role in synaptic plasticity and induction of dendritic spines, it is not surprising that mutations in Shank lead to defects in synaptic function and cause severe neurological disorders. Currently, the psychiatric diseases most intimately linked with Shank mutations are autism and autism spectrum disorders, which are a group of developmental pathologies that affect about 1% of the population (Baird et al, 2006; Zoghbi and Bear, 2012). Autism is clinically diagnosed by three core symptoms: deficits in communication, social interaction abnormalities, and stereotyped behavior (DSM, 2000; Peca et al, 2011). Even though the etiology of autism is not currently understood, it is considered as a genetic disorder because it is highly heritable and has much higher concordance rates among monozygotic twins than dizygotic twins (Huguet et al, 2013).

With accumulating evidence from genome-wide association studies, ASD has been increasingly linked to mutations in genes associated with the synapse. Thus far,

mutations in Fmr1 (Fragile X Syndrome), Tsc1, Tsc2 (tuberous sclerosis), Ube3a (Angelman's syndrome), Pten (hamartoma tumor syndrome), NF1 (Niemann Pick disease), Neuroligin, and Neurexin have all been strongly implicated in the mechanisms leading to autistic-like phenotypes (Zoghbi and Bear, 2012). Because these genes all encode either synaptic proteins or regulators of the synaptic network, it has been hypothesized that the molecular mechanisms underlying the cardinal autistic-like phenotypes share a common pathway (Zoghbi and Bear, 2012; Spooren et al, 2012). Due to the key scaffolding role of Shank at the synapse and its interactions with many of the abovementioned proteins, it is likely that by studying the mechanisms of Shank, we can shed light on a common synaptic etiology of ASD.

Shank3 as an Autism Candidate Gene

The Shank family proteins have been directly linked to autism through genome-wide association studies, clinical cases, and the generation of animal models of autism (Durand et al, 2007; Moessner et al, 2007; Gauthier et al, 2007; Schnutgen et al, 2009; Welch et al, 2007; Jiang and Ehlers, 2013). Phelan-Mcdermid Syndrome (PMS) is an ASD caused by microdeletions on 22q13.3 and is characterized by global developmental delay, hypotonia, and autistic-like phenotypes (Phelan and McDermid, 2012). Interestingly, studies aimed to identify the causal mutation for the phenotypes in PMS consistently indicate Shank3 as the main contributor (Phelan and McDermid, 2012; Wilson HL et al, 2003; Dhar et al, 2010). Subjects carrying ring form chromosome 22 but functional Shank3 do not show the autistic-like phenotypes, suggesting that only Shank3

mutations account for the cardinal autistic-like symptoms in the patients (Jeffries et al, 2005). Furthermore, genetic reports in recent years found that recurring breakpoints, deletions, and nonsense mutations in Shank3 can lead to autism that is not PMS (Durand et al, 2007; Moessner et al, 2007; Gauthier et al, 2009). This indicates that mutations in Shank3 alone can cause autism, and that by studying the basic function of Shank3, one could shed light on the pathology of monogenic autism.

Autism Spectrum Disorders

Diagnosis

Autism spectrum disorders (ASD) are a set of neurodevelopmental disorders defined by impairments in social interaction, verbal and nonverbal communication, and repetitive/stereotyped behavior (DSM V). They are often comorbid with intellectual disability, anxiety, motor deficits, sleep disorders, gastrointestinal irregularities, epilepsy, sensorimotor gating deficits, and attention-deficit/hyperactivity disorder (Huguet et al, 2013). Due to recent progress in diagnosis, the ASDs are now known to affect 1 in 68 children, and 1 in 100 people worldwide. This prevalence produces a tremendous social burden, costing about $35 billion annually in the US (Ganz, 2006).

Leo Kanner and Hans Asperger initially identified autism in the 1940s. They both described cases of young children displaying deficits in social integration and intense interest in specific action sequences (Asperger, 1944; Kanner, 1943). In the 70 years since their discovery, significant progress has been made in diagnosis and social

awareness. It is now recognized that the symptom onset for autism is in early childhood, typically within the first three years of life (Lord, 2000). Numerous patient studies show that the symptom profile for autism patients is quite heterogeneous (Miles, 2011). Even though the core deficits of social impairment and restricted interest are present in all patients, the spectrum of severity and specific symptoms are highly variable. The Diagnostic and Statistical Manual of Mental Disorders has categorized ASD into several main conditions including autism, Asperger, and pervasive developmental disorder, not otherwise specified (PDD-NOS). In Asperger, the symptoms do not include delay in early language development. In PDD-NOS, the patients do not display symptoms that are easily categorized into the other conditions.

Clinical Features

The symptoms of ASD begin within the first three years of life. Newborns do not display affinity for physical touch; they do not reach out to be held or rocked. They are typically prone to bouts of intense crying and are difficult to console. They are not comforted by hugs and are more easily calmed by being left alone. They do not hold or initiate eye contact. However, these symptoms are subtle and are easily missed by parents. The first blatant signs of abnormality are typically related to delays in language development within the second year (Miles, 2011).

For most ASD patients, the symptoms manifest gradually. However, for about 30% of ASD children, they undergo normal development during the first few months of life but then begin a pattern of regression. For example, they may learn to speak and then

suddenly lose their language ability. They initially have the ability to maintain eye contact, but stop this action as well. They do not usually engage in spontaneous imaginative games. While healthy children like to role-play and engage in extended sequences of being a nurse or firefighter, ASD children do not typically participate in such pretend games. They do not assign personality to toys, but rather treat them as props. For example, many ASD children tend to line their toys up in a specific order or sort them in particular sequences. There is little to no evidence of theory of mind in their voluntary games (Miles, 2011).

It is possible that the impairment in social interaction contributes to the delay in language development. A prevalent characteristic in ASD patients is the failure to practice turn taking in conversations, to properly sustain the logical flow of communication with others. ASD children have trouble learning that language can be used to name objects, make requests, and gain attention. The inability to understand how language can be applied could contribute to their delayed speech acquirement. When they do begin verbal communication, their initial speech is typically marked by pronoun reversal, echolalia, and aberrant intonation and inflections. In addition, their first utterances are usually fragments of sentences rather than single words. They do not understand the meaning of each word in these fragments (Miles, 2011; Lord et al, 2004). Thus not only is the language development delayed, the manner in which it develops in ASD patients is also different from the trajectory of healthy infants.

The other ASD cardinal symptom of repetitive movements can develop quite early on or not until about 4 years later after the children learn to engage in relatively complex and independent physical movements (Stefanatos, 2008; Lord et al, 2004; Volkmar et al, 2005; Werner and Dawson, 2005; Ozonoff et al, 2010; Miles, 2011). Early symptoms of repetitive movement can include subtle behaviors such as body rocking and uninterrupted staring. Other manifestations can include licking, page flicking, stereotypical finger movements, body spinning, or constant running. The duration of the stereotypes varies, but can last up to hours. The cause of the repetitive movements is not known. However, a salient characteristic of ASD patients is their affinity for stable routines. Many of them adopt elaborate routines comprised of specific sequences of words, objects, events, and people. It is common for children with autism to display aggressive and self-injurious outbursts when their daily routines are changed. It is possible that when under stress, repetitive behaviors reassure the patients of the lack of change and provide a source of comfort (Miles, 2011)

The deficits in sensory gating in many ASD patients may contribute to their lack of desire for change. Children with autism often show extreme sensitivity to certain sounds such as vacuum cleaners or distant chatter. Many sounds that are typically ignored by healthy controls may cause great discomfort to autism patients. The same deficits in hypersensitivity apply to other senses including touch, smell, taste, and vision. For example, the texture of certain fabrics may trigger great distress while physically harmful stimuli such as lacerations and burns are ignored. Thus, it is likely that these abnormalities in sensory integration may incentivize autism patients to develop a specific

routine to avoid the sensory discomfort associated with new activities (Miles, 2011). It should be noted that due to these aberrant sensory responses to physical stimuli, autism patients have a significantly increased risk of harming themselves and may require assistance to avoid injury.

Unfortunately, for most ASD children, recovery in pathology is limited. Many patients will need stable familial and societal assistance (Seltzer et al, 2004; Howlin et al, 2004; Howlin et al, 2000; Farley et al, 2009). A study that followed ASD patients over a period of 20 years showed that over 50% of the patients lived with their parents and only about 10% lived independently (Farley et al, 2009). According to other longitudinal studies, fewer than 5% of children with autism make complete recovery (Nordin and Gillberg, 1998).

Etiology

Genetic Contribution

Genetic susceptibility plays a large component in ASD etiology. Twin studies show that in monozygotic twins, the heritability of autism is ~90% (Bailey et al, 1995; Piven et al, 1997; Chakrabarti et al, 2001), whereas the concordance rate for dizygotic twins is ~24% (Ritvo et al, 1985). This significant increase in risk in monozygotic twins compared to dizygotic twins has been robustly replicated across multiple twin studies across decades (Abrahams and Geschwind, 2008; Devlin and Scherer, 2012; Freitag, 2007). Moreover, the risk of ASD is ten times greater for a sibling of an ASD patient than for the general population. Comprehensive genetic analyses show that a Mendelian or

chromosomal cause or predisposition in up to 40% of young patients of ASD (Schaffer and Mendelsohn, 2008; Miles, 2011). Large-scale genome analyses have identified novel robust copy number variants (CNV) and single nucleotide variants (SNP) associated with ASD for 5-15% of the patients (Huguet et al, 2013). Multiple exome sequencing studies have also revealed new deleterious de novo mutations in 3.6 to 8.8% autism patients (Sahin and Sur, 2015; Huguet et al. 2013; Kong et al, 2012; Neale et al, 2012; O'Roak BJ et al, 2011; O'Roak et al, 2012; Sanders et al, 2012).

Additional evidence that strengthen the genetic basis to ASD are the syndromic autism disorders with known genetic causes. Patients with syndromic autism display a cluster of other distinct phenotypes and have autism only as a secondary diagnosis. Examples include Fragile X, Rett, and Tuberous Sclerosis. Each of these disorders is caused by mutations in a single known genetic variant. DNA modifications mimicking these mutations in cultured cells and animal models have largely recapitulated the human patient pathology and bolstered the causal gene role in these conditions.

Non-Genetic Contribution

Because the heritability for ASDs is not 100%, it is important to note the contribution of non-genetic factors. Large bodies of evidence suggest that stochastic, epigenetic, and environmental influences increase the risk for ASD (Huguet et al, 2013; Sahin and Sur, 2015). Stochastic factors in autism refer to the contribution of noise, random variation in large populations. For example, across many individual samples, it is

possible that noisy variability in gene transcription or other processes involved in gene expression could result in phenotype manifestation (Person et al, 2011).

Advances in neurobiology have revealed the importance of epigenetic understanding in psychiatric disease mechanisms. Genomic imprinting, a canonical epigenetic process, has been cited as a candidate mechanism for autism in multiple cases. The paternal copy of the gene *UBE3A* is imprinted or silenced in neurons in healthy individuals. However, abnormal imprinting or lack thereof causes nonphysiological expression levels of *UBE3A* and has been linked to autistic-like pathology in human patients and mouse models (Chamberlain and Lalande, 2010). DNA methylation is another epigenetic process that controls gene expression and is heavily dependent on both the paternal and maternal experiences. *REELIN* is a gene regulated by methylation. It has been shown to be a critical gene in neuronal migration and maturation. Studies show that *REELIN* concentrations are significantly decreased in autism patients, highlighting the possible causal role of methylation irregularity (Schanen, 2006; D'Arcangelo, 2014). Other candidate genes in ASD have also been shown to be heavily methylated or involved in methylation mechanisms including MECP2 and FMR1.

Even though past environmental theories of cold maternal care in ASD have been debunked, new environmental theories have arisen from a large collection of clinical cases and mouse models. Studies of premature infants show that perinatal cerebellar hemorrhagic injury is linked to significantly higher risk of developing long-term developmental deficits including ASD symptoms (Limperopoulous et al, 2007;

Limperopoulous et al, 2010; Sahin and Sur, 2015). They show that injured infants have a ten times greater risk of developing neurological abnormalities and almost 40 times greater risk of displaying autistic-like phenotypes compared to healthy control infants (Limperopoulous et al, 2007).

There is also a host of growing literature on the contributing role of the immune system in ASD pathogenesis. Tissue from autism patients showed significantly higher activation of microglia and astrocytes in the brain. Neuroinflammation was found in multiple brain regions including the cerebellum, cerebral cortex, and white matter. Increased concentrations of cytokines were found in the brain and cerebral spinal fluid of both children and adults with ASD (Vargas et al, 2005). This suggests that neuroinflammation is a stable lifelong symptom. In addition, activation of the maternal immune system during pregnancy also has been significantly linked to ASD development in the fetus. Reports show that exposure to viruses such as rubella or cytomegalovirus prenatally multiplies the risk for disease (Hyman et al, 2006; Moy and Nadler, 2008; Patterson, 2009). It is possible that activation of the maternal immune affects the development of the fetal immune system in the brain. The elevated cytokine profile in the fetus could be an amendatory response to the maternal infection (Patterson, 2009). It is also possible for the infected maternal immune system to affect the peripheral immune system of the fetus because the placenta is the source of hematopoetic stem cells for the growing fetus (Gekas et al, 2005; Patterson, 2009). In support of this theory, some studies indicate that the placenta mediates stress during pregnancy and can lead to neurodevelopmental disorders (Bronson and Bale, 2015).

Another growing area of research on non-genetic contributions to ASD focuses on the interactions between the gut microbiome and autism. Studies show that the gastro-intestinal tracts are initially sterile upon birth (Koenig et al, 2011; Breitbart et al, 2008). Gut microbes then colonize the tracts immediately after birth, and evolve into the adult microbiome within the first three years (Koenig et al, 2011). Basic research demonstrate that the gut microbiome may be important for nutrient absorption and immune system development (Mull et al, 2013). It is important to note that the human genome does not encode enzymes necessary for breaking down many plant polysaccharides, whereas the gut microbiome encodes a spectrum of such enzymes (Gill et al, 2006; Mulle et al, 2013). It is also worth noting that the infant microbiome contains a significantly higher proportion of genes necessary for degrading lactate, which is an important source of energy for newborns (Koenig et al, 2011). These evidence collectively suggest an active role in nutrient intake for the gut microbiome. Other studies show that the gut microbiome is actively involved in training the immune system. Animal studies indicate that the presence of specific bacteria species is essential for the proper development of certain immune cell types (Gaboriau-Routhiau et al, 2009; Mazmanian et al, 2005).

More direct evidence linking the microbiome to ASD show that children with ASD display a significantly different microbiome profile compared to healthy controls. The concentrations of *Clostridium* or *Desulfovibrio* in stool samples from ASD patients are significantly higher compared to children with normal neural development (Finegold et al, 2011; Parracho et al, 2005; Song et al, 2004). The level of Bifidobacterium species was significantly decreased in ASD patients compared to same-age healthy children. In

addition, the concentrations of volatile organic compounds and free amino acids were also found to be significantly different in the stool samples from ASD patients and healthy controls (De Angelis et al, 2013). It is possible that the altered microbial profile in the ASD patients is a contributing factor to abnormal nutrient intake and immune system adaptation, and thus causes aberrant neural development. However, it is also likely that the different microbiome is merely a product of the rigid eating habits of the ASD patients and only reflects the consequences of already existing neural phenotypes. Future studies are necessary to elucidate the exact relationship between the gut microbiome and ASD pathogenesis.

The Genetics of Autism

Even though the contribution of non-genetic factors is important for ASD pathology, research over the last seven decades strongly indicate that genetics still plays the main causal role. Early large-scale efforts at identifying the common variants contributing to risk failed to provide clear candidates (Iyengar and Elston, 2007). Results from many additional large-scale studies that take advantage of both rapidly advancing technological developments and increased population samples demonstrated the vast heterogeneity and complexity of ASD genetics.

To date, high-resolution karyotype analyses showed that fewer than 5% ASD patients have microscopically visible cytogenetic abnormalities. Fluorescence in situ hybridization (FISH) revealed that another 3-5% patients have chromosomal abnormalities. Almost every chromosome has been associated with a cytogenetic

abnormality in ASD, with a few chromosomes that have significantly higher frequency than others (Reddy, 2005; Vorstman et al, 2006; Lintas and Persico, 2009; Miles, 2001; Huguet al, 2013). The most frequent chromosomal abnormalities have been detected at 2q37, 7q11, 15q11-13, 16p11, 22q11.2, and 22q13.3 (Vorstman et al, 2006).

Increasingly, the use of array comparative genomic hybridization (aCGH), which is also known as chromosomal arrays (CMA), is replacing the use of karyotype analyses in genetic screening for ASD. The first such study in the 2000s tested 29 ASD patients and found that 8 patients had copy number variants linked to ASD (Jacquemont et al, 2006). A second aCGH study also showed a significantly higher frequency of de novo copy number variants (CNV) in ASD patients. This study used a denser CGH array with a larger cohort size and found CNV in 10% of the ASD patients and only 1% in the healthy controls (Sebat et al, 2007). Many similar studies using aCGH or single nucleotide polymorphism (SNP) arrays were conducted (Christian et al, 2006; Cooper GM et al, 2011; Gilman et al, 2011; Glessner et al, 2009; Itsara et al, 2010; Marshall et al, 2008; Pinto et al et al, 2010; Sanders et al, 2011; Szatmari et al, 2007). Taken all together, about 4000 ASD patients, 1000 unaffected siblings, and 600 healthy controls were screened. While only about 1.9 % of control individuals and 1.4% unaffected siblings showed rare de novo CNVs, about 7% of ASD patients were shown to have such mutations. The data consistently showed that ASD patients have significantly more de novo CNVs in contrast to the individuals in the control group (Huguet et al, 2013).

In addition to investigating the burden of chromosomal abnormalities and CNVs in ASD patients, studies have also been performed to analyze the role of de novo coding-sequence variants. The optimization of next-generation sequencing technologies and decreasing cost of large-scale sequencing platforms have facilitated whole-exome sequencing and whole-genome sequencing in patients. Multiple studies analyzed the exome in about 1000 ASD patients and 800 unaffected siblings (Iossifov et al, 2012; Kong et al, 2012; Neale et al, 2012; O'Roak et al, 2012; Sanders et al, 2012). The results showed that when the exome was analyzed globally, there was no significant difference between the ASD patients and healthy controls. However, when the analysis was performed on only brain-expressing genes, the difference between ASD probands and undiagnosed sibalings became quite dramatic, indicating that the causative genes reside within the central nervous system (Sanders et al, 2012; Huguet et al, 2013).

Further analyses showed that the majority of the de novo mutations originated in the paternal chromosome. The de novo mutations were three times more likely to be attributed to the paternal allele than the maternal allele (Kong et al, 2012; Kumar et al, 2008). A study on the genome-wide mutation rates in a cohort of 78 parent-offspring trios reported that the age of the father at conception increases the frequency of mutations in the offspring, with about 2 mutations per year. Based on the data, an exponential model predicts that the total number of mutations on the paternal chromosome would double every 16.5 years (Kong et al, 2012).

Even though these large-scale studies revealed many novel gene candidates for autism pathogenesis, they also demonstrated that the contribution of each mutation to the disease is quite small. None of the uncovered hits can account for more than 1% of the ASD patient population, further highlighting the genetic complexity of autism (Huguet et al, 2013). It is worth noting that more sophisticated genomic technology and analyses may provide more useful information in the future. One possible strategy for advancing our understanding is to overcome some technical difficulties associated with sequencing certain difficult-to-sequence regions such as GC-rich stretches on the genome. Because current exome sequencing is unable to completely cover all coding regions, it is possible that more penetrant mutations have gone undetected (O'Roak et al, 2012; Huguet et al, 2013). Adopting different criteria for subject recruitment could also lead to novel findings. For example, categorizing patient samples based on distinct phenotypes and linking significant hits to these specific isolated symptoms may advance our understanding of the relationship between mutations and behaviors (Huguet et al, 2013).

Due to the genetic heterogeneity in ASD and the relatively low contributions by single gene mutations, one of the dominant hypotheses posits that there are "multiple hits" for many ASD patients. Several large-scale studies have found a significant proportion of ASD individuals harboring more than one genetic mutation (Girirajan et al, 2012; Girirajan et al, 2010; Leblond et al, 2012). In 2010, Girirajan et al found that in more than 2000 children who were diagnosed with congenital defects and intellectual disability, about 10% of them harbored two CNVs. They observed that patients with two large CNVs were at eight times more risk for developmental abnormalities compared to

their healthy controls (Girirajan et al, 2010). In addition, in a study characterizing patients with 16p11.2 microdeletion, the results showed that about 25% of them harborered a second large CNV. This frequency in the patient group was significantly higher than the second-hit frequency in the control group (Girirajan et al, 2012). Also, in Sato et al, 2012, they demonstrated that in all patients with SHANK1 deletion, there was also a mutation in the protocadherin gamma 11-encoding gene. It is possible that the interaction between the two mutations caused the development of ASD (Sato et al, 2012).

Consistent with the multiple hits hypothesis of ASD is the common variant common disease model, which claims that common single nucleotide polymorphism variants cause the disease. Common SNPs are defined as the variants found in at least 5% of the population (Voineagu, 2012). Genome-wide association studies (Wang et al, 2009; Weiss et al, 2009; Anney et al, 2010) showed that the effect of single common variants is small. No common SNPs were found with an odds ratio of greater than 1.5 (Berg and Geschwind, 2012). Due to the lack of significant single common variant hits from GWAS studies, Klei et al used a novel method to consider all common SNP variants simultaneously and estimate the contribution of all such common variants to ASD. They screened a large cohort of samples including 2000 families with ASD and about 4000 healthy controls. The results showed that the SNPs have an additive effect on ASD symptoms, accounting for about 60% of the variance for ASD patients from multiplex families and 40% for the patients from simplex families (Klei et al, 2012). Even though the effect of common variants on ASD pathogenesis is evident, due to their small individual effect, it remains difficult to identify these common SNPs.

Another etiological hypothesis for ASD is the rare variant common disease model, which states that rare variants including copy number variants and rare SNPs contribute significantly to ASD development (Zhao et al, 2007). To that end, many studies have been conducted to identify both inherited and rare mutations in ASD individuals (Berg and Geschwind, 2012). Multiple themes emerged from the compiled results. First, the results consistently showed that the number of inherited rare copy number variants did not differ significantly between ASD patients and healthy controls (Levy et al, 2011; Sanders et al. 2011; Szatmari et al, 2007; Marshall et al, 2008). Second, the results showed that in ASD patients, the size of the rare copy number variants was significantly larger than those in control samples (Levy et al, 2011; Sanders et al, 2011; Szatmari et al, 2007; Marshall et al, 2008). Two studies published in 2012 showed that for SNPs, the total number of mutation was also not significantly different between patients and healthy siblings. However, when the analysis was restricted to only gene-disrupting SNPs, the effect became significant with the mutation rate being statistically higher in the ASD probands compared to matched controls (Iossifov et al, 2012; Sanders et al, 2012). Iossifov et al showed that AD patients harbored twice as many splice-site, nonsense, and frame-shift mutations (Issofov et al, 2012). Consistently, Sanders et al also reported that the number of non-synonymous and nonsense de novo SNPs was significantly higher in ASD individuals (Sanders et al, 2012).

Interestingly, identifying rare variants, much like identifying common variants, proves to be a difficult task despite the challenges being different. One hurdle is posed by the typically multi-genic nature of copy number variations, which renders it ambiguous

which gene is the causal contributor. Sophisticated analyses of the intersection of these GWAS results with data obtained from other methods including systems biology approaches and animal models have generated a small list of ASD candidate genes including Shank2 and Shank3 (Levy et al, 2011; Sanders et al, 2011; Berg and Geschwind, 2012). Another challenge stems from the sheer rarity of these rare mutations. Because the rate of rare mutations is by definition quite low, it is possible for the rare variants to have only one occurrence in a typical genomic sample size. Such low frequencies do not provide enough evidence for robust statistical conclusions regarding disease association and causality. Much larger sample sizes are thus required for validating the contributions of rare variants (Freimer and Sabatti, 2004).

Currently, due to the heterogenous etiology of ASD, there are many possible models of ASD risk. The identification of monogenic syndromic ASDs support the Mendelian model, which claims that at least a small proportion of ASD pathogenesis is due to single causative genetic mutations. For the rest of the ASD patient population, a spectrum of polygenic models may apply. In addition to the common variant common disease and rare variant common disease models, it is likely that in some patients, a combination of the two models to varying degrees may be the culprit (Berg and Geschwind, 2012). Despite our incomplete understanding of ASD genetic etiology, current data have identified and replicated some key genetic contributors including Shank3. Additional functional characterizations and animal model studies have significantly illuminated interesting genetic pathways and networks of ASD.

Shank3 Contributes to Syndromic and Non-Syndromic ASD

One of the prominent genetic contributors associated with ASD is Shank3, which is a gene encoded by the q terminal end of chromosome 22. Studies show that it contributes to about 1% of all ASD cases, which is quite striking considering the thousands of genes currently linked to the heterogeneous disease. Importantly, genetic studies have linked Shank3 mutations to both idiopathic and syndromic ASD, highlighting its prevalent role in autistic phenotypes. Shank3 mutations were first discovered to be linked to Phelan-McDermid syndrome, a neurodevelopmental disorder frequently associated with autism. Patients with Phelan-McDermid syndrome suffer from severe developmental delay, intellectual disability, hypotonia, language development aberrations, and autistic phenotypes (Phelan, 2007; Jiang and Ehlers, 2013). The syndrome is caused by deletions of 22q13.3, with the deletion size ranging from 0.1 to 10 Mb (Wilson et al, 2003; Dhar et al, 2010). Despite the variability in deletion size, almost all of the cases of Phelan-Mcdermid syndrome have included deletion of Shank3 except for one report in which two children harbor deletions proximal to Shank3 (Wilson et al, 2008). Case studies of patients with deletions specific to Shank3 or balanced translocations within Shank3 reported that they have symptoms indistinguishable from Phelan-Mcdermid patients with much larger deletions (Wong et al, 1997; Anderlid et al 2002; Bonaglia et al, 2006; Jiang and Ehlers et al, 2013). This indicates that Shank3 is a major key contributor to the pathogenesis of Phelan-Mcdermid syndrome. It is important to note that Shank3 also contributes significantly to non-syndromic or idiopathic ASD. Microdeletions and point mutations in Shank3 have been discovered in patients of non-

syndromic ASD in multiple studies over the last decade (Moessner et al. 2007; Durand et al, 2007; Marshall et al, 2008; Gauthier et al, 2010; Waga et al, 2011; Gong et al. 2012; Boccuto et al, 2013).

Many different types of molecular defects in Shank3 have been identified in human patients. These include microdeletions (Dhar et al, 2010; Boccuto et al, 2013), microduplication (Okamoto et al, 2007), intragenic deletions (Bonaglia et al. 2011), point mutations (Boccuto et al. 2013; Durand et al. 2007), translocations with breakpoints (Bonaglia et al, 2006), and terminal deletion of 22q13.3 (Wilson et al, 2003), and ring form of chromosome 22 (Jeffries et al, 2005). Different types of de novo sequence mutations in Shank3 have also been documented in ASD patients. These include splice site, missense, and frameshift mutations (Waga et al, 2011; Schaaf et al, 2011; Moessner et al, 2007; Hamdan et al, 2011; Gong et al, 2012; Gauthier et al, 2009; Gautheier et al, 2010; Boccuto et al, 2013; Durand et al, 2007). Examinations of the patients indicate that the different Shank3 mutations give rise to a spectrum of clinical severity (Jiang and Ehlers, 2013). It is possible that the symptom severity depends on Shank3 dosage (Jiang and Ehlers, 2013). It is also possible that the specific isoforms disrupted by the mutations play a key role in symptom presentation. Further studies are needed to determine the cause of clinical heterogeneity.

Shank3 and the Synapse

Previous literature indicate that at the excitatory synapse, the Shank family of proteins serve as key scaffolding proteins that help mediate synapse remodeling by

recruiting important signaling molecules. The Shank family of proteins, Shank1-3, characteristically contain five protein-protein interaction domains including the N-terminal ankyrin repeats, SH3 domain, PDZ domain, proline-rich region, and a C-terminal SAM domain (Boeckers et al, 1999; Ehlers, 1999; Lim et al, 1999; Sheng and Kim, 2000). Shank1-3 use these domains to interact with and regulate numerous proteins and receptors at the PSD. Through the PDZ domain, Shank binds to guanylate kinase-associated protein (GKAP or SAPAP), which interacts with PSD95. The PSD95/SAPAP/Shank postsynaptic complex regulates the function of NMDA receptors, which are essential to long-term potentiation6. Through the proline-rich region, Shank binds to Homer, which interacts with group 1 mGluRs, which play a key role in long-term depression (Tu et al, 1999). In addition to neurotransmitter receptors, evidence also indicate that Shank interacts with voltage-gated L-type calcium channels through both the PDZ domain and the Src homology 3 domain (Zhang et al, 2005). Therefore, due to its ability to assemble a wide range of proteins critical for synaptic function, the Shank family proteins are considered to be "master" scaffolding proteins (Baron et al, 2006; Kreienkamp, 2008; Sheng and Kim, 2000; Hayashi et al, 2009). Many studies, both in vitro and in vivo, indicate that Shank plays a key role in dendritic spine. It has been biochemically shown that Shank interacts with many actin-binding proteins including Cortactin (Du et al, 1998; Naisbitt et al, 1999), Abp1 (Qualmann et al, 2004), and Abi-1 (Proepper et al, 2007). In addition, studies have reported that when Shank1 is overexpressed in hippocampal neurons, it causes significant spine head enlargement and maturation through the recruitment of IP3 receptors to ER (Sala et al, 2001).

Furthermore, reports indicate that artificial expression of Shank3 in normally aspiny cerebellar granule cells leads to the formation of dendritic spines. This suggests that the mere presence of Shank3 is sufficient signal for the generation of functional dendritic spines (Roussignol et al, 2005).

Shank3 and Mouse Model of ASD

Based on the plethora of evidence linking Shank3 to autism, our lab generated a mouse model of autism by deleting exons 13-16 in the PDZ domain of Shank3. This eliminated two major isoforms of Shank3. The resulting animal (heretofore referred to as Shank3B) captured two cardinal phenotypes of autism: social interaction deficits and repetitive behavior. We compared social interaction between wildtype and knockout by using the three-chamber assay. While the wildtype mice preferred to interact with another animal, the knockout mice preferred to spend time in the empty chamber alone. We quantified the time that the test animal spent in all of the chambers, and found that there was a significant deficit in social interaction in the knockout mice (Peca et al, 2011). Through video surveillance, we also found that the knockout mice showed repetitive behavior such as compulsive grooming, which was severe enough to cause visible skin lesions. We quantified the time that the animals spent grooming and found that the knockout mice groomed almost twice as much as the wildtype controls. This phenotype has about 35% penetrance in the general colony and 100% penetrance in females that have given birth to 4-6 colonies (Peca et al, 2011). Additional Shank3 knockout models generated in other labs show similar phenotypes (discussed in Chapter 3). The ability of

the Shank3 knockout to capture key phenotypes of autism render it a novel and attractive animal model for studying the molecular and circuit mechanisms of the disease. It further solidifies the link between Shank3 and autism, and strongly suggests that by understanding the basic functions and properties of Shank3, we can provide insight on the etiology of autism.

Mouse Models as a Readout for Gene Function

Genetically modified mouse models have become a prevalent tool for studying gene function at the molecular, cellular, circuit, and behavioral level. The use of transgenic mouse lines provides several advantages for neurobiologists. First, the human genome shares about 85% homology with the mouse genome at both the nucleotide and protein level (Makalowski et al, 1996; Batzoglou et al, 2000). Second, the mouse genome has been well characterized for over a century, providing a rich platform for future genetic studies. Third, many different technologies have been developed and applied for manipulating the mouse genome, facilitating mutation experiments for gain-of-function and loss-of-function studies. Fourth, the short generation time and ease of handling of these small animals are ideal for relatively fast-paced research projects.

However, there are important caveats to consider when interpreting results from animal models. Despite the similarity between the mouse and human genomes, the two species have dramatic differences in their neurobiology and anatomy. It is difficult to directly correlate mouse behaviors with human behaviors. For example, social interaction in human subjects is immensely complex with multiple layers of nuances and facets.

Even though mice are highly social animals, one cannot draw conclusive parallels between aspects of their social interaction with those of humans. In our study, we use the behavior of the mice as a functional readout of the mechanistic impact of the target gene. The presence or lack of differences in behavioral data indicate the neurobiological consequence of gene expression in different circuits. These studies give us insight on the native properties of the gene in the context of the whole organism. It is important to note that we do not equate our animal behavioral results with their exact counterparts in humans.

Chapter 2: FULL METHODS

Animal Model

Generation of *Shank3CKI*: The *Shank3*$^{fx/fx}$ targeting vector was designed by inverting the PDZ domain (exons 13 to 16) and flanking it with the FLEx cassette, which is composed of one pair of LoxP sites staggered with one pair of Lox2722 sites. *Shank3*$^{fx/fx}$ conditional knock-in mice were generated by homologous recombination in R1 embryonic stem cells and implanting the correctly targeted cells in C57 blastocysts using standard procedures. Correct locus insertion of the targeting construct into the genomic DNA was determined by PCR genotyping using two primers End_F (5'-GGCAGACTCCACACAGTTCCTG-3') and LoxR (5'-GTATCCTATACGAAGTTATTCCGGGTCGAC-3'). Subsequent mouse genotyping was determined by PCR of mouse tail or ear DNA using three primers. For the wildtype (WT) allele, primer FuncF2 (5'-CGTTTGACACACATAAGCACC-3') and primer FuncFlipR4 (5'-CTCCACCTAGCTGAATTTCCC-3') were used to produce a band of 340 bp. For the knockout (Fx) allele, primer FuncF2 (5'-CGTTTGACACACATAAGCACC-3') and primer Gen_Flx_R1 (5'-GCTGACATCACATTGCTGCC-3') were used to produce a band of 481 bp. For the rescue allele, primer FuncF2 (5'-CGTTTGACACACATAAGCACC-3') and primer FuncFlipR4 (5'-CTCCACCTAGCTGAATTTCCC-3') were used to produce a band of 408 bp.

Chimeric males were crossed to C57BL/6J females from Jackson Labs. The F1 hybrids were crossed with C57BL/6J β-Actin Flp to remove the Neomycin cassette. All progeny were bred onto the pure C57BL/6J (Jackson Labs) for at least two generations before being bred onto a mixed background with 129S1/SvlmJ (Jackson Labs). Heterozygotes were initially bred with heterozygotes to produce experimental animals. All germline *Shank3*$^{fx/fx}$ (KO) and germline rescue (GR) mice along with their respective wildtype littermates were produced by breeding heterozygotes with heterozygotes. For the adult *Shank3* rescue experiments, the *Shank3* conditional knock-in line was crossed with CAGGS-CreER (Guo et al, 2012). In order to produce enough animals for all necessary experiments, breeding strategy was switched to heterozygotes crossed with homozygotes and homozygotes crossed with homozygotes for all conditions (*Shank3*$^{fx/+}$*:CreER*$^{+/-}$ bred with *Shank3*$^{fx/fx}$*:CreER*$^{-/-}$; *Shank3*$^{fx/fx}$*: CreER*$^{+/-}$ bred with *Shank3*$^{fx/fx}$*:CreER*$^{-/-}$; *Shank3*$^{+/+}$ *:CreER*$^{+/-}$ bred with *Shank3*$^{+/+}$*:CreER*$^{-/-}$; *Shank3*$^{+/-}$*:CreER*$^{+/-}$ bred with *Shank3*$^{+/+}$*:CreER*$^{-/-}$). It should be noted that all animals in the rescue condition were produced from the same litters as the animals in the knockout condition. The animals were randomly assigned to different conditions. No computerized randomization program was used.

Animals were housed by genotype at a constant 23°C in a 12 h light/dark cycle (lights on at 07:00, lights dark at 19:00) with ad libitum food and water. Rescue treatment i.e. tamoxifen feeding was initiated on mice at 2-4.5 months. All electrophysiological and behavioral experiments were done at least 6 weeks after treatment in adult mice with the

experimenter being blinded to the genotypes. Only age-matched male mice were used for behavioral assays. All experimental procedures were inspected and approved by the MIT Committee on Animal Care.

Behavior

Open Field: An automated Omnitech Digiscan apparatus (AccuScan Instruments) was used to assess spontaneous locomotion as previously described (Welch et al, 2007). Anxiety-like behaviors were assessed by the following parameters: time spent rearing and frequency of rearing. Locomotion was evaluated by the total distance traveled. The first 30 minutes were evaluated for all parameters. Statistical analysis was done using one-way ANOVA with Bonferroni multiple comparison tests.

Zero Maze: An elevated zero maze was illuminated such that the open arm was lit by 60 lux, and the dark arm was lit by 10-20 lux. Animals were habituated with 10-20 lux for at least one hour before test. The animal was introduced into the closed arm and allowed to freely explore the maze for 5 minutes, which was videotaped. An observer blinded to the genotype performed analysis using an automated tracking software Noldus Ethovision. Anxiety-like behavior was assessed by the percentage of time spent by the animal in the open arm during the 5-min interval. Statistical analysis was done using one-way ANOVA with Bonferroni multiple comparison tests.

Rotarod: Animals were placed on a rotarod apparatus (Med Associates) that accelerates 4-40 rpm for 5 minutes. Each animal was tested for three trials with 1-2 hours between trials in a single day. All trials were videotaped. Latency to fall was manually analyzed for each trial by a blinded observer on Noldus Observer. The change in the latency to fall over the course of three trails indicates the quality of motor coordination. Statistical analysis was done using two-way repeated measures ANOVA with Bonferroni post-hoc tests.

Grooming: Animals were individually placed into a novel cage and allowed to habituate. Grooming behavior was videotaped for 2 hours from 19:00 to 21:00h with red light (2 lux). An observer blinded to the genotype manually quantified grooming behavior using Noldus Observer. All instances of face-wiping, scratching/rubbing of head and ears, and full-body grooming were counted as grooming behavior. Statistical analysis was done using one-way ANOVA with Bonferroni multiple comparison tests.

Novel Object Phobia: Animals were habituated in the behavior room (6 lux) for at least one hour prior to test. After test begins, each animal was placed into a 30 cm x 30 cm chamber (6 lux) containing a thin layer of bedding. After 15 minutes of the animal habituating to the chamber, a novel object was introduced to the center of the arena. The animal was allowed to explore the object for 5 minutes. An observer blinded to the genotype quantified the interaction of the animal with the object using NoldusEthovision. All instances of the nose of the animal being within 1.5 X the diameter of the object was

counted as close interaction.Statistical analysis was done using one-way ANOVA with Bonferroni multiple comparison tests.

Social Interaction: A modified version of the three-chamber social interaction assay was used as previously described (Peca et al, 2011; Yang et al, 2012; Sheng and Kim, 2000). Only age-matched males were used for all tests. S129 males were used as stranger mice and were habituated to the test chamber for 3 sessions (20 minutes each) one or two days prior to the behavioral assay. On the day of the test, both test and stranger animals were habituated to the test room for at least one hour before the start of the assay. The left and right chamber of the three-chamber apparatus were both lit by 4-6 lux during the test session. Each test animal was first placed into the center chamber with open access to both the left and right chamber, each of which contained an empty wired cup placed upside down. This allowed the animal to habituate to not only the social apparatus, but also the cups that will eventually contain the stranger mice. After 15 minutes of habituation, the test animal was moved back to the center chamber briefly before the next session. During the social phase, an age-matched stranger mouse was placed randomly into one of the two side chambers while a novel object was placed into the other side chamber. The test animal was allowed to freely explore the social apparatus and demonstrate whether it prefers to interact with the novel object or the novel mouse. This social phase was also 15 minutes. The placement of the stranger mouse and the object was alternated between test mice to eliminate any confounds due to chamber bias. Time spent by the test animal in close proximity (~5 cm) to the cup containing either the

stranger or the object was calculated. Analysis was done by an observer blinded to the genotype on Noldus Ethovision. One-way ANOVA with Bonferroni *post hoc* test was used for statistical analysis.

Oral Gavage

Tamoxifen Preparation and Feeding: Tamoxifen (Sigma #T5648) was dissolved in corn oil at 20 mg/ml through vortexing. Freshly prepared tamoxifen was protected from light by aluminum foil and kept for 2-3 days at room temperature. Animal feeding needles from Harvard Apparatus (cat #52-4025) were used for oral gavage. To avoid toxicity of tamoxifen, the following dosages were used for adult animals:

Mice at 17-21g body weight were fed 5 mg/day

Mice at 22-25g body weight were fed 6 mg/day

Mice at 26-29g body weight were fed 7 mg/day

Mice at 30-35g body weight were fed 8 mg/day

The adult animals were fed for 5 consecutive days followed by two weeks of rest. Then the animals were fed for 5 more consecutive days followed by another two weeks of rest. Corn oil was fed as a control. The mice fed with tamoxifen and mice fed with corn oil were housed separately to avoid contamination.

For induction of Shank3 expression in P20-P21 animals, mice that weighed 7-9 g received 0.1 ml of tamoxifen or corn oil per day for two to three consecutive days. Mice

that weighed 10-12g received 0.15 ml of tamoxifen or coil per day for two to three consecutive days.

Mechanistic Studies:

Western blot:

PSD and synaptosomal fractions of the striatum, cortex, and cerebellum were prepared as previously described (Welch et al, 2007; Peca et al, 2011). Purified fractions were separated on SDS-PAGE and quantified using Odyssey Licor. β-Actin and Tubulin were used as loading controls. Specific primary antibody for SAPAP3 was prepared as previously described (Welch et al, 2007; Peca et al, 2011). Commercial antibodies used include SHANK3 (Santa Cruz SC-30193), GluR1 (Millipore MAB2263), GluR2 (Neuromab 75-002), NR1 (BD Biosciences 556308), NR2A (Millipore 07-632), NR2B (Millipore 05-920), Homer1 (Chemicon AB5877, Synaptic Systems 160022), Homer3 (Synaptic Systems 160303), mGLUR5 (Upstate 06-451), CaMKIIa (Millipore 05-532), Shank1 (Synaptic Systems 162002), Shank2 (Cell Signaling 12218S), B-Actin (Sigma A5441), and Tubulin (Sigma T5168). Statistical analysis was done using two-tailed Students' t-tests.

Dendritic Spine Analysis:

Mice from WT (N=5), KO (N=4, 1 had to be euthanized due to lesion development), and TM (N=5) conditions at 6 to 12 months old, age-matched males were used. The pAAV-hSyn1-EGFP-P2A-EGFPf-WPRE-HGHpA construct was designed in-house and sent for

commercial viral packaging by Upenn Viral Core with serotype 2/9. To achieve sparse labeling, ~8-30 uL of this virus was injected through the retro-orbital route into each mouse. Three weeks after viral injection, the mice were transcardially perfused and sectioned into 200 micron slices. Immunohistochemistry was performed by staining the slices with anti-GFP antibody (Invitrogen A11122) for 48 hours and 24 hours of secondary antibody incubation. The stained slices were then surrounded by a 240-um depth spacer (Electron Microscopy Sciences) and mounted with Vecta Shield Mounting Media.

Confocal images were taken with a 60X objective of the dorsal striatum. Spine count on intact neurons began 30-40 um away from the soma and was extended for 10-60 um from the origin. Spine density was analyzed automatically by Neuron Studio. All virus injections, imaging, and software analysis were done with the experimenter blinded to the mouse genotypes. Statistical analysis was done using one-way ANOVA, Newman-Keuls post-hoc test.

Electrophysiology

Dorsal and ventral striatum: Acute striatal slices were prepared from 3-7 months old age-matched mice. Animals were anesthetized by avertin intraperitoneal injection (tribromoethanol, 20mg/ml, 0.5mg/g body weight) and transcardially perfused with ice-cold oxygenated NMDG-based cutting aCSF solution (mM): 92 N-methyl-D-glucamine (NMDG), 2.5 KCl, 1.20 NaH2PO4, 30 NaHCO3, 20 HEPES, 25 glucose, 2 thiourea, 5

Na-ascorbate, 3 Na-pyruvate, 0.5 CaCl2, 10 MgSO4 (~300mOsm, 7.2-7.4pH). Following decapitation, brains were removed for sectioning in the same ice-cold cutting aCSF using a Vibratome 1000 Plus (Leica Microsystems, USA). For all dorsal striatal recordings, 300 μm coronal slices were prepared, unless otherwise stated. For all NAc core recordings, 300 μm parasagittal slices were prepared and NAc core was identified by the presence of anterior commissure. Slices were recovered in the same cutting aCSF solution at 32°C for 12 min and transferred to room-temperature carbogenated regular aCSF(mM): 119 NaCl, 2.5 KCl, 1.2 NaH2PO4, 24 NaHCO3, 12.5 glucose, 2 MgSO4.7H2O, 2 CaCl2.2H2O (~300mOsm, 7.2-7.4pH). Slices were allowed to recover at least ≥1h and transferred to a recording chamber (RC-27L, Warner Instruments) prior to recordings. Stimulations were performed using a platinum iridium concentric bipolar electrode (CBAPC75, FHC). For dorsolateral striatum coronal slices, electrode was placed at the corpus callosum to mainly stimulate corticostriatal axons. For dorsolateral striatum parasagittal slices, electrode was placed at the cortex between layer V and VI. For ventral striatum parasagittal slices, electrode was placed dorsally to the anterior commissure at the border between NAcc core and the cortex. Afferents were stimulated with 0.1ms stimulation step (Isoflex, AMPI) delivered at 0.05Hz frequency (unless otherwise stated). Slices were visualized under IR-DIC (infrared-differential interference contrast) using a BX-51WI microscope (Olympus). All slice preparations, recordings and data analysis were performed with experimenter blinded to the genotypes.

Cortex: Acute brain slices were prepared from 3-7 month-old mice as follows. Briefly, mice were deeply anesthetized by intra-peritoneal injection of avertin solution (20 mg/ml, 0.5 mg/g body weight) and then transcardially perfused with 20 ml of carbogenated (95% O_2, 5% CO_2) ice cold cutting solution with the composition (in mM): 105 NMDG, 105 HCl, 2.5 KCl, 1.2 $NaH2PO_4$, 26 $NaHCO_3$, 25 Glucose, 10 $MgSO_4$, 0.5 $CaCl_2$, 1 L-Ascorbic Acid, 3 Sodium Pyruvate, 2 Thiourea (pH 7.4, with osmolarity of 300–310 mOsm). The brains were rapidly removed and placed in ice-cold and oxygenated cutting solution. Coronal slices (300 μm) were sliced using Leica VT1200S (Leica Microsystems) and then transferred to recovery chamber at 32 °C with carbogenated cutting solution for 8 min, followed by transferring to holding chamber containing aCSF that contained (mM): 119 NaCl, 2.3 KCl, 1.0 $NaH2PO_4$, 26 $NaHCO_3$, 11 Glucose, 1.3 $MgSO_4$, 2.5 $CaCl_2$ (pH was adjusted to 7.4 with HCl, with osmolarity of 300–310 mOsm) at room temperature. Slices were allowed to recover for at least two hours in holding chamber before recording and used for experiment typically between 3~7 hours after slicing. Layer 5 pyramidal cells with a prominent apical dendrite were visually identified with a microscope equipped with IR-DIC optics (BX-51WI, Olympus) mainly by location, shape and pClampex online membrane test parameters.

Extracellular field recordings: Slices were prepared from a daily group of mice containing all the 3 genotypes/treatments on randomized order, and recordings were obtained at RT with carbogenated regular aCSF (~2 ml/min rate). Borosilicate glass recording microelectrodes (King Precision Glass) were pulled on a P-97 horizontal puller

(Sutter Instruments) and backfilled with 2M NaCl. Recording electrode was placed ~400μm away from stimulating electrode and field population-spike was evoked by a 0.1ms stimulation step (Isoflex, AMPI) delivered at 0.05Hz frequency. Input-output functions were generated through consecutive rounds from 0.1-1.0 mA in 0.1 mA increments (triplicate measurements *per* stimulation intensity). Three components were resolved in the recording traces: stimulation artifact, negative peak 1 (NP1, presynaptic fiber volley) and field population spike. Amplitude for each component was determined by the average peak amplitude from triplicated measurements *per* stimulation intensity. Data was amplified using a MultiClamp 700B and sampled at 10 KHz using a Digidata 1440A acquisition system. Analysis was performed blinded to genotype using pCLAMP 10 software (Axon Instruments/Molecular Devices).

Whole-cell recordings: Borosilicate glass recording microelectrodes (King Precision Glass) were pulled on a P-97 horizontal puller (Sutter Instruments) and backfilled with CsGlu (mM: 110 CsOH, 110 D-Gluconic acid, 15 KCl, 4 NaCl, 5 TEA-Cl, 20 HEPES, 0.2 EGTA, 5 Lidocaine N-ethyl chloride, 4 MgATP, 0.3 NaGTP). Internal pH was adjusted to ~7.3 with KOH and osmolarity adjusted to ~300 mOsm with K2SO4. Typical internal resistance was around 3-5 MΩ. MSNs were visually identified based on their shape, size and location under IR-DIC (infrared-differential interference contrast), using a BX-51WI microscope (Olympus). After seal rupture and internal equilibrium (5min to allow proper dialysis of Cs+ internal), cells were recorded with series-resistance values <20 MΩ (experiments were discarded if changed by >20%). All voltage clamp traces

were recorded in the presence of 50 μM PTX (picrotoxin, Tocris) with theoretical liquid junction potential not corrected-for. Signals were filtered at 2 KHz, digitized at 10 KHz and data acquired using a MultiClamp 700B amplifier and a Digidata 1440A. All analyses were performed blinded to the genotype. Grubb's test was used to remove single outliers.

Miniature EPSCs: Slices were perfused with RT carbogenated regular aCSF at a rate of approximately 2 ml/min. Voltage clamp traces were recorded at holding potential -70 mV in the presence of 50 μM PTX (picrotoxin, Tocris) and 1 μM TTX (tetrodotoxin, Tocris). Analysis of miniature EPSCs was performed using pCLAMP10 (Axon Instruments, Molecular Devices) and Minianalysis software (Synaptosoft Inc, USA) by manually clicking of individual events.

Paired-pulse ratios: Slices were perfused with carbogenated regular aCSF at ~30 °C, ~2 ml/min rate. Stimulus intensity was set to evoke 150–400 pA EPSC at holding potential -70 mV. Two EPSCs (inter-stimulus interval of 50 ms) were evoked for 10 consecutive traces. PPR was calculated by dividing the second EPSC peak amplitude by the first one.
AMPAR/NMDAR ratios: Slices were perfused with carbogenated regular aCSF at ~30 °C, ~2 ml/min rate. Stimulus intensity was set to evoke 150–400 pA EPSC at holding potential -70 mV. An average EPSC was obtained (~10 traces) at -70 mV and then at +40 mV. AMPAR/NMDAR ratio was calculated as the ratio of the average EPSC peak amplitude at -70 mV (AMPAR EPSC) to the average amplitude of the EPSC recorded at

+40 mV, 50ms after afferent stimulation. For pharmacologically isolated AMPAR/NMDAR ratios, dual-component evoked EPSC at +40mV was recorded before and after DL-APV bath application (50 μM, Abcam). NMDAR EPSC was obtained by digitally subtracting the average EPSC amplitude after APV application (AMPAR EPSC). For NR2B/total NMDAR ratio, dual-component evoked EPSC at +40 mV was recorded after ifenprodil bath application (3 μm, Tocris), before DL-APV bath application. Average NR2B EPSC was determined by digital subtraction and its peak amplitude was divided by NMDAR peak amplitude to obtain an NR2B/NMDA ratio.

Tail vein injections: Adult mice (ages 3-7 months) were anesthetized with a mix of 2.5% isofluorane/O2 circulated at a rate of 1L/min and put into restraint in a heating pad. The tail was swabbed with alcohol before injection and 200uL of virus preparation delivered through a single tail vein injection.

For the rescue experiments 200ul of AAV9.hSyn.eGFP.WPRE.bGH (~9e12 GC/ml titer) and AAV9.hSyn.HI.eGFP-Cre.WPRE.SV40 (~3e13 GC/ml titer) were used for single injections. For sparse labelling (sholl analysis experiment) 10-20ul of AAV9.hSyn.memGFP.WPRE.hGH (~4e13 GC/ml titer) was diluted in PBS to a final volume of 200ul and injected through the tail vein.

All virus were packaged by UPenn Vector Core; other viral preps using the same construct but packaged in our lab or using one other viral core packaging services, either

failed to cross the BBB or showed extremely low infection rates (around 5cells *per* 100μm coronal sections).

Brain sections IHC and imaging: Mice were anesthetized by isoflurane inhalation and transcardially perfused with PBS solution followed by 4%PFA (paraformaldehyde) fixative solution. Brains were kept in 4% PFA overnight at 4°C and then transferred to PBS and sectioned. Some mice brains were prepared for striatum electrophysiology and the remaining brain tissuewas fixed in 4% PFA (paraformaldehyde) solution to check for viral expression. Brains were kept in 4% PFA overnight at 4°C and then transferred to PBS and sectioned on a Vibratome (1000 Plus, Pelco International). After electrophysiology recordings, those slices were also kept in 4%PFA overnight at 4°C and later processed for IHC to check for viral expression, together with the remaining sections.Sections were washed 3x in PBS and incubated in PBS-0.5%Triton-X 100 for 2H RT, followed by another 3xPBS wash. After that, blocking was performed for 1H in PBS containing 15% NGS, 5% BSA and 0.2% Triton-X. Primary antibodies were incubated 48H at 4°C for detection of the respective antigens. Sections were washed 3XPBS, followed by 4°C 24H incubation with secondary antibody (species-specific Alexa-conjugated antibody, 1:1000, Invitrogen). Lastly, sections were washed 3xPBS, stained for DAPI, mounted inFluoro-Gel (EMS, 17985-10) and imaged using an epi-fluorescence microscope (Epi BX61, Olympus) ora confocal microscope (FV1000, Olympus).

Viral-infection cell count: Matched coronal sections (+1.60, +0.38, -0.40 and -2.30mm relative to bregma according to Franklin&Paxinos mouse brain atlas) were collected from each animal, coded in order to blind the experimenter and co-stained for GFP and NeuN. Sections were imaged with 20xobjective (UPLSAPO 20x NA:0.75) in a confocal microscope (FV1000, Olympus) at the highest focal plane (to avoid potential differences in labeling due to focal depth changes). Cells were counted from 200x200μm regions defined in both hemispheres *per* section according to different brain regions of interest (ROI) – M1, M2, striatum, GP and thalamus. Cells were automatically counted inside the different ROIs using ImageJ software with Fiji, Particle Analysis. Average infection *per* brain region was determined as the average percentage of GFP+/NeuN+ cells inside ROI.

IHC Antibodies: Mouse anti-parvalbumin (Swant #PV235,1:5000), Mouse anti-NeuN (Millipore #MAB377, 1:1000), Mouse anti-GFAP (Cell Signaling #3670P, 1:1000), Rabbit anti-GFP (Invitrogen #A11122, 1:1000), Rabbit anti-FosB (5G4, Cell Signaling #2251, 1:200), Goat anti-rabbit alexafluor-488 (Invitrogen #A11034, 1:1000), Goat anti-mouse alexafluor-555 (Invitrogen #A21424, 1:1000), Goat anti-rabbit alexafluor-555 (Invitrogen #A-21428, 1:1000).

Sholl analysis: Adult WT, KO and TM mice were sacrificed 3weeks after tail-vein injection of the membrane-GFP virus. Brains were processed as described in IHC methods above using rabbit anti-GFP antibody. Matched 100μm coronal sections from the entire striatum (16 slices total, bregma+1.4 through -0.10mm, according to Franklin

& Paxinos mouse brain atlas) were collected from each animal and coded in order to blind the experimenter. Isolated MSNs were imaged from DLS matching regions and identified by their typical morphology (high spine density and fairly short neuronal arborizations). Total of 1 MSN *per* section was acquired, unless no MSN meet the criteria at given sections (severed dendritic arborization or overlapping with surrounding neurons). Confocal z-stacks were acquired in 1μm steps using confocal microscope (FV1000, Olympus) and 40xobjective (UPLFLN 40xoil NA:1.30). Cell arborization was reconstructed and analyzed using Neurolucida software (MBF Bioscience). Values were plotted in Prism (Graph Pad) and compared by Two-way repeated measures ANOVA.

Statistical Analyses: All statistical analyses were performed using Prism (GraphPad Software). All data sets were analyzed using D'Agostino-Pearson omnibus test and Shapiro-Wilk test for normality. Data sets with normal distributions were analyzed for significance using either unpaired Student's two-tailed *t*-test or ANOVA measures with multiple comparison post-hoc test, using *P< 0.05, **P<0.01, ***P< 0.001; all data presented as means ± s.e.m. Data sets with non-normal distributions were analyzed using Kruskal-Wallis test with adjustments for multiple comparisons. Based on previously published literature on Shank3 models (Wang et al, 2011; Bozdagi et al, 2010; Peca et al, 2011; Yang et al, 2012), we chose similar sample sizes for all experiments performed. All behavior test results for the tamoxifen treated cohorts are the combination of at least two different large animal cohorts that showed the same results. All electrophysiological,

biochemical, and morphological data were obtained by counterbalancing experimental conditions with controls. Further details on particular statistical analyses can be found on the respective figures/results section for each data set.

CHAPTER 3: Adult Expression of Shank3 Rescues Selective Behaviors

I generated the Shank3 Fx/Fx mice, produced the PCRs shown, conducted the tamoxifen feedings, performed the biochemistry, and conducted the behavioral experiments. Patricia Monteiro performed the electrophysiology recordings and contributed to the open field experiments. Special thanks to Alexander Lim for contributing to the behavioral analysis; Triana Dalia for contributing to the mouse colony maintenance. Special thanks to Jing Lu for the LacZ data shown.

Critical Window?

Autism is a neurodevelopmental disorder that typically induces apparent symptoms in children before the age of 3 (Miles et al, 2011). Due to the early development of symptoms, it is not currently known whether the disease can be fully rescued. Furthermore, it is not known whether there is a critical time window for rescue that will efficiently reverse the pathology. Because there is little evidence of neurodegeneration in ASD in both human patients and mouse models, it is possible that the neural deficits can be improved.

Studying ASD is complicated by the vast etiological hetereogeneity. However, Shank3 is a monogenic cause of ASD, accounting for about 1% of all cases of ASD and 2% of ASD patients with intellectual disability (Leblond et al, 2014; Soorya et al, 2013; Betancur et al, 2013). It is a major scaffolding protein in the synapse and is critical for the maintenance of synaptic function. Due to the large proportion of ASD candidate genes localized to the synapse, studying Shank3 may elucidate general mechanisms of pathogenesis and shed light on how synaptic disruption contributes to the behavioral phenotypes in autism. Determining whether impaired synaptic structure and function can be improved in adulthood will significantly advance both our basic understanding of synaptic plasticity and disease reversibility.

To address these critical questions, we used an innovative approach to generate a novel Shank3 conditional knock-in mouse line. Using this transgenic model, we expressed Shank3 at different age points in our Shank3 conditional knock-in to determine

whether expression of Shank3 during adulthood, young adulthood, or at germline is necessary to reverse the autistic-like symptoms.

Targeting Strategy

To address whether adult reversal of physiological and behavioral abnormalities in *Shank3* mutant mice is possible, we adopted a genetic method that allows for inducible *Shank3* expression by Cre recombinase. Because *Shank3* duplication is linked to ADHD and bipolar disorder, and *Shank3* overexpression in mice leads to manic-like phenotypes and abnormal synaptic function (Moessner et al, 2007; Durand et al, 2007; Han et al, 2013), it is critical to maintain tight regulation of *Shank3* expression within its physiological concentrations to avoid potential confounds. Other targeting methods including inducible transgene expression and viral delivery do not provide such precise control (Chandler et al, 2007; Waehler et al, 2007). Thus, we generated a novel *Shank3* conditional knock-in mouse by using the Cre-dependent genetic switch (FLEx) strategy (Schnutgen et al, 2007), which enables the conditional manipulation of the *Shank3* gene at its endogenous genetic locus. To our knowledge this is the first engineered conditional mouse model of autism using FLEx strategy *in vivo*.

Targeting Shank3

Designing an effective targeting strategy for Shank3 to both efficiently delete the gene and re-express it is complicated by the intricate gene structure of the Shank3 gene. Shank3 maps onto chromosome 22 in the human genome and chromosome 15 in the mouse genome. In the mouse, it spans about 58 kb and contains 22 exons, 5 of which are

alternatively spliced. There are 6 predicted promoters and 5 CpG islands (Jiang and Ehlers, 2013). As a result of these multi-layered regulatory elements, the gene produces an extensive array of isoforms (Wang et al, 2014). Studies showed that these protein isoforms have specific expression patterns across the brain, leading to the hypothesis that these isoforms are cell-type specific and may therefore have distinct mechanistic functions (Wang et al, 2014; Peca et al, 2011; Han et al, 2014).

Biochemical analyses showed that the 22 exons encode 5 protein domains with exons 4-9 producing the ankyrin domain, exons 10 and 11 producing the SH3 domain, exons 13-16 encoding the PDZ domain, exons 20-21 encoding the Proline-Rich domain, and exon 22 generating the SAM domain. Previous studies show that the different domains mediate distinct protein-protein interactions (Roussignol et al, 2005; Hayashi et al., 2009). The Ankyrin domain has been shown to bind to alpha-Fodrin, while SH3 interacts with GRIP1 and Densin-180. The Proline-Rich domain binds to Homer, which in turn interacts with mGluRs. It also binds to Cortactin and Abp1. The SAM domain is well established for mediating Shank3 self-oligomerization. The PDZ domain mediates both direct interactions with AMPA receptors and indirect interactions with NMDA receptors. It also regulates the actin cytoskeleton by interacting with ProSAPiP1 and β-Pix. Mutations have been identified in all but the SAM domain in ASD patients (Moessner et al., 2007; Philippe et al, 2008; Boccuto et al., 2013; Bonaglia et al., 2011; Dhar et al., 2010; Gauther et al., 2009, 2010; Sarasua et al., 2011; Waga et al., 2011; Wilson et al., 2003; Jiang and Ehlers, 2013).

The relationship between the mutant variants and phenotype is not currently understood. Different human mutations in the Shank3 gene produce phenotypes of varying severity, suggesting that each mutation has different consequences on the Shank3 protein and function. For example, the mutation c.601-1G>A in the Ankyrin domain found in one patient with no other genes disrupted is correlated with mild intellectual disability, severe language deficits, but no ASD diagnosis. Another patient with the frameshift mutation p.A447fs in the SH3 domain had language impairment and a borderline score for ASD diagnosis. A third patient with a point mutation in the PDZ domain p.R656H showed developmental delay, mild intellectual deficits, and was diagnosed with ASD (Jiang and Ehlers, 2013). Thus, careful attention to the placement of the mutations and its impact on the protein isoform profile is necessary to elucidate the mechanisms of autism pathogenesis.

In order to study the reversibility of autistic phenotypes after development, we needed to generate a mouse model that properly recapitulates the phenotypes of autistic patients. To that end, we studied the existing literature on the different Shank3 mouse models. Several labs generated models that targeted the N-terminal Ankyrin domain (Bozdagi et al, 2010; Yang et al, 2012; Wang et al, 2011; Peca et al, 2011). These transgenic lines all displayed deficits at the synapse, whether morphologically or functionally. However, the behavioral phenotypes were quite mild (Jiang and Ehlers, 2013). Schmeisser et al, 2012 targeted exon 11 or the SH3 domain. Even though this line displayed stereotyped grooming behavior, there was little evidence of synaptic deficits or social interaction abnormalities (Schmeisser et al, 2012; Jiang and Ehlers, 2013). The

only mutant line that showed robust synaptic functional impairments and the full array of key autistic-like behavior phenotypes was the line that targeted the PDZ domain (Peca et al, 2011). This is consistent with the evidence showing that the PDZ domain is present in all major isoforms of Shank3 and is critical to the multiprotein scaffold complex in the PSD.

Thus, like in the SHANK3B mutant mice, we genetically targeted the PDZ domain, which includes exons 13 to 16. We inverted and flanked exons 13-16 with two staggered pairs of inward-facing non-matching Lox sites (Fig. 1). The introduction of Cre recombinase will catalyze the re-orientation of the inverted and double floxed exons 13-16, allowing correct gene transcription. Further inversion of the re-oriented exons will be prevented by the incompatibility of the remaining Lox sites, which are LoxP and Lox2722 (Fig. 1).

We introduced this novel Shank3 Flex cassette into the stem cells through electroporation, and used homologous recombination to replace the endogenous Shank3 gene. After completing an extensive screening process for positive clones that harbor the Flex cassette at the Shank3 locus, we then injected the healthiest stem cell colonies into mouse blastocysts. This novel mouse line successfully yielded germline transmission. To screen for positive pups, I used two different PCR protocols to both ensure the correct locus of insertion and the intactness of the Lox sites (Figure 2a and 2b). The mice used for experiments are maintained on a mixed background as described in Methods.

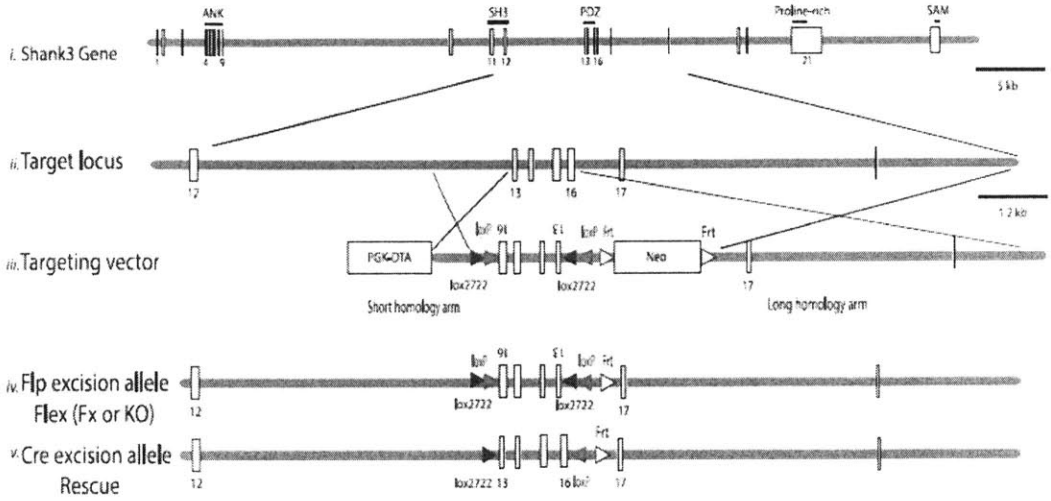

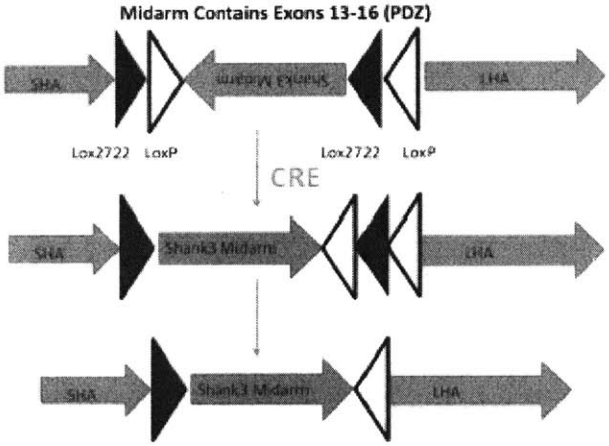

Figure 1. Flex Strategy. The midarm including exons 13-16 of Shank3 is flanked by staggered pairs of LoxP and Lox2722 sites. Upon Cre expression, the midarm is re-oriented in the 5' to 3' direction. The remaining LoxP and Lox2722 sites are incompatible for further Cre recombination, thus preventing further midarm re-orientation.

Figure 2a. PCR screen of germline transmission. A single band at 340 bp indicates wildtype; one band at 340 bp and one band at 480 bp indicate the presence of the floxed allele.

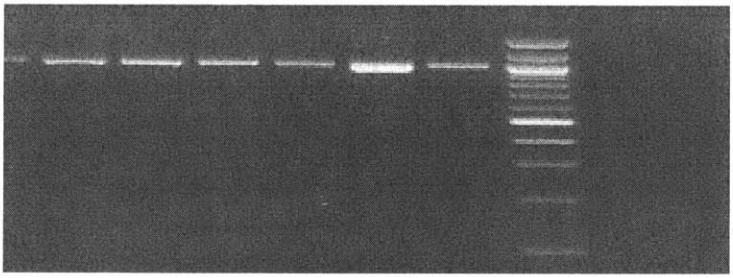

Figure 2b. PCR screen of the insertion of the Flex cassette in the correct locus in the germline transmission mice. A single band at 980 bp indicates the presence of the Flex cassette at the Shank3 locus.

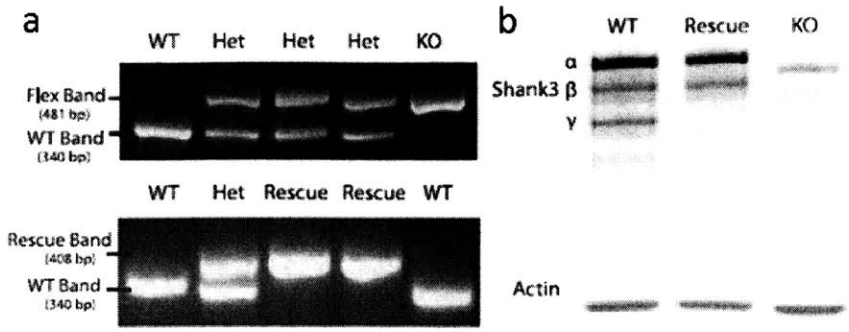

Figure 3. a) PCR genotyping showing the bands for Fx, Rescue, and WT. b) Western blot showing almost complete rescue of Shank3 expression upon Cre recombination, with exception of putative Shank3y isoform. This is likely due to disruption of a putative intronic promoter by the introduction of the LoxP sites.

In the absence of Cre, the *Shank3*$^{fx/fx}$ mice function as SHANK3 knockout (KO), and result in the deletion of most major isoforms of SHANK3 including the putative alpha, beta, and gamma bands (Fig. 3B; Fig. 4A, B). Similar to behavioral abnormalities previously reported on SHANK3 KO mice (Wang et al, 2011; Bozdagi et al, 2010; Peca et al, 2011; Yang et al, 2012), these *Shank3*$^{fx/fx}$ mice show significant deficits in exploratory behavior (Fig. 4C), anxiety (Fig. 4E), motor deficits (Fig. 4D), and display open wound lesions which suggest repetitive/stereotyped grooming behavior (Peca et al, 2011; Karayannis et al, 2014). In addition, they show impaired striatal neurotransmission in the dorsal striatum (Fig. 4F-G), consistent with our previous findings in *Shank3B* KO mice. These novel *Shank3*$^{fx/fx}$ mice thus recapitulate autistic-like phenotypes, enabling us to investigate the possibility of reversing those physiological and behavioral abnormalities in adulthood.

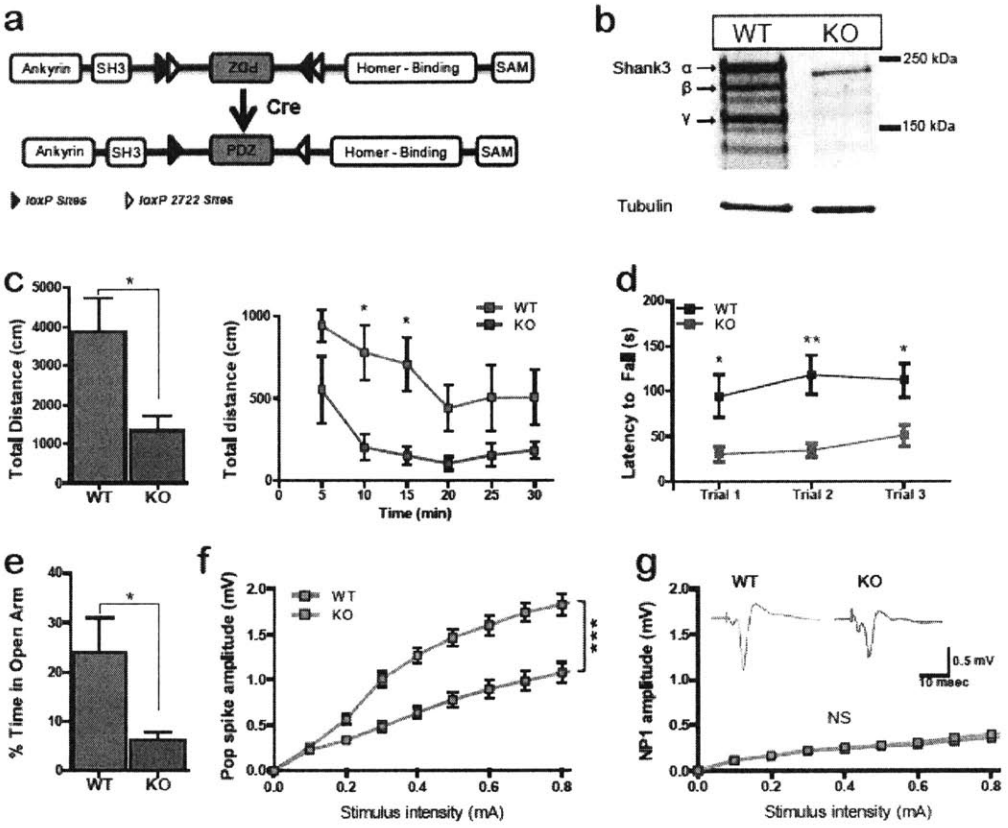

Figure 4. *Shank3*$^{fx/fx}$ mice have disrupted *Shank3* expression, striatal and behavioral deficits. **a**, Schematic domain structure of SHANK3 protein, with FLExed PDZ domain inverted; flanked domain can be re-oriented in presence of Cre recombinase. **b**, Western blot showing *Shank3* expression in PSD preparation from striatum (3ug total protein per lane), for wildtype (WT) and *Shank3*$^{fx/fx}$ (KO) mice. **c**, *Shank3*$^{fx/fx}$ mice show decreased total distance traveled in the open field test compared to WT. **d**, KO mice show impaired motor coordination in rotarod test. **e**, *Shank3*$^{fx/fx}$ mice spend less time at the open arm in elevated zero maze test. **f**, *Shank3*$^{fx/fx}$ mice show inefficient cortico-striatal transmission as measured by decreased pop spike amplitude in extracellular field recordings. **g**, Normal relationship of stimulation intensity to the negative peak 1 amplitude (NP1; action potential component) suggesting unaltered presynaptic function; insets show representative field traces from *Shank3*$^{fx/fx}$ and WT mice. *P< 0.05, **P<0.01, ***P< 0.001; all data presented as means ± s.e.m. (all behavior data from n=6 WT and n=7 KO mice); two-tailed *t*-test for **c** (left panel) and **e**; two-way repeated measures ANOVA with Bonferroni *post hoc* test for **c** (right panel), **d**, **f** and **g** (electrophysiology data from n=9 slices; 3 mice *per* genotype).

To achieve temporal control of *Shank3* expression, we crossed the *Shank3*$^{fx/fx}$ mice to an inducible CAGGS-CreER mouse line (CAGGS comprises a CMV enhancer and chicken β-actin promoter [Guo et al, 2002]) that activates global Cre function upon tamoxifen treatment (Fig. 5). This particular transgenic CreER line contains a transgene insert that carries a fusion protein of the Cre recombinase and a modified mouse estrogen receptor ligand-binding domain (Guo et al, 2002). The modified estrogen receptor does not bind to any natural ligand physiologically, but will only bind to 4-hydroxytamoxifen. This fusion protein is normally anchored to the cytoplasm, however, upon tamoxifen treatment, the fusion protein will be shuttled to the nucleus, where Cre can now induce DNA recombination. This extra layer of control regulated by tamoxifen exposure facilitates the temporal induction of Cre function. In the CAGGS-CreER, the CreER fusion protein is under the regulation of the strong pCAGGS promoter, which contains the CMV early enhancer and chicken β-actin promoter (Guo et al, 2002). We have characterized the expression pattern of this CreER line by crossing it with a Rosa26$^{floxSTOP\text{-}LacZ}$ reporter line and treating the progeny with tamoxifen. After 5 days of consecutive oral gavage, this line demonstrates brain-wide expression of Cre (Fig 5A; courtesy of Dr. Jing Lu). We further confirmed this data by crossing the mouse line with another reporter line, Rosa26$^{floxSTOP\text{-}TdTomato}$. The expression pattern is consistent with the data shown (Fig 5B).

a

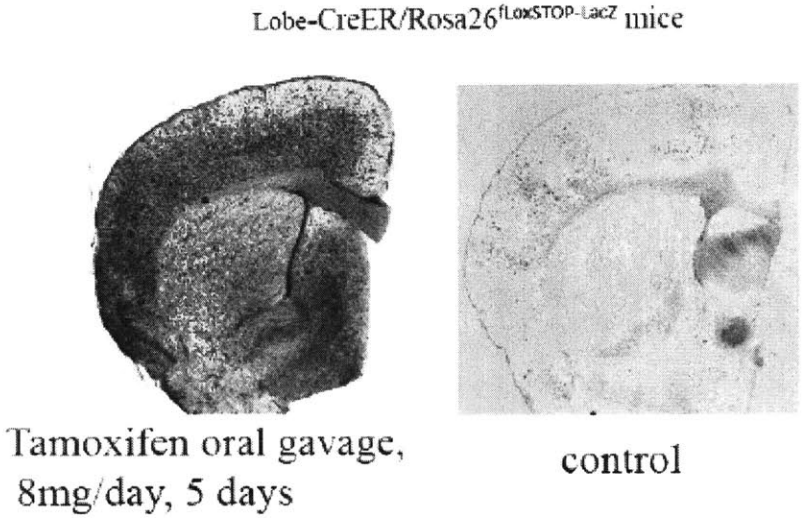

b

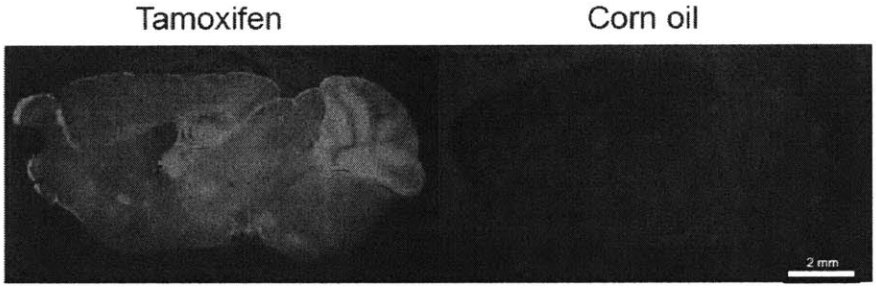

Figure 5. Tamoxifen-inducible Cre strategy leads to broad reporter expression. **a,** Coronal sections from pCAGGS-CreER+/-:Rosa26-floxSTOP-LacZ fed with tamoxifen(left panel) and vehicle (right panel). **b**. Sagittal sections from pCAGGS-CreER+/-:Rosa-stopflox-tdTomato+/- mice after feeding with tamoxifen (left panel) or corn oil (right panel). Results show specific induction of tdTomato reporter expression upon tamoxifen-induced Cre expression but not in the absence of Cre (corn oil feeding); pCAGGS promoter consists of the CMV early enhancer with chicken β-actin promoter (Guo et al, 2002).

When the *Shank3*$^{fx/fx}$*:CreER*$^{+/-}$ mice reached 2-4.5 months, we used oral gavage to deliver 5 consecutive daily doses of tamoxifen followed by a 2-week hiatus and then another 5 consecutive daily doses of tamoxifen to ensure complete Cre-mediated re-orientation of exons 13-16 (Fig. 6A). All experiments post-feeding were performed on the following three groups: *Shank3*$^{+/+}$*:CreER*$^{+/-}$ treated with tamoxifen (WT), *Shank3*$^{fx/fx}$*:CreER*$^{+/-}$ treated with tamoxifen (TM), and *Shank3*$^{fx/fx}$*:CreER*$^{+/-}$ treated with corn oil vehicle (KO). Synaptosomal preparations show that tamoxifen treatment of *Shank3*$^{fx/fx}$*:CreER*$^{+/-}$ mice restores the expression of most major SHANK3 isoforms including the alpha and beta isoforms to the wildtype level at synapses (Fig. 6B).

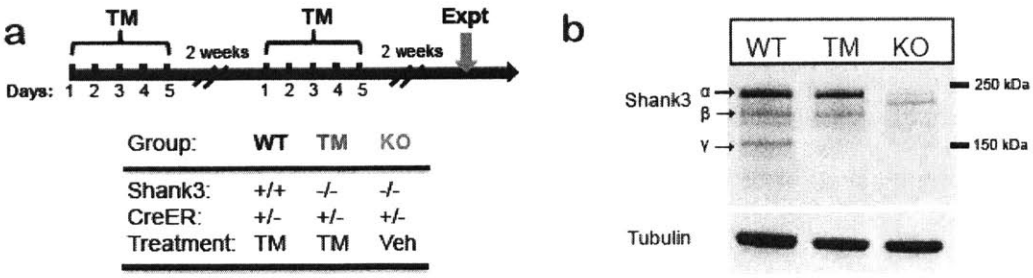

Figure 6. Adult tamoxifen feeding efficiently restores Shank3 expression. a, Feeding scheme and mouse genotype for all groups oral gavaged. **b**, Western blot from striatal synaptosome preparation after tamoxifen feeding shows restoration of most SHANK3 isoforms.

After optimizing the tamoxifen treatment protocol, we tested how adult Shank3 expression may alter behavioral abnormalities. Since striatal defects have been strongly linked to repetitive/compulsive behaviors (Welch et al, 2007) and *Shank3* KO mice show overgrooming (Peca et al, 2011), we videotaped WT (*Shank3*$^{+/+}$:*CreER*$^{+/-}$ treated with tamoxifen), TM (*Shank3*$^{fx/fx}$:*CreER*$^{+/-}$ treated with tamoxifen), and KO (*Shank3*$^{fx/fx}$:*CreER*$^{+/-}$ treated with corn oil) mice after treatment, and quantified their grooming time. The results indicate that while there is significant increase in the percentage of time spent grooming in the KO mice treated with corn oil compared to WT mice, KO mice treated with tamoxifen exhibit significantly reduced grooming time (Fig. 7A-B). In addition, during the tamoxifen treatment, we noticed that some *Shank3*$^{fx/fx}$:*CreER*$^{+/-}$ mice that initially developed lesions began to heal and regrow their lost fur (Fig. 7C), providing further support that repetitive/excessive grooming phenotype is reversible in the *Shank3*$^{fx/fx}$ mice.

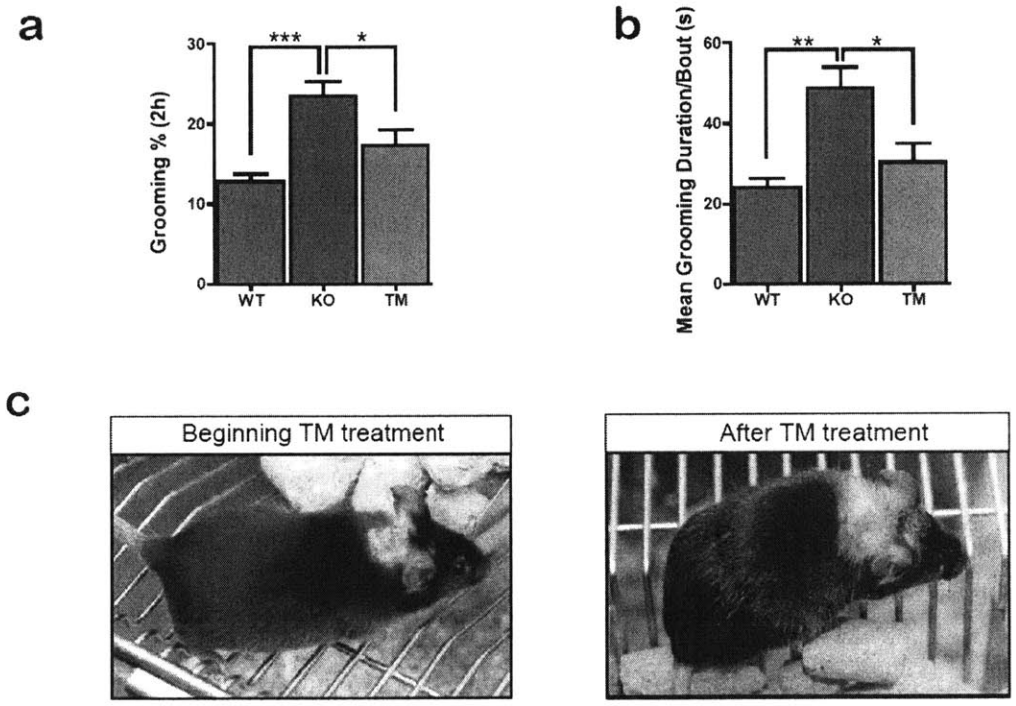

Figure 7. Adult *Shank3* expression rescues grooming-induced lesions. **a**,**b**, Significantly reduced repetitive grooming behavior (both in terms of total time spent grooming and mean grooming duration *per* bout) in KO mice after tamoxifen feeding. **c**, *Shank3*$^{fx/fx}$ mouse showing pronounced neck lesion at the beginning of tamoxifen feeding and picture of the same mouse showing lesion healing and regrown fur after tamoxifen feeding scheme. *P<0.05, **P<0.01, ***P<0.001; all data presented as means ± s.e.m; one-way repeated measures ANOVA with Bonferroni *post hoc* test for **a**,**b** (n=9 WT, n=9 TM and n=12 KO mice).

One of the defining features of autism is the impairment in social interaction. Thus, we used a modified three-chamber assay to probe voluntary social interaction (Peca et al, 2011; Yang et al, 2012; Chao et al, 2010). After habituating to the three-chamber box, the test mice were given a choice of either interacting with a novel object or a novel mouse. We measured the duration and frequency of close interaction between the test mouse and its target of interest to determine the level of social preference. We found that while WT mice demonstrated strong preference for the novel mouse, KO mice displayed no preference for either the object or the novel mouse (Fig. 8). This result is consistent with previous reports indicating that *Shank3* deletion leads to social interaction deficits in mice (Wang et al, 2011; Bozdagi et al, 2010; Peca et al, 2011; Yang et al, 2012). Interestingly, we found that TM mice behave similarly to their WT controls in that they show strong preference for the novel mouse in both duration and frequency of interaction (Fig. 8). These data show that, similar to repetitive grooming behavior, social interaction deficit can also be rescued in adulthood.

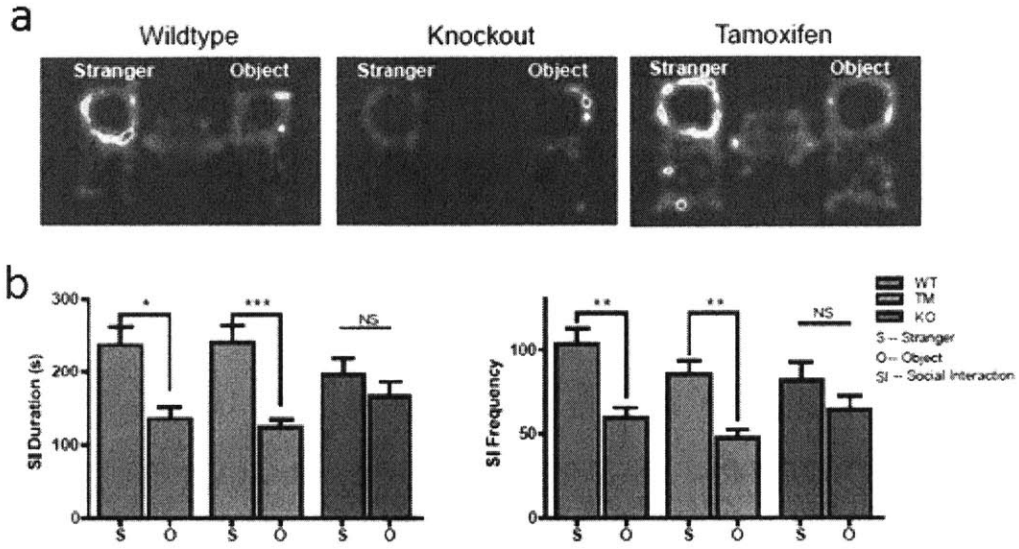

Figure 8. Adult *Shank3* expression rescues social interaction. a, Representative heat map analysis from the social interaction test for all groups (1 WT, 1 TM and 1 KO). **b,** KO mice (red bars) showed no preferential interaction between a stranger mouse and an inanimate object, as assessed by interaction duration and frequency; this behavior is rescued after tamoxifen treatment, with TM group (blue bars) showing preference for social interaction (stranger); the same social preference is observed in WT mice (grey bars). *P<0.05, **P<0.01, ***P<0.001; all data presented as means ± s.e.m **b**, Social interaction duration data (left panel) was analyzed using one-way repeated measures ANOVA with Bonferroni *post hoc* test. Social interaction frequency data (right panel) was analyzed using Kruskal-Wallis test with Dunn's multiple comparison test due to the distribution not being normally distributed (n=22 WT, n=30 TM and n=30 KO).

Encouraged by the rescue of repetitive grooming and social deficits, we ran a battery of other behavior tests to assess the extent of behavioral rescue. In contrast to the social interaction and grooming behaviors, adult *Shank3* re-expression has minimal impact on anxiety-like behavior and motor coordination deficit (Fig. 9). In the open field test, TM (*Shank3*$^{fx/fx}$:*CreER*$^{+/-}$ treated with tamoxifen) mice showed no significant difference from the KO mice (*Shank3*$^{fx/fx}$:*CreER*$^{+/-}$ treated with corn oil) in exploratory behavior (Fig. 9A) and anxiety-like behavior including rearing time and rearing frequency (Fig. 9B). This result was further corroborated by our observations from the elevated zero maze test (Fig. 9C). In addition, we found no significant recovery in motor coordination deficit after re-expressing *Shank3* in adulthood (Fig. 9D). Interestingly, we also discovered that the Shank3 KO mice exhibited novel object phobia, and that this deficit is also not improved after Shank3 restoration (Fig. 10).

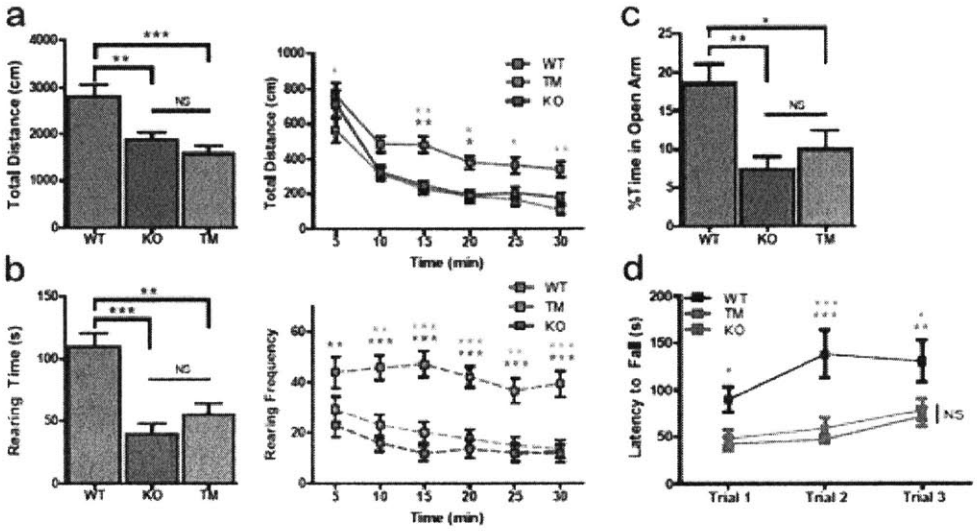

Figure 9. Restoring *Shank3* expression in adulthood does not rescue anxiety and rotarod deficits. a, Open field results indicate that tamoxifen feeding in adults does not rescue total locomotion in the *Shank3*$^{fx/fx}$ mice. **b**, Other parameters from open field test including rearing time and rearing frequency show that anxiogenic behavior is not rescued after tamoxifen feeding. **c**, *Shank3*$^{fx/fx}$ mice spend less time exploring the open arm; this behavior is also not rescued in the tamoxifen group compared to the control groups. **d**, Motor coordination measurement from rotarod is not rescued in adult *Shank3*$^{fx/fx}$ mice. *P < 0.05, **P<0.01, ***P < 0.001; One way ANOVA for **a** (left panel), **c**; Kruskal-Wallis test with Dunn's multiple comparisons for **b** (left panel). Two-way repeated measures ANOVA with Bonferroni *post hoc* test for **d; a-c**: n=18 WT, n=25 TM and n=27 KO; **d**: n=13 WT, n=19 TM and n=21 KO.

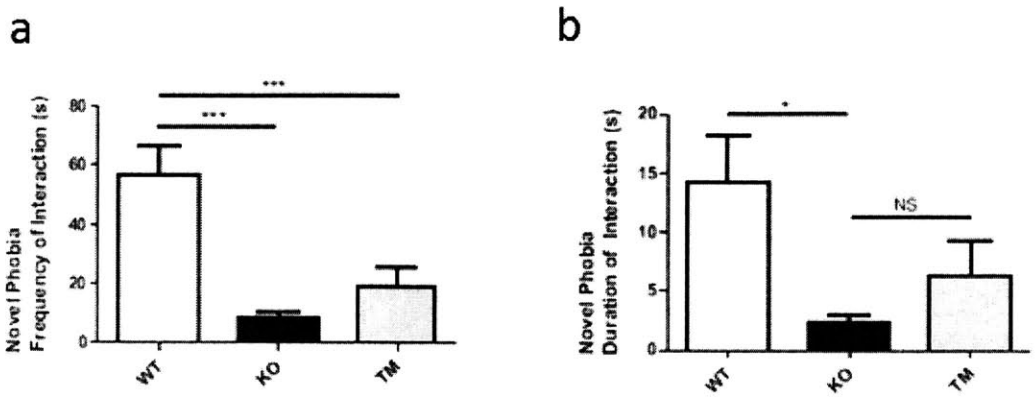

Figure 10. Adult Shank3 expression does not rescue novel object phobia. Novel object phobia results indicate that Shank3 Fx/Fx display fear towards novel objects in both frequency (**a**) and duration (**b**) of interaction, which are not rescued by tamoxifen feeding in the adult mice. *$P < 0.05$, **$P<0.01$, ***$P < 0.001$. Two-way repeated measures ANOVA with post hoc two-tailed t-test for **a, b**. N=13 WT, N=19 TM, and N=21 for KO mice.

To address whether the lack of rescue in these behavior phenotypes is indeed due to adult gene expression, we crossed *Shank3*$^{fx/fx}$ mice to a transgenic line that expresses Cre under the β-actin promoter, enabling germline rescue of *Shank3* expression. The germline rescue (GR) mice show no significant differences in striatum physiology (Fig. 11), exploratory behavior (Fig. 12A), anxiety (Fig. 12B-C), and motor coordination (Fig. 12D) from their wildtype littermates, indicating that, unlike in adulthood, restoring *Shank3* expression at the germ cell stage can restore all behavioral phenotypes. Together, these data strongly suggest that there are certain developmental defects that are irreversible by adult re-expression of *Shank3*.

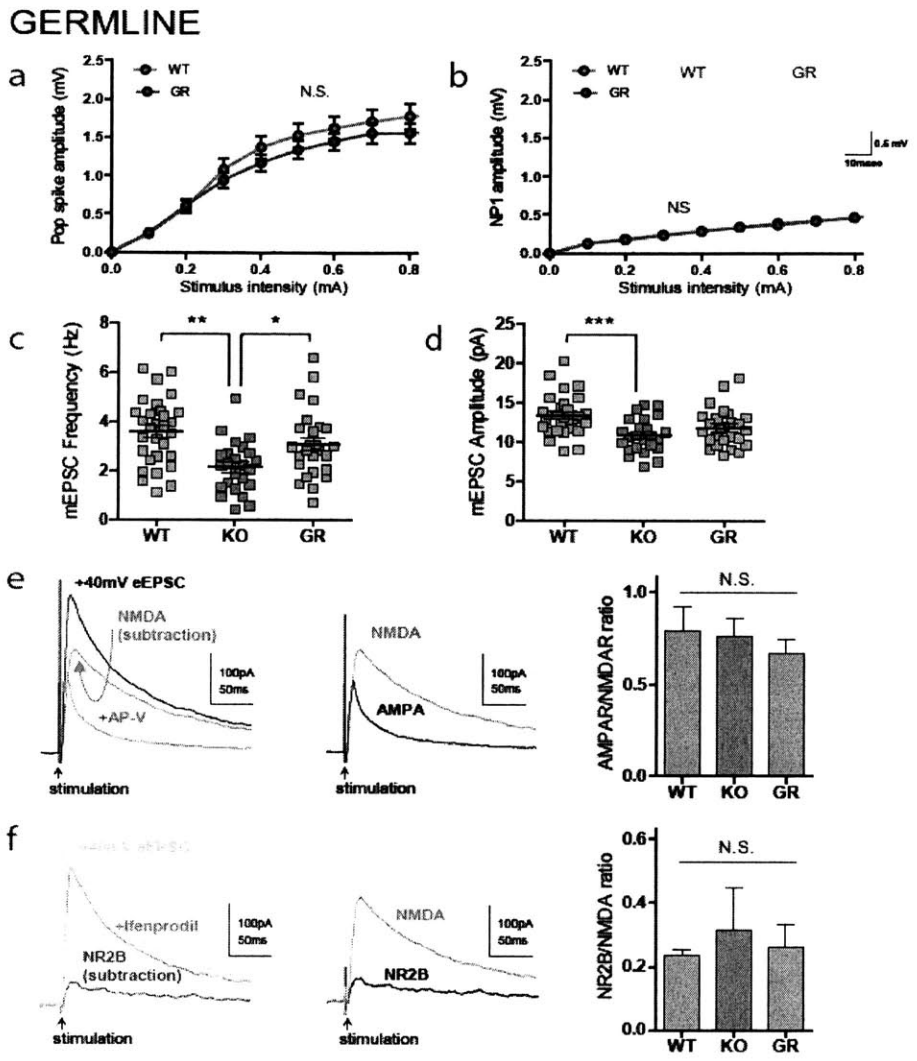

Figure 11. Dorsal striatum electrophysiological measurements in germline rescue (GR)

a,**b**, Normal pop spike amplitude (a) and NP1 (b) in genetically rescued GR mice (insets show representative field traces). **c**,**d**, Reduced mEPSC frequency in KO mice compared to WT and GR. A reduction in mEPSC peak current amplitude is observed between KO and WT group only (WT=30, KO=24, GR=26 MSNs). **e**, Representative traces (left) and bar graph (right) for pharmacologically isolated AMPAR/NMDAR ratio (WT=9, KO=9, GR=8 MSNs). Dual-component evoked EPSC at +40 mV recorded before and after APV bath application. **f**, Representative traces (left) and bar graph (right) for NR2B/NMDAR ratio in WT, KO and GR groups (WT=6, KO=5, GR=7 MSNs). Dual-component evoked EPSC at +40 mV recorded before and after ifenprodil bath application. *p<0.05; **p<0.01; ***p<0.001 (ANOVA). Data are means ±s.e.m.

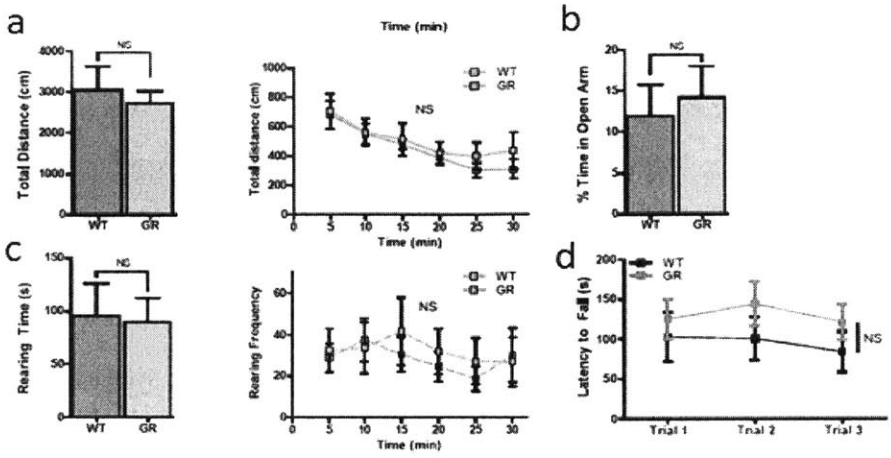

Figure 12. Restoring *Shank3* expression in adulthood does not rescue anxiety and rotarod deficits. a-d, Germline rescued *Shank3*$^{fx/fx}$ mice show that all previous parameters for open field, elevated zero maze and rotarod tests can be rescued if *Shank3* expression is restored at germ cell stage; results indicate the existence of a critical period such that adult expression of *Shank3* cannot rescue these behaviors. *$P < 0.05$, **$P<0.01$, ***$P < 0.001$; Two-tailed *t*-test for **a** (left panel) **b** (left panel) and **c**; Two-way repeated measures ANOVA with Bonferroni *post hoc* test **d**; All data presented as means ± s.e.m. (**a-d**: n=10 WT and n=8 GR mice).

It is possible that *Shank3* re-expression during a developmental period between the germline stage and adulthood can yield significant improvement in behaviors that cannot be altered through adult *Shank3* re-expression. To test this, we treated P20-21 mice with two to three consecutive doses of tamoxifen to efficiently induce *Shank3* expression (Fig. 13A), and assayed their behaviors in adulthood (Fig 13-14). As previously reported (Guy et al, 2007), we observed that treatment of mice with tamoxifen at young age leads to some toxicity including reduced body weights in the WT mice and affected their motor coordination compared to the KO fed with corn oil (Fig. 14D). However, even with the TM toxicity, we found that on the rotarod, the developmentally treated TM mice performed significantly better than their KO counterparts (Fig 14A-B). The P20-21 treated TM mice also showed significantly improved anxiety on the elevated zero maze compared to the KO (Fig. 13F).

We also treated the KO mice at P10 and assayed for their behavior when they reached adulthood. We found that this early rescue significantly improved their performance in the open field, which was not rescued with P21 treatment. We also ran the zero maze, and found that consistent with the P21 treatment, the P10-treated mice also performed significantly better than their vehicle-treated counterparts (Fig. 15). Overall, these behavioral results showed that earlier intervention yields more behavioral improvement than adult treatment, further supporting the developmental origin of the behavioral abnormalities that are irreversible in adults.

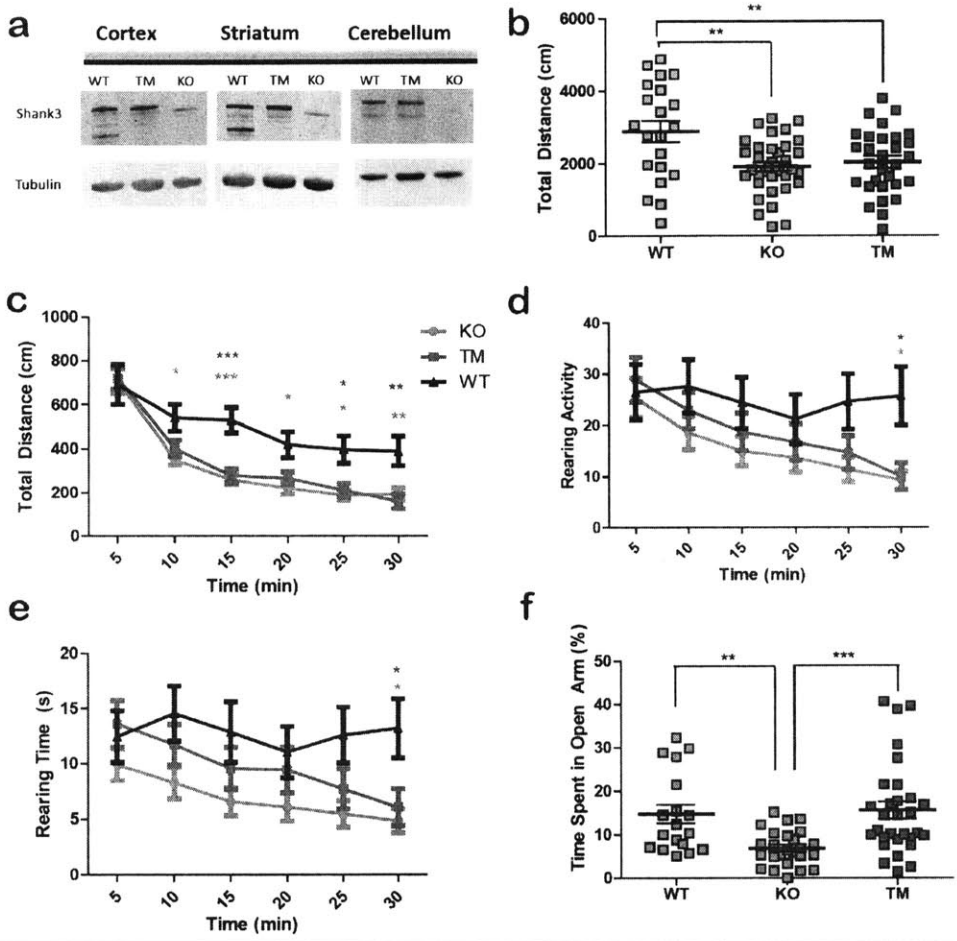

Figure 13. Expression of Shank3 at P20-21 rescues some behavioral measurements of anxiety in adulthood

a, Representative western blots showing efficient Shank3 re-expression in cortex, striatum, and cerebellum in mice that were treated with tamoxifen at P20-P21. **b**, The total distance traveled as measured by the open field was not improved in the tamoxifen condition compared to the KO condition. One-way ANOVA, Bonferroni post-hoc test. **c**, The open field total distance plotted across 5-minute time bins, showing that there is no difference between KO and TM conditions across time. **d.** Rearing activity measured by open field plotted across time, showing that TM performs in between WT and KO for most of the 30 -minute test. **e.** Rearing time measured by open field plotted across time, also showing that the intermediate performance of TM between that of WT and KO. (**b** to **e)** WT N=21, KO N=36, TM N=30. Two-way ANOVA, Bonferroni post-hoc test. **f.** Activity on the zero maze shows that the TM condition shows significantly improved performance compared to that of the KO condition. There is no difference between WT and TM. WT N=18, KO N=25, TM N=30. Kruskal-Wallis test, Dunn's Multiple Comparison test. All data presented as means ±s.e.m.

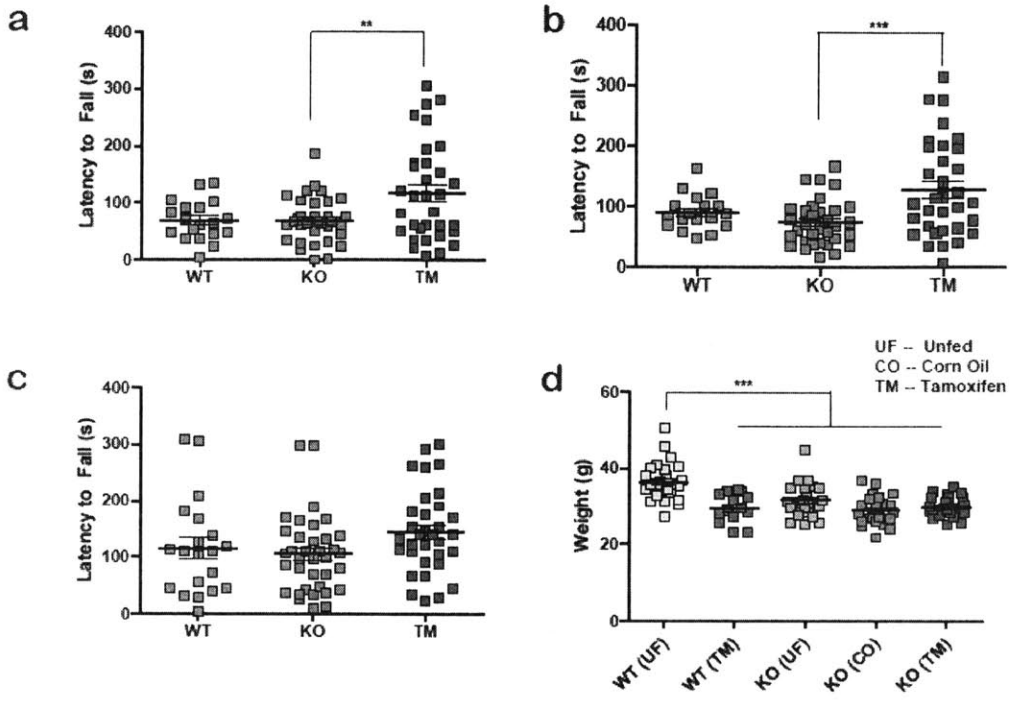

Figure 14. Expression of Shank3 at P20-21 rescues some behavioral measurements. a, Representative western blots showing efficient Shank3 re-expression in cortex, striatum, and cerebellum in mice that were treated with tamoxifen at P20-P21. **b**, The total distance traveled as measured by the open field was not improved in the tamoxifen condition compared to the KO condition. **c**, The open field total distance plotted across 5-minute time bins, showing that there is no difference between KO and TM conditions across time. **d.** Rearing activity measured by open field plotted across time, showing that TM performs in between WT and KO for most of the 30 -minute test. **e.** Rearing time measured by open field plotted across time, also showing that the intermediate performance of TM between that of WT and KO. (**b** to **e)** WT N=21, KO N=36, TM N=30.Two-way ANOVA, Bonferroni post-hoc test. **f.** Activity on the zero maze shows that the TM condition shows significantly improved performance compared to that of the KO condition. There is no difference between WT and TM. WT N=18, KO N=25, TM N=30. Kruskal-Wallis test, Dunn's Multiple Comparison test. All data presented as means ±s.e.m.

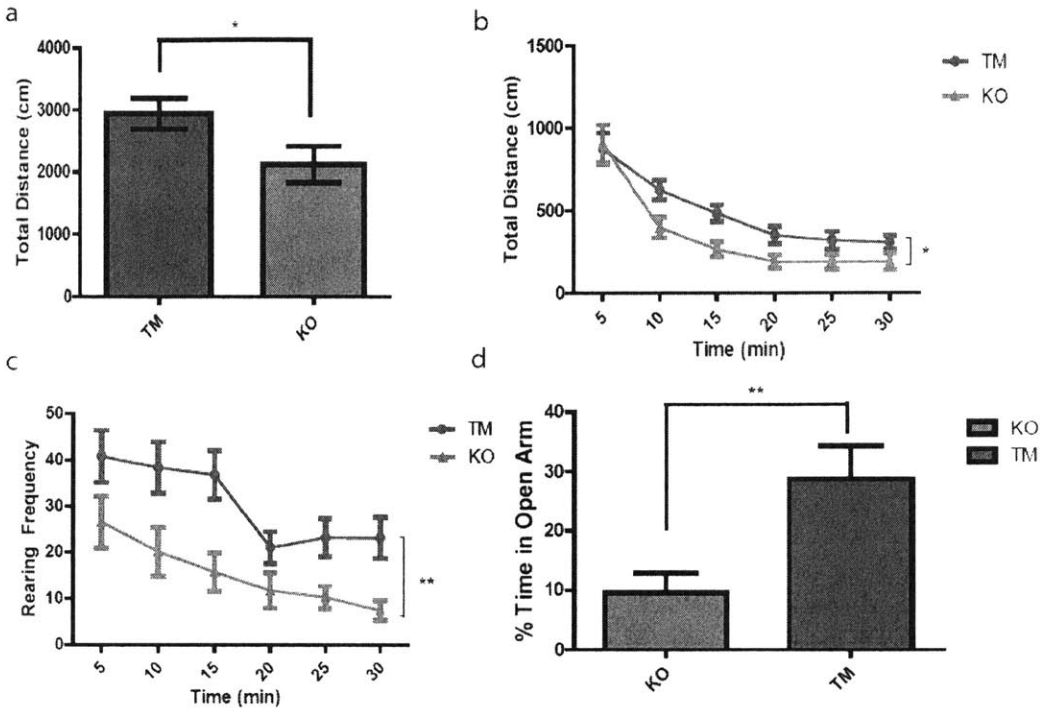

Figure 15. Expression of Shank3 at P10 rescues more behavioral measurements. a, Restoration of Shank3 expression at P10 improves total distance measured in open field. Student's two-tailed t-test. **b,** Open field total distance plotted across 5-minute time bins, showing that TM perform better than KO. **c**, The open field rearing frequency plotted across 5-minute time bins, showing that there is significant improvement in TM. **b-c**, Two-way ANOVA, Bonferroni post-hoc test. **a-c,** KO N=19, TM N=16 **d.** Activity on the zero maze shows that the TM condition shows significantly improved performance compared to that of the KO condition; KO N=11, TM N=11; Student's two-tailed t-test. *P<0.05, **P<0.01, ***P<0.0001

Discussion

Previous studies aiming to determine the adult reversibility of ASD phenotypes focused on MECP2 (Guy et al, 2007) and Syngap1 (Clement et al, 2012). While the results from MECP2 rescue showed that the disease phenotypes can be efficiently reversed, the data from Syngap1 study showed the opposite effect, indicating that the behavioral deficits are permanent (Guy et al, 2007; Clement et al, 2012). The difference in these conclusions highlights the inherently distinctive mechanisms of these two genes. MeCp2 is a general transcription factor that regulates the expression of most of the genome. Mutations in this gene are the primary cause for Rett Syndrome, which is characterized by severe developmental abnormalities, motor defects, and repetitive hand movements. Up to 80% of the patients have seizures (Jian et al, 2006). Syngap1 is a ras GTPase-activating protein that localizes to the PSD. It has been shown to play a role in regulating NMDA plasticity and the insertion of AMPA receptors. Mutations in this gene cause intellectual disability (Hamden et al, 2009; Kim et al, 1998). Thus, the different critical windows for these two ASD candidate genes demonstrate the striking mechanistic heterogeneity in autism, and underscore the importance of investigating the pathways involved in multiple key players in the disease. It is important to note that due to the syndromic burden of MECP2 and Syngap1, studies on these two genes did not characterize behavioral phenotypes that are specific to autism such as social interaction, and how adult gene therapy could impact them.

Using a novel transgenic strategy, we investigated the critical window of Shank3. Our study showed that the adult restoration of Shank3 expression selectively rescues the autistic-like phenotypes social interaction and stereotyped behavior, but have no impact on anxiety and motor deficits. This is a different result from both the MECP2 and the Syngap1 studies, highlighting the unique mechanisms of the master scaffolding PSD protein. This selective behavioral rescue suggests that different neural networks may underlie the behaviors tested. It is possible that specific cell types or brain regions have varying degrees of plasticity, thereby causing the contrasting behavioral results. It is also possible that the improvements and deficits are due to complex interactions between multiple brain regions.

Our results also demonstrated that early postnatal intervention is more effective in reversing the disease phenotypes. P21 re-expression improved the rotarod deficits and some anxiety measurements including the zero maze. P10 re-expression showed further improvement in anxiety as demonstrated by the open field results. These data indicate that Shank3 expression restoration during early postnatal development is the most effective in improving behavioral deficits. This is consistent with the mechanistic function of Shank3 in regulating synaptic function and structure. Many previous studies show that the peak of endogenous Shank3 protein expression coincides with the peak of synaptogenesis (Wang et al, 2014). It is possible that early restoration of Shank3 facilitates the proper formation of synaptic function across all brain regions to enable healthy behavioral development.

CHAPTER 4: ADULT SHANK3 RESTORATION RESCUES STRIATAL SYNAPTIC NETWORK AND NEUTROTRANSMISSION

I performed the tamoxifen feeding, biochemical purification, and western blots. Special thanks to Kasey Han for assisting with the western blots. Patricia Monteiro, Yang Zhou, Jin-Ah Kim, and Zhanyan Fu performed the electrophysiology.

Shank3 in Synapse Formation and Function

Shank3 is a master scaffolding protein in the postsynaptic density in the excitatory synapse, critical in the regulation of synaptic transmission and structure. Through its multidomain structure, Shank3 recruits and interacts with many neurotransmitter receptors including NMDA receptors, AMPA receptors, mGLURs, and L-type calcium channels. It also binds with a host of actin cytoskeleton regulating proteins such as Bpix and Cortactin (Chua et al, 2012). Due to its vast wide-ranging protein network, Shank3 mediates synaptic responses to external stimuli and propagates changes in the cytoskeletal structure in synaptic morphology.

Previous studies have shown that Shank3 expression is abundant throughout the brain and multiple organs outside of the central nervous system including the heart, lungs, and kidney. In the brain, it is most highly expressed in the striatum (Peca et al, 2011). In situ studies showed that Shank3 protein expression peaks around P21 in the rodent cortex, coinciding with the peak of synaptogenesis, suggesting a role for Shank3 in synapse formation. Subsequent in vitro studies showed that deletion of Shank3 leads to alterations in the dendritic spine structure including changes in the length, thickness, and density of the spines. Biochemical analysis also demonstrated significant reductions in the concentrations of neurotransmitter receptors and scaffolding proteins in the PSD after Shank3 deletion. Functional characterizations consistently showed impairment in synaptic signaling and transmission. In comparison, overexpression studies of Shank3 established the ability of Shank3 to induce spine growth in culture. Ectopic expression of

Shank3 in aspiny cerebellar granule cells led to the formation of dendritic spines in vitro, leading to the recruitment of some synaptic proteins in these new structures.

In addition to evidence *in vitro*, mouse models of Shank3 mutations also demonstrate the critical role of Shank3 in proper synaptic development in vivo. In almost all of the reported Shank3 mutant mouse lines, the PSD protein network is significantly altered (Bozdogai et al, 2010; Yang et al, 2012; Wang et al, 2011; Peca et al, 2011; Schmeisser et al, 2012). In the Ankyrin domain-deletion models, decreased concentrations of GluA1, NR2A, Homer1b/c, and SAPAP were identified. When the PDZ domain is targeted, similar reductions of NMDAR and AMPAR were shown along with other PSD proteins including PSD-93. In the SH3-domain model, NR2B and Shank2 concentrations were increased possibly due to compensation mechanisms (Schmeisser et al, 2012).

These biochemical perturbations led to functional deficits in synaptic transmission. In the Ankyrin-domain models, varying degrees of excitatory transmission were reported including impaired AMPAR-mediated basal transmission, decrease in paired-pulse ratio, and reduced long-term potentiation (LTP) (Bozdagi et al, 2010; Yang et al, 2012). Wang et al, 2011 also reported similar reductions in LTP, although they did not detect alterations in the basal synaptic transmission (Wang et al, 2011).

Consistent with these protein and functional aberrations, synaptic structure was disrupted in vivo as well. Different spine labeling methods performed across multiple labs yielded similar results, indicating that Shank3 deletion reduces dendritic spine density. This result has been replicated in both the hippocampus and the striatum. All together, these in vivo and in vitro studies reliably demonstrate that Shank3 expression is critical for proper synaptic development and function across the brain.

Critical window for synapse restoration

A key question that our current study addresses is the role of Shank3 in the synapse after development. If an organism initially develops without Shank3 regulating its synaptic formation, would adult restoration of Shank3 be able to correct the synaptic deficits and restore proper neural transmission? Can post-developmental Shank3 expression rescue aberrant synaptic morphology?

A prevalent hypothesis in the field is that neural plasticity is limited in adulthood. In the 1920s, after painstaking observations of the brain, Ramon y Cajal declared. "Once development was ended, the fonts of growth and regeneration of the axons and dendrites dried up irrevocably. In the adult center the nerve paths are something fixed and immutable, nothing may be regenerated" (Ramon y Cajal, 1929). The seminal study by Hubel and Wiesel furthered this view by showing that in the cat visual cortex, early visual impairment is irreversible post development (Hubel and Wiesel, 1970). They used monocular deprivation during early development and adulthood in the animals. They

observed that while early monocular deprivation produced permanent synaptic alterations in the visual cortex, it had no effect in the adult brain. They determined a clearly defined critical window in the brain for visual development and provided strong evidence that neural plasticity is negligible in the mature brain.

However, in the last few decades, there emerged an accumulating body of evidence supporting some post-developmental neural malleability, challenging the notion that the brain is "set" during the early postnatal period. The first line of evidence stemmed from the breakthrough discovery of neurogenesis in the adult brain across multiple species. Initial characterizations of neurogenesis were completed in rodents and brids (Altman and Das, 1965; Goldman and Nottebom, 1983). Multiple labs then demonstrated that there are also actively dividing progenitor cells in the dentate gyrus in the adult human brain, which then mature into neurons (Eriksson et al, 1998). Additional studies showed that there is evidence of neurogenesis in the human striatum as well. Based on existing literature, adult neurogenesis appears to be experience-dependent, regulated by environmental stimuli (Gage, 2004). Another line of evidence supporting adult neural plasticity is from the studies demonstrating the remarkable ability of damaged axons to regenerate post-development. Since the pioneering work by Raisman, Bjorklund, and Aguayo and colleagues, many labs have reported the successful regrowth of damaged axons in the adult system. Collectively, these remarkable studies demonstrate the continued presence of synaptic growth and remodeling in the adult brain, putting forth the possibility of neural restoration in the adult Shank3 mutant model.

Results

Previous reports indicated that *Shank3* deletion *in vivo* significantly decreases the concentration of multiple PSD scaffold proteins and receptor subunits (Peca et al, 2011). However, it is unknown whether re-expressing *Shank3* after development can rescue the recruitment of various proteins to the synapse and improve synaptic transmission. Because SHANK3 is the only SHANK protein family member highly enriched in the striatum, a region strongly implicated in certain behaviors associated with autism (Peca et al, 2011; Rothwell et al, 2014), mechanistic characterizations were primarily carried out on striatal neurons.

Consistent with our previous findings, we found that the synaptic concentrations of scaffold proteins SAPAP3 and Homer1b/c and glutamate receptor subunits NR2A, NR2B and GluA2 are significantly reduced in striatal synaptosome preparations of KO mice. We found that in the tamoxifen rescue condition, the synaptic levels of these postsynaptic proteins are significantly increased compared to those in the KO, reaching the level of WT controls (Fig. 16). This molecular rescue at the synaptic level shows for the first time that restoring *Shank3* expression in the adult brain can efficiently recruit major scaffolding and signaling proteins to the synapse and assemble the PSD protein network even after the developmental period. We also probed for other postsynaptic proteins including PSD95, mGluR5, CaMKIIa, NR1, GluA1, SHANK1, and SHANK2, but we did not find any differences in these synaptic markers across genotypes (Fig. 16).

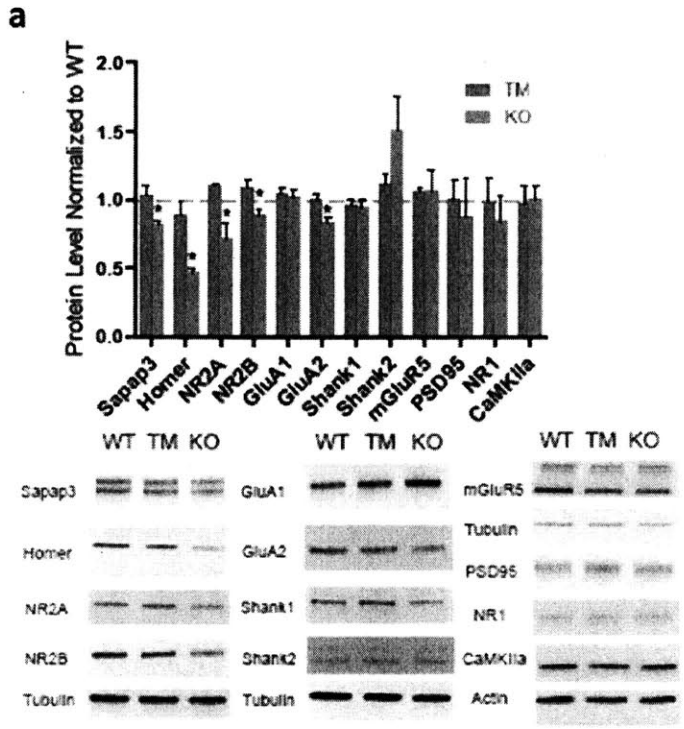

Figure 16. Adult rescue of PSD proteins in the striatum. Western blot analysis of synaptosomal fractions from striatal tissue after feeding scheme; PSD proteins are significantly increased in TM group compared to KO; No difference between the TM and WT controls; 10 μg of protein per lane with tubulin as loading control and normalized to wildtype levels. *P< 0.05, **P<0.01, ***P< 0.001; all data presented as means ± s.e.m. Student's two-tailed *t*-test for **c** (n=3 WT, n=4 TM, n=3 KO; each sample represents combined striatal tissue from 2 mice).

The encouraging synaptic molecular repair after adult *Shank3* expression prompted us to investigate whether there were parallel changes at the functional level. We prepared acute brain slices from tamoxifen treated adult mice and controls to simultaneously test their striatal physiology. As expected, $Shank3^{fx/fx}:CreER^{+/-}$ (KO) mice treated with corn oil show significantly reduced field population spikes. However, the reduced field responses in $Shank3^{fx/fx}:CreER^{+/-}$ mice treated with tamoxifen are rescued to WT levels (Fig. 17 A-B). We then performed whole-cell recordings and found that $Shank3^{fx/fx}:CreER^{+/-}$ (KO) mice treated with corn oil have reduced mEPSC frequency compared to WT mice ($Shank3^{+/+}:CreER^{+/-}$ treated with tamoxifen), similar to our previous findings in Shank3B KO mice (Peca et al, 2011). Interestingly, mEPSC frequency can be rescued in the tamoxifen condition ($Shank3^{fx/fx}:CreER^{+/-}$ [KO] treated with tamoxifen) compared to KO and WT groups (Fig. 17C).

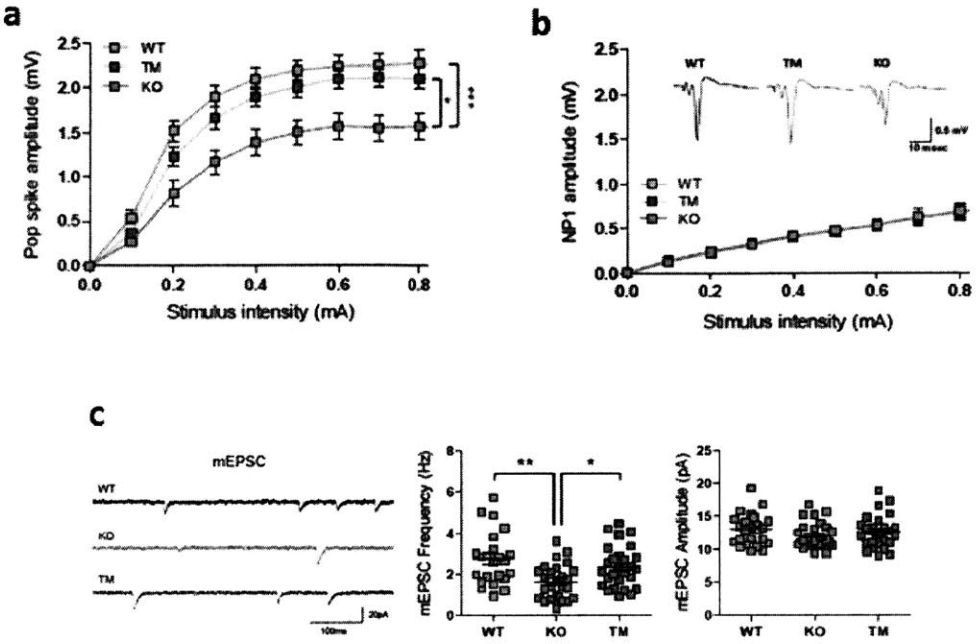

Figure 17. Adult rescue of striatal neurotransmission. a, Representative field traces for WT mice fed with tamoxifen and KO mice fed with tamoxifen (TM) or corn oil (KO). Indistinguishable relationship of stimulation intensity to the NP1 amplitude *per* group suggests unaltered presynaptic function. **b,** Rescued mEPSC frequency in the striatum in the TM compared to the KO. Representative mEPSC traces for WT, KO, and TM. *P< 0.05, **P<0.01, ***P< 0.001; all data presented as means ± s.e.m. Two-way repeated measures ANOVA, with Bonferroni post hoc test for **a** and **b** (n=12 slices from 4 WT, n=12 slices from 4 TM and n=12 slices from 4 KO mice). One-way ANOVA with Bonferroni post hoc test for c (n=23 cells for WT, n=26 cells for KO, and n=27 cells for TM).

We further measured evoked AMPAR/NMDAR ratio and paired-pulse ratio (PPR) in both parasagittal (primarily cortico-striatal) and coronal (mixed cortico-striatal and thalamo-striatal) sections using both differential voltage clamping and pharmacological isolation approaches. We found no differences between WT and KO groups (Fig. 18,19), consistent with our previous report (Peca et al, 2011). In addition, pharmacologically isolated NR2B/NMDA ratio also showed no differences across genotypes (Fig. 18C). Overall, these results suggest that a primary defect of striatal physiology in KO mice is the reduced mEPSC frequency, and this defect can be improved by restoring Shank3 expression in adulthood.

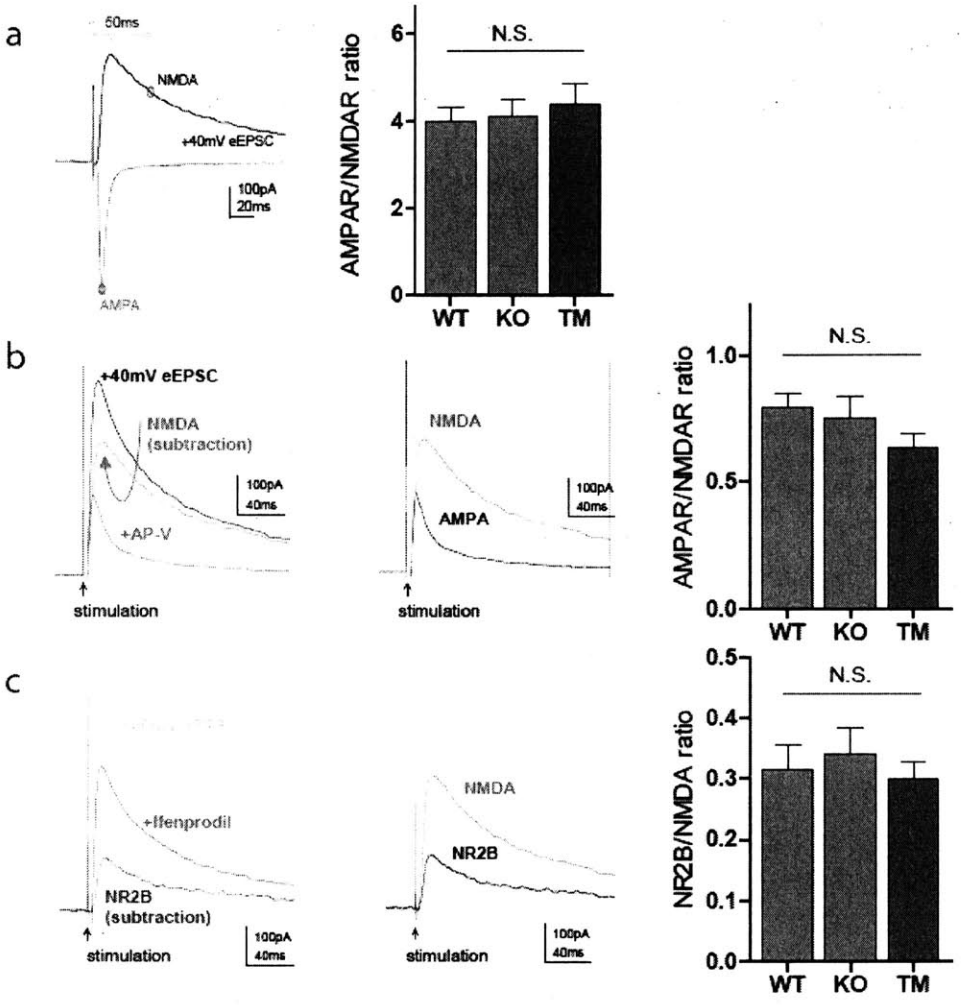

Figure 18. Additional measurements of dorsal striatum synaptic function in tamoxifen rescue (TM)

a, Representative traces (left) and bar graph (right) for AMPAR/NMDAR ratio in WT, KO and TM groups (WT=30 MSNs, KO=33 MSNs, TM=33 MSNs). AMPAR/NMDAR ratio calculated as the ratio of the EPSC peak amplitude at −70mV (AMPAR EPSC) to the amplitude of the EPSC recorded at +40 mV, 50ms after afferent stimulation. **b**, Representative traces (left) and bar graph (right) for pharmacologically isolated AMPAR/NMDAR ratio (WT=20 MSNs, KO=20 MSNs, TM=23 MSNs). Dual-component evoked EPSC at +40mV recorded before and after APV bath application. **c**, Representative traces (left) and bar graph (right) for NR2B/NMDAR ratio in WT, KO and TM groups (WT=16 MSNs, KO=16 MSNs, TM=22 MSNs). Dual-component evoked EPSC at +40mV recorded before and after ifenprodil bath application. All data presented as means ±s.e.m.

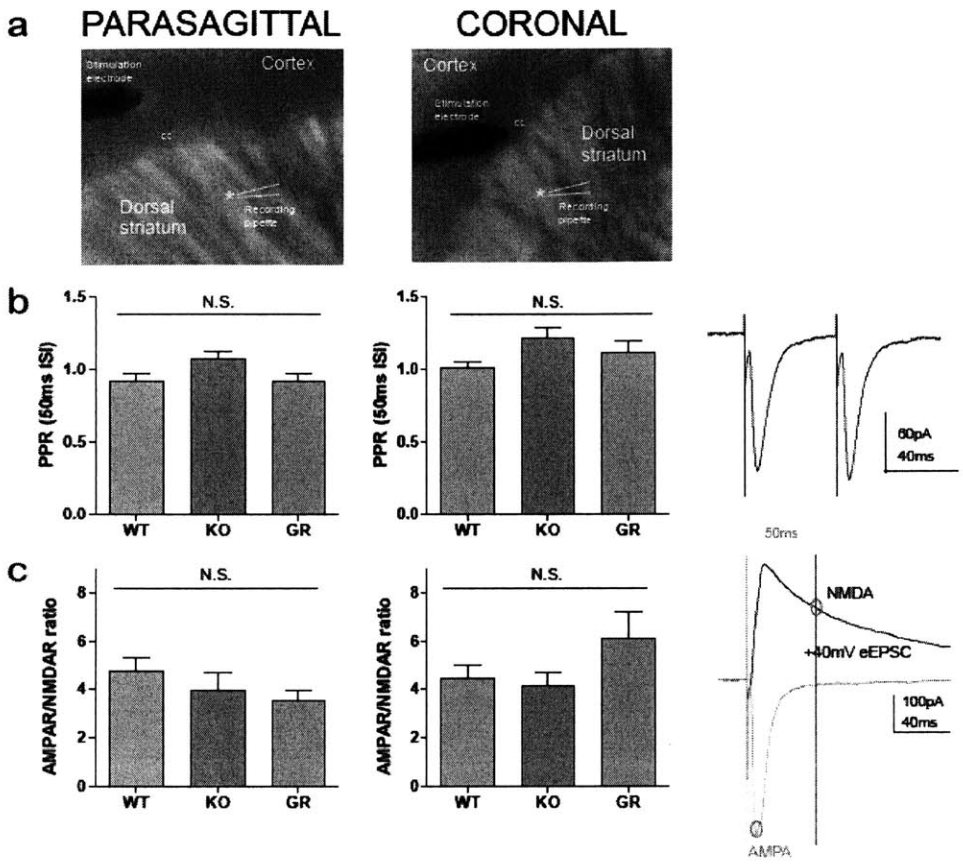

Figure 19. Additional measurements of synaptic function in dorsal striatum by cortical and *corpus callosum* (cc) evoked stimulation (parasagittal and coronal slices respectively)

a, IR-DIC images showing representative placement of the stimulation electrode in the cortex (left) or corpus callosum (right) to evoke EPSCs in dorsal striatum using parasagittal (left) and coronal slices (right). **b**, Representative traces (right) and summary bar graphs for paired-pulse ratios (PPR) of evoked EPSCs in dorsal striatum MSNs, showing similar magnitude in parasagittal (left bar graph) and coronal slices (right bar graph). No differences were found between genotypes . **c**, Representative traces (right) and summary bar graphs of AMPAR/NMDAR ratios evoked in parasagittal (left bar graph) and coronal slices (right bar graph) from all 3 genotypes (WT, KO, GR). AMPAR/NMDAR ratio calculated as the ratio of the EPSC peak amplitude at −70 mV (AMPAR EPSC) to theamplitude of the EPSC recorded at +40 mV, 50ms after afferent stimulation (panel c, right side). All data presented as means ±s.e.m.

Currently, the neurobiological mechanisms of social deficits of ASD are not well understood. Given that ventral striatum has been associated with social interaction (Dolen et al, 2013), we measured miniature excitatory synaptic transmission (Fig 20A), AMPAR/NMDAR ratio (Fig 20B), and PPR (Fig 20C) in ventral striatum/nucleus accumbens. However, we did not observe any basic synaptic transmission differences across genotypes (Fig. 20).

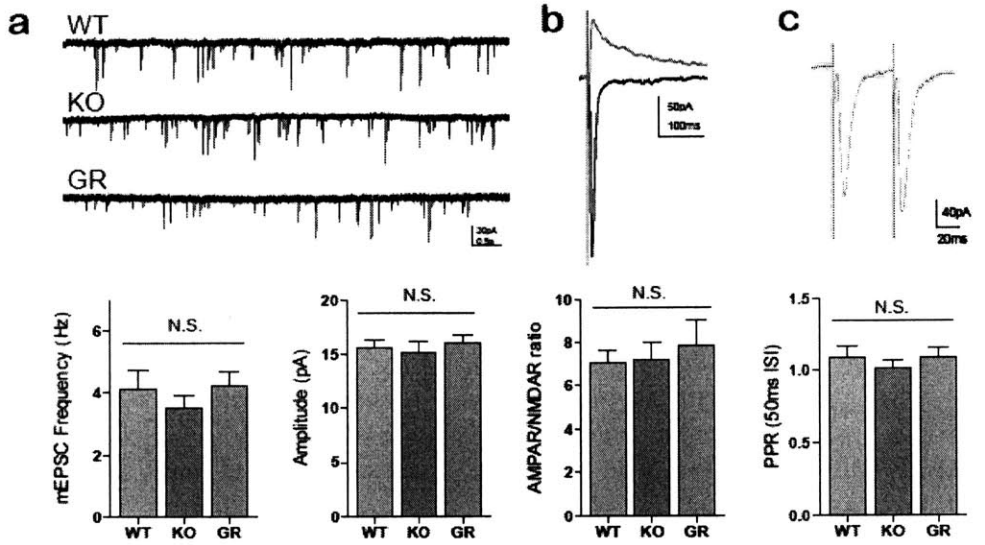

Figure 20. Whole-cell measurements of excitatory synaptic function in ventral striatum.

a, Representative traces (top) and summary bar graphs (bottom) of mEPSCs in NAc-MSNs (WT=22, KO=16, GR=18 MSNs). **b,** Representative traces (top) and summary bar graph (bottom) of AMPAR/NMDAR ratio in NAc-MSNs. AMPAR/NMDAR ratio calculated as the ratio of the EPSC peak amplitude at −70 mV (AMPAR EPSC) to the amplitude of the EPSC recorded at +40 mV, 50ms after afferent stimulation (WT=19, KO=16, GR=15 MSNs). **c,** Representative traces (top) and summary bar graph (bottom) of paired-pulse ratios in NAc-MSNs (WT=25, KO=22, GR=19 MSNs). All data presented as means ±s.e.m.

Because the cortex and cerebellum have been linked to anxiety and motor coordination, we used biochemistry to assess postsynaptic protein composition in these brain regions (Gross et al, 2002; De Zeeuw and Ten and Brinke, 2015). In the cortex, Shank3 expression is restored to WT level in TM mice (Fig. S6A). However, we found no significant differences in other postsynaptic proteins between WT and KO mice except the upregulation of SHANK2 (Fig. 21B-C), which may compensate for the loss of SHANK3. Consistently, we did not find functional differences in mEPSC recorded from the prefrontal cortex (Fig. 22A-C). In the cerebellum, Shank3 expression is also restored to WT level in the TM mice (Fig. 23). However, we did not find significant differences in other postsynaptic proteins except a reduction of GluA1, which is rescued in TM mice (Fig. 23B-C). The circuit mechanisms of anxiety and motor coordination deficits in the Shank3 KO mice may involve other brain regions or could be the collective consequence of connectivity deficits across many brain regions.

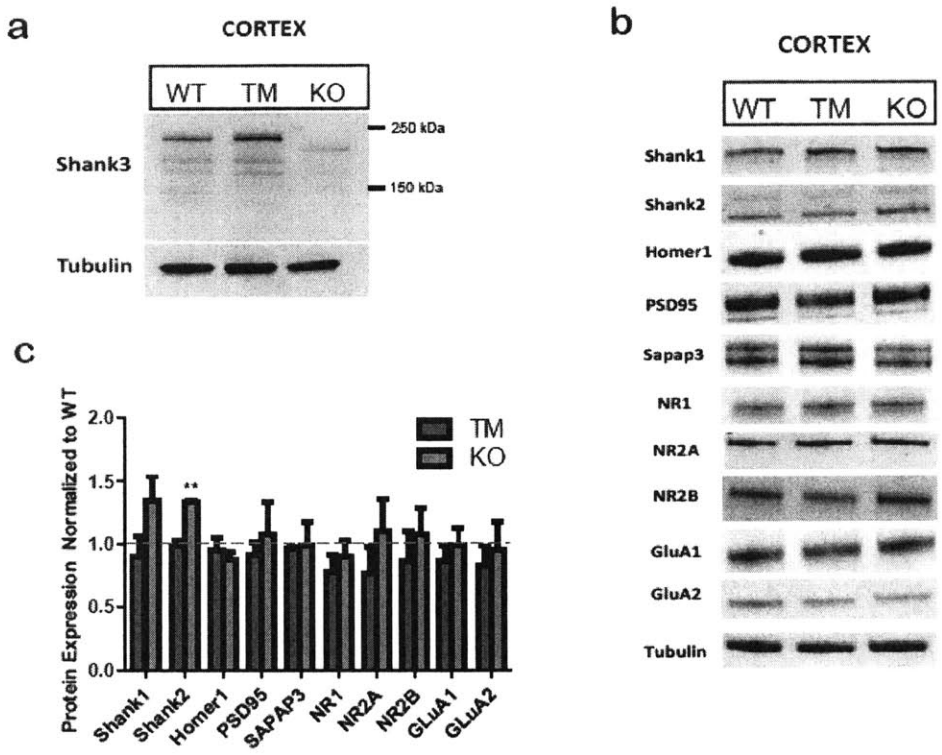

Figure 21. Western blots on synaptosome preparations in the cortex in the adult treated mice show minimal difference across genotypes. **a,** Repesentative western blot on Shank3 in the cortex in the adult treated tamoxifen mice, showing that most major Shank3 isoforms are restored in the TM mice. **b**, Representative western blots on synaptic proteins including scaffolding proteins and neurotransmitter receptors in the adult cortex across genotypes. **c**, Western blot quantification of multiple synaptic markers in the adult treated mice in the cortex. All data WT N=3, TM N=3, KO N=3; each sample is from tissue taken from two animals. All data presented as means±s.e.m.

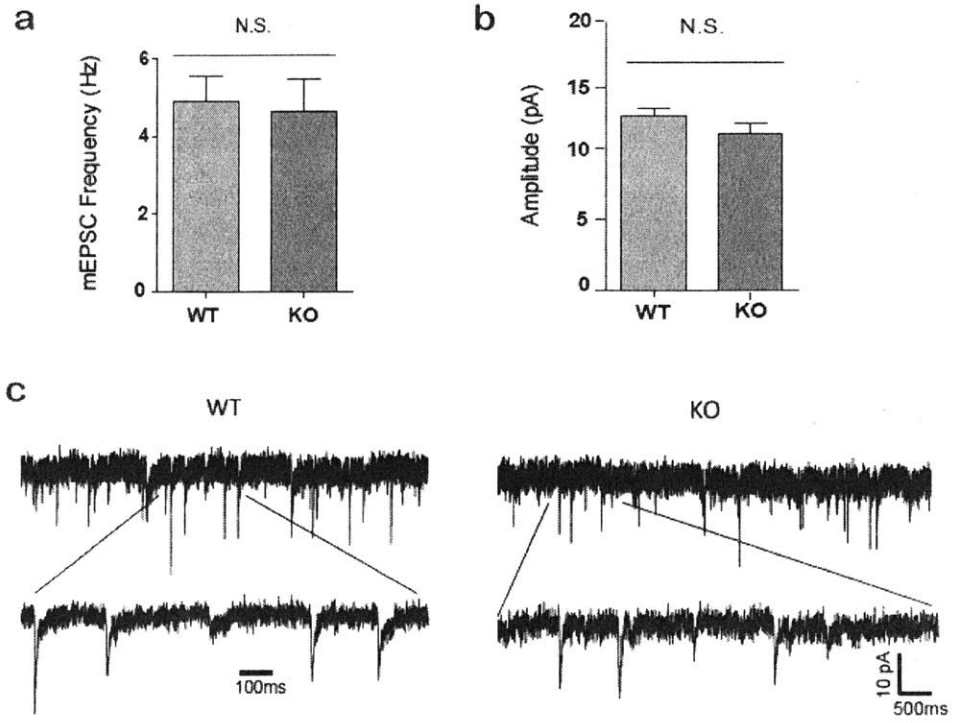

Figure 22. Whole-cell measurements of excitatory synaptic function in the cortex.

a, Summary bar graph of mEPSC frequency in the prefrontal cortex in the adult WT and KO. **b**, Summary bar graph of mEPSC amplitude in the prefrontal cortex in the adult WT and KO. **a,b,** WT N=13, KO N=10 cells; Student's unpaired t-test. All data presented as means ±s.e.m. **c**, Representative traces from mEPSC recordings in the WT and KO in the adult prefrontal cortex.

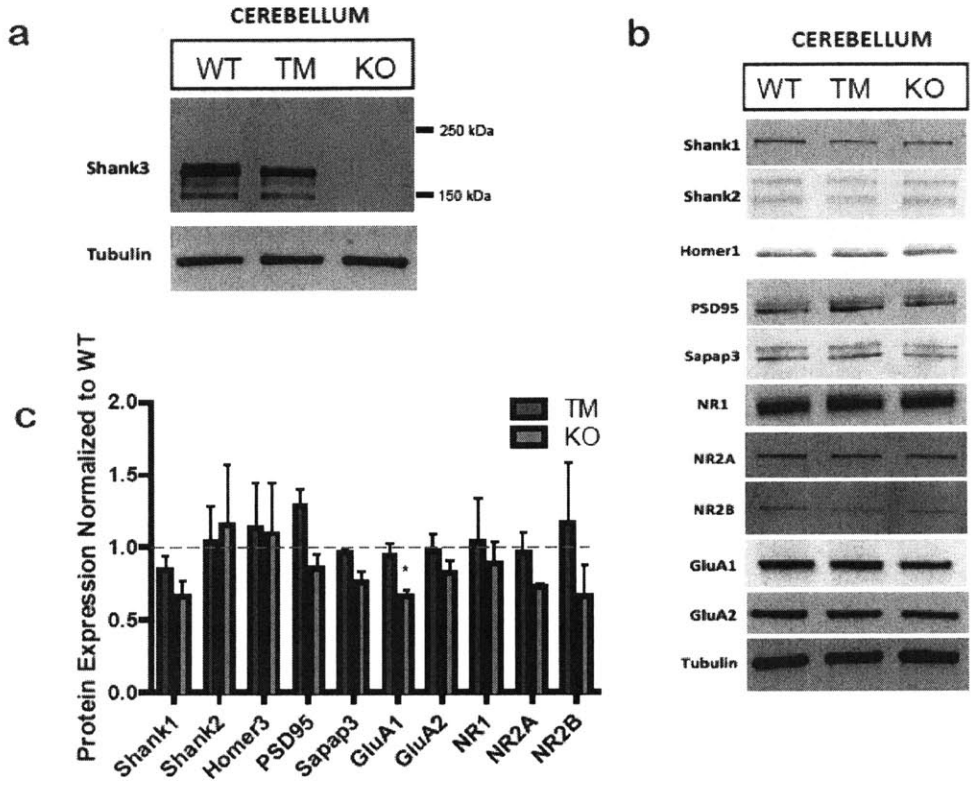

Figure 23. Western blots on synaptosome preparations in the cerebellum in the adult treated mice show minimal difference across genotypes.

a, Representative western blot on Shank3 in the cerebellum in the adult treated tamoxifen mice, showing that Shank3 isoforms are restored in the TM mice. **b**, Representative western blots on synaptic proteins including scaffolding proteins and neurotransmitter receptors in the adult cerebellum across genotpypes. **c**, Western blot quantification of multiple synaptic markers in the adult treated mice in the cerebellum. All data WT N=3, TM N=3, KO, N=3; each sample is from tissue taken from a single animal. All data presented as means ±s.e.m.

Discussion

In the current study, we showed for the first time that in the adult mouse brain, *Shank3* expression can alter the PSD protein composition and improve striatal neurotransmission. To our knowledge, this is the first demonstration of the ability of Shank3 to reconstruct the synaptic protein network in the adult brain. Our results indicate that Shank3 restoration can correctly recruit the key postsynaptic neurotransmitter receptors and scaffolding proteins to the PSD, enabling recovery in the synaptic transmission.

Because our biochemical characterizations are derived from large-tissue fractions, more fine-grained electrophysiological analysis was necessary to determine the impact of Shank3 at different levels of neural function. From our whole-cell recordings, we found that the frequency of mEPSC in the medium spiny neurons was significantly reduced in the KO and recovered in the TM. This together with the lack of difference in the PPR indicated that Shank3 affects primarily postsynaptic response with minimal impact on the presynaptic function. This is consistent with our previous study on the Shank3B mice and with the well-documented postsynaptic localization of Shank3. Interestingly, we found no difference in the AMPA/NMDA ratio across the genotypes. It is possible that due to the biochemical reductions in both AMPA and NMDA receptors in the PSD, the ratio remains unchanged. Together, these results indicate that the primary function of Shank3 is in the postsynaptic glutamatergic neurotransmission, and that adult restoration of Shank3 is able to induce functional recovery.

An interesting question to address is the role of Shank3 in brain regions other than the striatum. We showed previously that Shank3 deletion causes many behavioral phenotypes including anxiety, motor deficits, social interaction, and repetitive behavior. Thus, it is highly likely that many other cell types and brain regions are regulated by Shank3 expression. In addition, the lack of behavioral rescue in anxiety and motor coordination indicate that there must be some regions regulated by Shank3 that are not plastic in the adult brain. However, even though we probed the regions most associated with these behaviors in literature including the cortex, nucleus accumbens, and cerebellum, we were not able to identify any circuits that were not improved after Shank3 expression. It is possible that the lack of specific behavioral rescue is due to complicated interactions between multiple brain regions, which are difficult to detect using current technologies. It is also likely that other brain regions that we did not analyze are responsible for the phenotypes. Further studies are necessary to elucidate these mechanisms.

CHAPTER 5: NOVEL VIRAL METHOD FOR NEURONAL SPARSE LABELING AND GENE THERAPY

I and Patricia Monteiro optimized the tail vein injection conditions and piloted the retro-orbital injections. I commercialized the memGFP virus for tracing, conducted tamoxifen feeding, and performed the behavioral experiments. Patricia Monteiro performed the tail-vein injections, electrophysiology, and cell quantification. Xian Gao performed the retro-orbital injections and spine counting. Patricia Monteiro, Xian Gao, and I completed the imaging. Qiangge Zhang designed the memGFP construct. Special thanks to Heather Zanewski for the sholl analysis. Special thanks to Will Stockton for assistance with the cell quantification. Special thanks to Kasey Han for assistance with spine counting. Special thanks to Shijing Feng for assistance with behavioral analysis.

Introduction:

Invented in 1873, the Golgi silver impregnation technique has remained one of the most frequently used methods for characterizing neuron morphology (Nicolls, 2001). Since then, other popular techniques for neuron labeling have developed including Lucifer Yellow filling, biocytin staining, and transgenic reporter animals. However, all of these methods are hampered by low throughput data collection, high labor intensity, low turnaround rate, and predisposition to neuronal damage. Here, we present a novel rapid, reliable, and high throughput tracing technique that enables systemic sparse labeling of neurons across the whole brain. Using a modified AAV9 viral vector, we demonstrate the ability of this virus to reliably target neurons in animals of multiple ages. In addition, we show that this technique provides optimal signal to noise ratio to facilitate reliable sholl analysis and dendritic spine characterization in multiple brain regions.

AAV Modifications for Neuronal Tracing

The wildtype Adeno-associated virus is a small parvovirus carrying a single-stranded deoxyribonucleic acid that is about 4.7 kb. The DNA can be either positive or negative ended, containing two inverted terminal repeat (ITR) sequences. A member of the Dependovirus genus, it requires the assistance of other helper viruses such as adenovirus or Herpes simplex virus to complete its life cycle. In the 1980s, recombinant AAVs (rAAVs) were produced by removing 96% of the viral genome, leaving only the ITRs and the encapsidation signal (Samulski et al, 1982; Hermonat and Muzyczka, 1984; McLaughlin et al, 1988; Bourdenx et al, 2014). Further optimizations in viral engineering

led to successful production of safe, non-replicative independent rAAVs that can reliably carry transgenes in vivo (Bourdenx et al, 2014).

The distinctive properties of rAAV render it a desirable tool for genetic engineering. Studies have shown that it mediates stable and efficient transduction of both dividing and non-dividing cells for a sustained period of time. Devoid of its viral genes, it typically resides as a nonintegrated episome in the nucleus, thus minimizing pathogenic interruption of the host genome. In non-dividing cells, it is known to persist throughout the life cycle of the cell, highlighting its longevity. Unlike many other viral vectors, rAAVs do not cause cytotoxicity. Wildtype AAVs are a common small virus that infects many species including humans. However, no disease has been reported to be associated with AAV infection, supporting the view that it is non-pathogenic (Weinberg et al, 2013). Lastly, about 12 different species of rAAVs have been produced through pseudotyping with either natural or engineered capsid serotypes, providing a wide spectrum of cell tropism. Several of the serotypes, notably serotype 9, show high infectivity in the central nervous system through systemic injection, demonstrating their ability to cross the blood brain barrier (Bourdenx et al, 2014).

Here we take advantage of the safe stable brain-tropism of AAV9 by tailoring its genome to facilitate neural tracing. Previous studies showed that the ability of systemic AAV9 to infect neurons is regulated by the age of the organism. These reports show that in the rodent, systemic injection of AAV9 in the neonatal brain results in widespread

neural infection whereas adult injection of AAV9 is limited to glia labeling (Faust et al, 2009; Chakrabarty et al, 2013). In our current study, we overcome this challenge by adopting the Syn1 promoter, which enables neuron-specific targeting. We demonstrate that AAV9 driven by Syn1 promoter efficiently and specifically transduces neurons across multiple ages including late adulthood. In addition, we modified the reporter transgene to optimize fluorescent signal to enable reliable characterization of dendritic branching and spine quantification. We also show that with high systemic viral dosages, the infection rate increases significantly throughout the brain and remains neuron-specific. Altogether, our results introduce a novel reliable high-throughput neural tracing technique, as well as new advancements in achieving more effective gene therapy.

Results:

To characterize the expression pattern of systemic virus in the brain, we injected diluted AAV9-hSyn1-GFP into the tail vein of adult mice. After three weeks, we perfused and immunostained for the GFP signal. We found that the virus efficiently crosses the blood brain barrier resulting in widespread viral infection in the brain, and that the signal was sparse enough to enable isolated morphology characterization (Figure 24). We costained for multiple markers to determine the cell types infected by the virus. We found that all virally labeled cells that were positive for GFP were also positive for NeuN. However, we found no colocalization of GFP and GFAP, indicating that the virus is neuron-specific and does not infect astrocytes. We also determined that some GFP positive cells were also positive for parvalbumin. This demonstrates the advantage of this

novel tracing technique to provide cell-type information, which is not provided by other existing tracing methods (Figure 25).

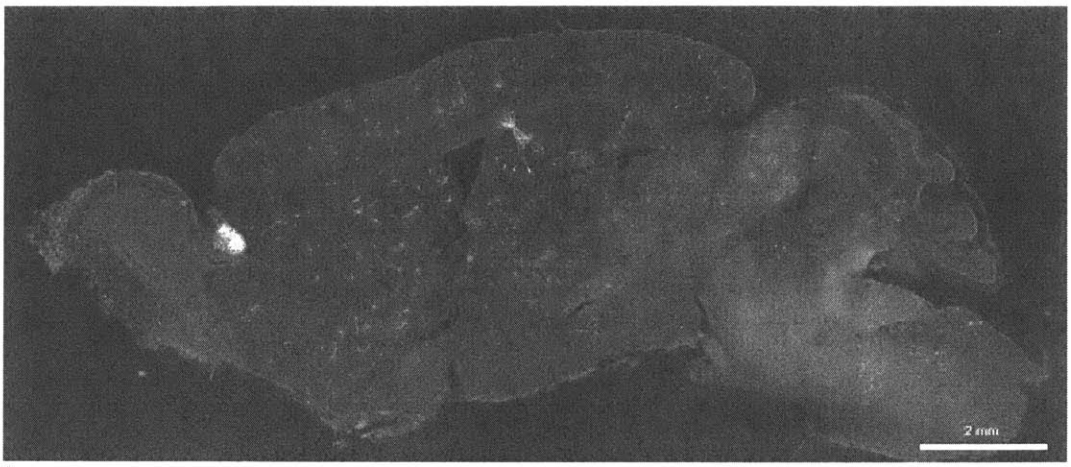

Figure 24. Systemic viral delivery in adult mice achieves brain-wide sparse labeling. Sagittal section showing neuronal infection after systemic delivery of a small amount of GFP virus through tail-vein injection.

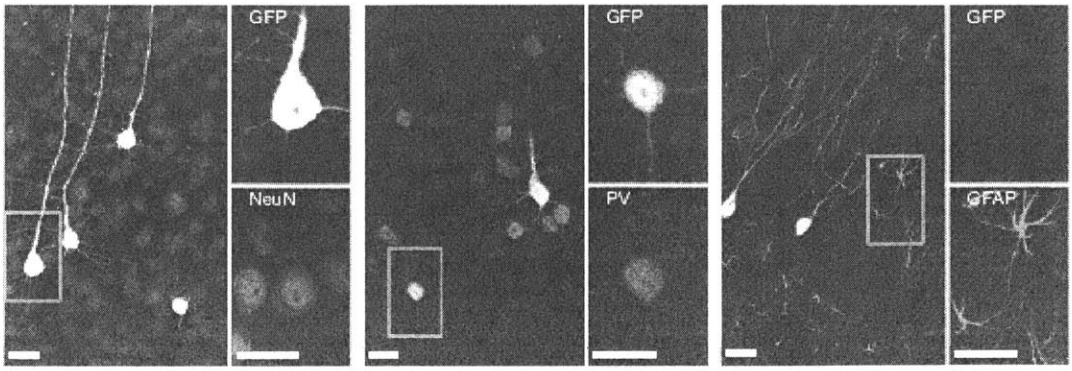

Figure 25. Systemic AAV9 labels different neuronal populations. Representative images from cortex and dentate gyrus showing GFP expression in neuronal populations (scale bars=20μm).

Using the low viral titre, we injected the virus systemically to study the dendritic branching in WT, KO, and TM conditions of the Shank3 knock-in line. Three weeks after injection, we perfused the animals and used antibody enhancement. In a blinded manner, we completed the sholl analysis in the dorsolateral striatum, consistent with our previous mechanistic studies. We found that the low-titre enabled labeling sparse enough for individual cell characterization with minimal branching overlap across cells. Our quantification showed that there was no difference in dendritic branching between the genotypes. Because the raw values were similar to those of medium spiny neurons reported in literature, the results indicate that the precision of this viral technique is comparable to that of traditional tracing methods (Figure 26).

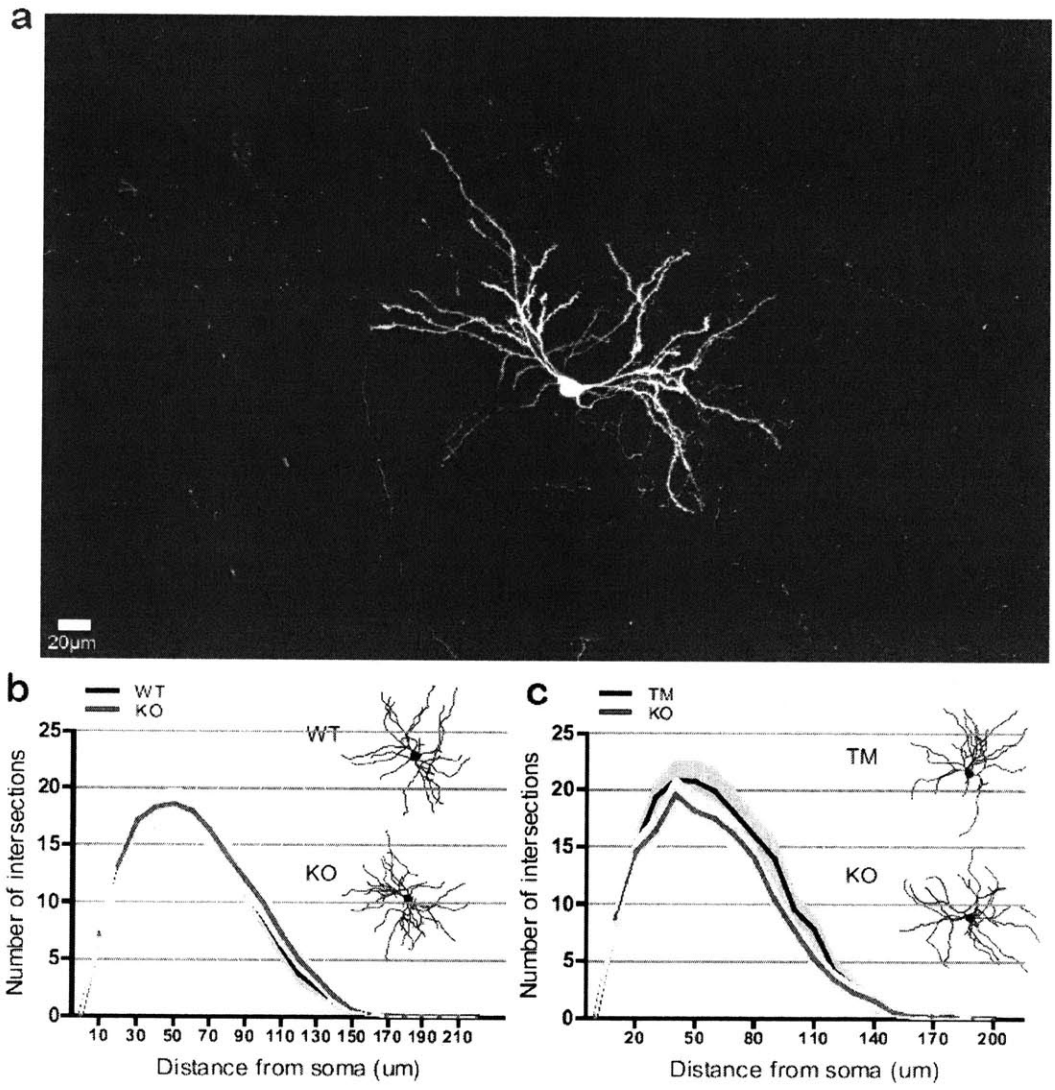

Figure 26. Sholl analysis of MSNs in dorsolateral striatum of WT, KO, and TM mice. a, single MSN expressing membrane-targeted GFP after tail-vein injection (diluted virus) allows for sparse labeling of cels and visualization of tis detailed neuronal processes. This technique allows co-staining, offering an advantage over the classical Golgi staining technique. **b**, Sholl analysis does not reveal obvious morpholiglca differences between WT (black) and KO mice (red); insets show examples of neurons (top: TM; ottom: KO). Two-way repeated measures ANOVA for a and b (for a n=21 from 2 WT and n=23 from 2 KO; for b n=12 from 3 TM and n=12 from 3 KO.

Previous *in vitro* and i*n vivo* studies have shown that *Shank3* manipulation can lead to significant changes in the total spine density (Sala et al, 2001; Roussignol et al, Roussignol et al, 2005; Peca et al, 2011). It is, however, unclear whether post-developmental *Shank3* expression can also affect spine structure. To address this, we used systemic viral injection to sparsely label neurons with GFP in the WT, KO, and TM mice after treatment. We imaged and analyzed the dendritic spines in the dorsal striatum from all three conditions. Similar to our previous report on *Shank3B* KO mice, we observed a significant reduction of MSN spine density in the dorsal striatum of KO mice compared to WT mice. Surprisingly, the total spine density was significantly increased in the TM treated mice compared to the KO mice (Fig 27). To our knowledge, this is the first indication that the ability of *Shank3* to promote spine formation or maintenance is not restricted to any developmental critical period, highlighting the continued structural plasticity in the adult striatum. Interestingly, the spine density in the TM condition is significantly higher than that of the WT. One possibility for this phenomenon is that adult *Shank3* expression induces dendritic spines that may not be pruned and regulated by the same processes that occur in development. Furthermore, these results demonstrate that this novel viral method is sensitive enough for dendritic spine quantification.

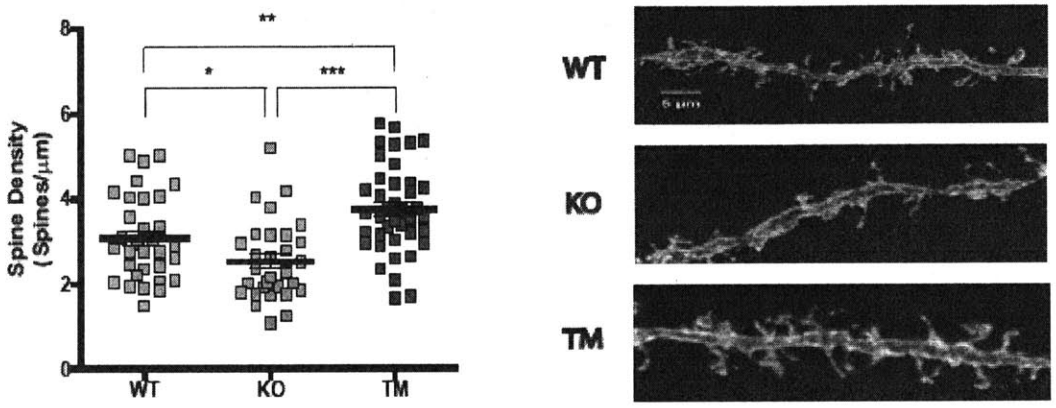

Figure 27. Adult restoration of Shank3 expression increases dendritic spine density in the striatum. a) Quantification of dendritic spine density. Increased spine density in the TM compared to the KO, while spine density in the KO is lower than that of the WT. b) Representative confocal images of dendritic spines from WT, KO, and TM. *P< 0.05, **P<0.01, ***P< 0.001; all data presented as means ± s.e.m. One-Way ANOVA, Newman-Keuls Multiple Comparison test (n=32 dendritic segments for WT, n=30 for KO, and n=40 for TM).

Systemic viral delivery rescues grooming

Because Shank3 is a key scaffold protein expressed widely thorough the brain, its mutation or deletion would affect many complicated pathways and circuits. Thus, it is likely that the most promising route of treatment for human patients is gene therapy, which would enable the correct expression of the causal gene and restore the deficient pathways and circuits. Due to our encouraging findings that adult expression of Shank3 can improve selective autistic-like phenotypes, we aimed to determine if a translational rescue strategy can yield similar results.

To achieve brain-wide adult expression of Shank3, we tested some conditions to determine the optimal injection protocol for high infection rate. We compared the efficiency of single injection versus two weekly injections. We found that surprisingly, the two weekly injections led to decreased infection rate relative to the single injection. This could be due to the development of antibodies in between the viral delivery that would then neutralize the virus (Figure 28).

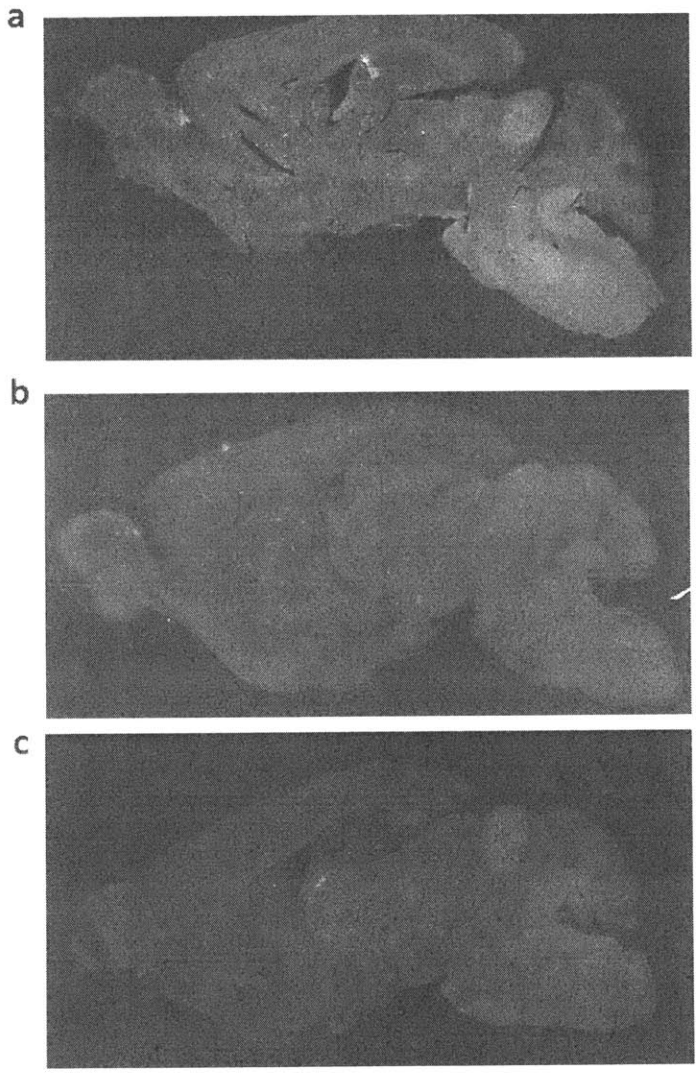

Figure 28. Single injection of AAV9 achieves more efficiency than double injections. **a**, Representative sagittal section showing single injection of AAV9-hSyn1-GFP. **b**, Representative sagittal section showing the same viral titre delivered with two injections separated by a week. **c**, Representative sagittal section shwoing AAV9-hSyn1-GFP-Cre virus delivered through single injection.

Using single injections, we systemically injected AAV9-hSyn1-GFP-Cre through the tail vein in Shank3$^{fx/fx}$ (KO) mice aged 2-4.5 months. As age-matched controls, we injected AAV9-hSyn-GFP-Cre into Shank3$^{+/+}$ (WT) and AAV9-hSyn1-GFP into Shank3$^{fx/fx}$ (KO). Neuronal infection in the cortex and basal ganglia (regions putatively associated with anxiety, social interaction, and stereotyped behavior), were quantified as percentage of GFP^{+} cells per NeuN^{+} cells. The neuron-specific expression pattern shows that with this strategy it is possible to cross the adult blood brain barrier (BBB) and lead to robust transgene expression in several neuron populations throughout the brain (Figure 29).

a

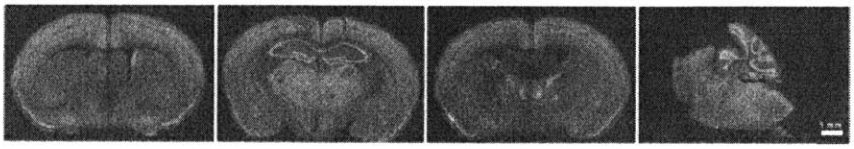

b

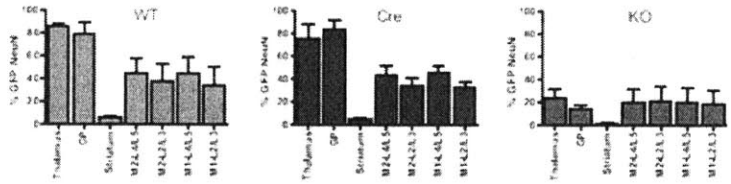

Figure 29. High titre systemic injection leads to increased neuronal labeling across brain regions a, Systemic injection of higher titer virus leads to broad neuronal infection and robust cre-GFP expression; this strategy was used to systemically provide cre in adult mice and test for possible rescued phenotypes. **b**, quantification of neuronal infection in the motor cortex, thalamus, striatum, and GP of tail-vein injected mice (expressed as percentage of GFP+ cells per NeuN+ cells).

Six weeks post viral injection, we performed a battery of behavioral assays and electrophysiological recordings. The results showed that stereotyped grooming can be significantly rescued with this strategy (Figure 30). While 4 out of 11 Shank3$^{fx/fx}$ injected with AAV9-hSyn-GFP developed lesions, 0 out of 11 Shank3$^{fx/fx}$ injected with AAV9-hSyn-GFP-Cre showed lesions. In addition, we found that consistent with our tamoxifen treatment, systemic viral injection did not rescue anxiety or motor coordination (Figure 30). Results from the three-chamber assay showed that while there is a trend for improvement in social interaction in both duration and frequency, the effect is not statistically significant (Figure 30). A minor trend was also observed for striatal field recordings without reaching any statistical significance (Figure 31). These results are likely due to the much fewer number of cells infected by the systemic virus compared to the number of cells targeted in the global CreER mouse line used in the tamoxifen rescue strategy. Further optimization of the efficiency of viral transduction of neurons may greatly improve the effectiveness of the treatment. We used retro-orbital injection to deliver the AAV9-hSyn1-Cre-GFP virus at P10 and observed increased infection rate (Figure 32). This suggests that viral delivery earlier in development may provide more widespread viral rescue. Overall, this viral approach highlights the exciting potential for ameliorating autistic-like phenotypes through systemic delivery of Shank3-based gene therapy.

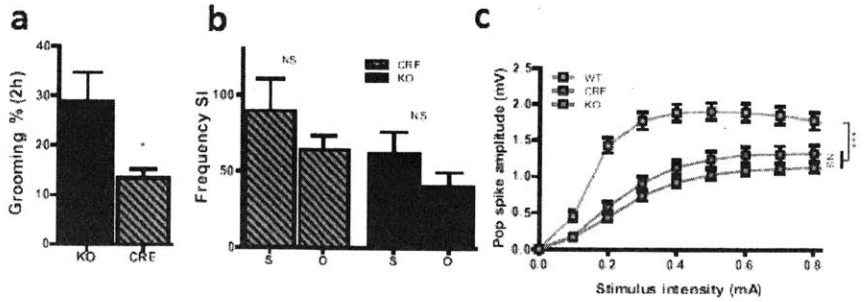

Figure 30. High-titre systemic viral injection rescues grooming, but not striatal neurotransmission. a , KO cre-injected mice spend significantly less time grooming compared to control KO GFP-injected mice. **b**, KO cre-injected mice show a trend for social preference that does not reach statistical significance; KO GFP-injected mice also show no social preference. **c**, Reduced striatal field responses in KO mice injected with cre-GFP and GFP compared to controls. *P<0.05, **P<0.01, ***P<0.0001; two-tailed *t*-test for c and d. (n=11 KO and n=10 Cre mice); two-way repeated measures ANOVA, with Bonferroni *post hoc* test for f; all data data presented as means ± s.e.m. Field recordings n=24 slices from 8 mice per group.

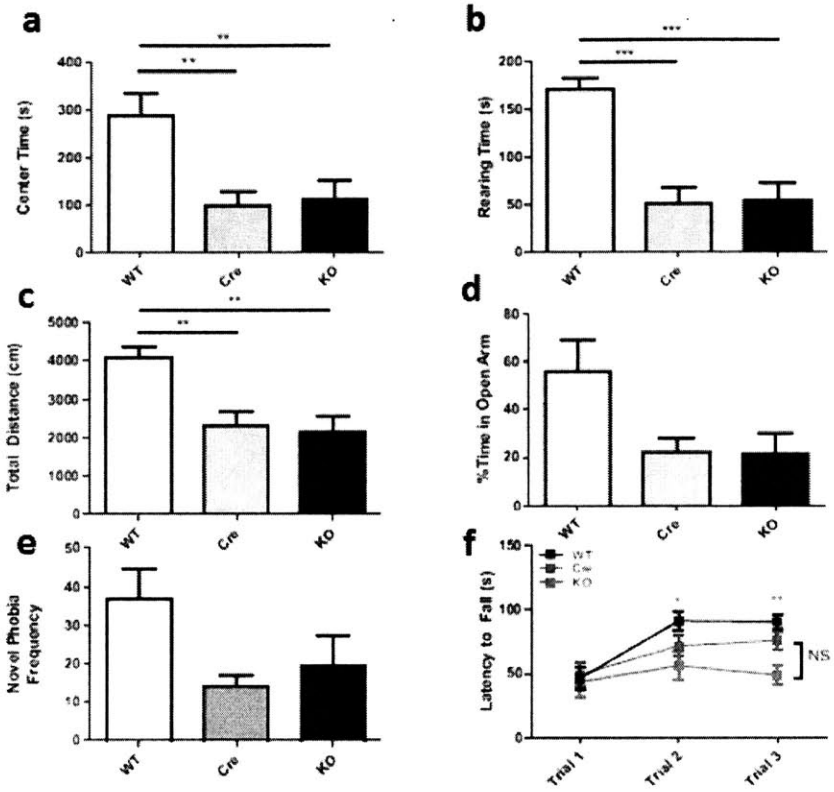

Figure 31. Adult AAV9 systemic delivery and resultant mice behavior. a,b, Open field results show that tail-vein injection does not rescue anxiety in adult Shank3$^{fx/fx}$ mice. **c,** Locomotion in the open field is also not rescued. **d,** Results from the elevated zero maze confirm that anxiety is not rescued. **e,** Tail-vein injection cannot rescue the fear of novel objects in the Shank3$^{Fx/Fx}$. **f,** Motor coordination is also not rescued as is indicated by the latency to fall during rotarod. One-way ANOVA with Bonferroni post hoc tests for **a-e**. Two-way repeated measures ANOVA with post hoc tests for **f**. *P<0.05, **P<0.01, ***P<0.0001; data for all panels are presented as means ± s.e.m.; n=11 per group for **b to d**. n=8 for WT, n=7 for KO, n=8 for Cre for **e**. n=8 for WT, n=9 for KO, n=8 for **e**. n=10 for WT, n=11 for KO, and n=10 for Cre for **f**.

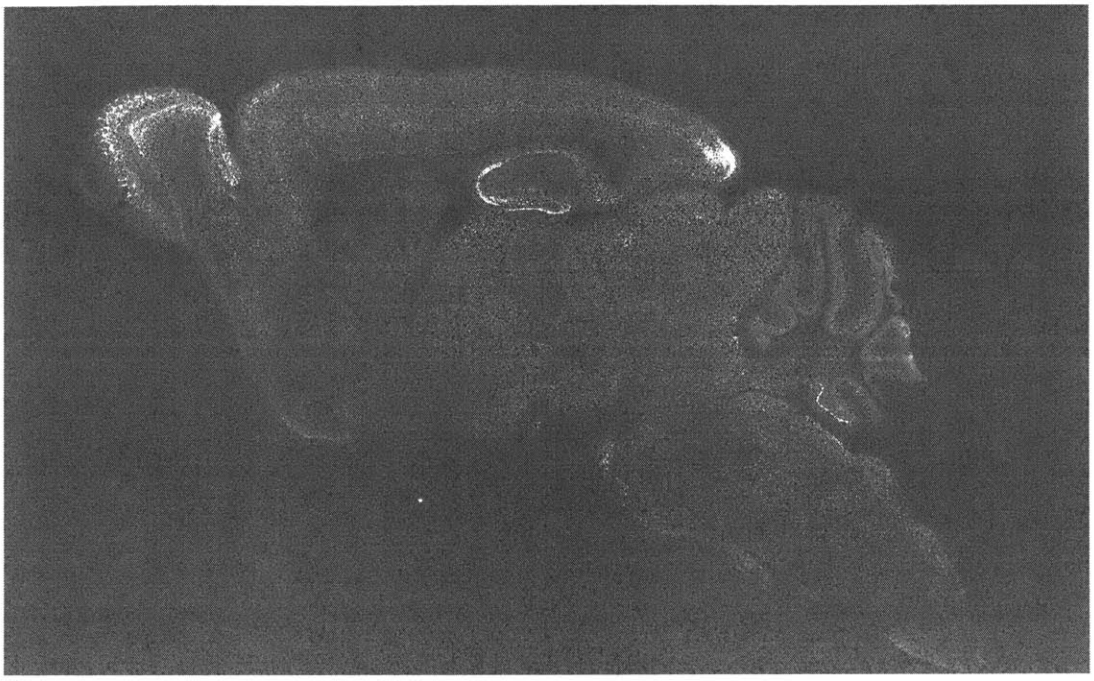

Figure 32. AAV9 systemic delivery at P10 achieves high efficiency. Representative sagittal section showing the result of AAV9-hSyn1-GFP-Cre delivery at P10 through the retroorbital route. The virus labels the infected nucleus with GFP, demonstrating the remarkable infection efficiency at P10.

Discussion

In the current study, we present a novel reliable and efficient method for studying neuronal morphology. Understanding how neuronal and synaptic structures alter in response to environmental stimuli and genetic manipulations is key to advancing our knowledge of neuronal mechanisms. By tailoring the genome of the AAV9 viral vector and optimizing injection conditions, we show that it can be used to trace dendritic branching and quantify spine density across multiple ages of the organism. Because the systemic sparse labeling is brain-wide, the technique can be used to simultaneously characterize multiple cell types in multiple brain regions. In addition, the short experimental window and the non-invasiveness of the injection render it an ideal tool for characterizing neuronal structures in high-throughput studies.

We also demonstrate that systemic injections of high viral titre can infect a substantial proportion of neurons across the brain. To our knowledge, the neuronal infectivity shown here in the adult brain is significantly higher than previously reported for AAV-mediated gene delivery methods. The high post-developmental neuronal targeting could be due to the combination of different promoters, route of injection, and viral preparation. Additional studies are necessary to elucidate the mechanisms of viral infectivity and further optimize the delivery efficiency. Overall, our results show that systemic AAV9 provides a powerful tool for understanding basic neuronal properties and provide a promising avenue for effective gene therapy.

Chapter 6: Conclusions, Limitations, and Future Directions

Possible Limitations and Alternative Approaches:

Truncated Protein Isoform

Through biochemistry, I have shown that in the Fx/Fx mice, a truncated form of the full-length Shank3 alpha isoform remains. To determine the components of this truncated isoform, I purified RNA from the brain tissue from these Fx/Fx mice and used a series of PCR that amplified from different exons of Shank3. I found that I was able to reliably obtain PCR products from primers targeting all of the exons except for exons 13-16, the exons that comprise the PDZ domain. This showed that the truncated isoform does not contain the PDZ domain. The molecular weight of the truncated isoform on the western blot also matches the predicted size of the full-length alpha isoform of Shank3 missing the PDZ domain, further supporting this conclusion. Altogether, the evidence suggest that in the Fx/Fx allele, due to the presence of the fLEx cassestte flanking the inverted PDZ domain, transcription of the Shank3 alpha isoform continues until it reaches the PDZ domain, where it skips over the domain, and re-starts from the Proline-Rich domain and completes after the SAM domain.

This truncated isoform is not detected in the WT striatal tissue, indicating that it is not a protein form that is normally expressed in the striatum. It is therefore possible that this new isoform harbors different properties from a Shank3 null. Biochemical data from differential biochemical fractionation show that it is present in the whole cell lysate fraction, the synaptosome fraction, and the purified postsynaptic density fraction. Because this truncated isoform shows a similar intracellular expression profile as the WT Shank3 isoforms, it is possible that this truncated form functions as a dominant negative or a gain of function mutant. More detailed

experiments and analysis would be necessary to determine how this truncated isoform differs from the null condition.

One possible set of experiments to address these questions could be done by culturing neurons from the Fx/Fx mice and using RNAi manipulation. One could compare the effect on the cells (i.e. dendritic spine morphology and neurotransmission) before and after knocking down the truncated isoform to produce the null condition. If the defects in cell morphology and neurotransmission are worsened in the null compared to the Fx/Fx, this would suggest that the mutant protein still harbors some Shank3 function and is most likely not a dominant negative form. However, if the results are not different in the mutant condition compared to the null condition, the conclusion would be unclear. It is possible that both the dominant negative and null conditions produce a floor effect.

An alternative approach to determine whether the mutant protein is a dominant negative is to characterize the heterozygote conditions. One could compare the defects in the heterozygote truncated protein condition (which would contain one WT Shank3 allele and one Fx/Fx allele) with the defects in the heterozygote null (which would contain one WT Shank3 allele and one null allele). If the Fx/Fx mutant is a dominant negative, one would expect the heterozygote Fx/Fx condition to display more severe phenotypes compared to the heterozygote null condition. Our lab has previously demonstrated that a single point mutation in the Proline-Rich domain in the Shank3 gene leads to the Shank3 protein null condition (Zhou et al, 2015). Thus, one could use the brain tissue from the heterozygotes from this Shank3 null line and compare them with the heterozygote tissue from the Fx/Fx line for this experimental approach.

Another possibility is that the truncated protein isoform is a gain-of-function mutant. It could either serve new functions or have enhanced protein activity. Based on our data on reduced

protein recruitment to the PSD, decreased dendritic spine density, and reduced excitatory neurotransmission in the Fx/Fx mice, it does not seem likely that there is enhanced Shank3 activity due to the Fx/Fx mutation. However, it is possible that the mutant truncated protein isoform has new biological functions compared to the WT Shank3 protein. To address this, one would have to conduct much more comprehensive characterizations in the Fx/Fx line. For example, one could use biochemistry to determine the effect on additional protein pathways, conduct sholl analysis and cell body measurements, perform a much more thorough battery of electrophysiology. Conducting much more complete characterizations of the Fx/Fx neuronal morphology, protein network, and function and comparing these parameters with both WT and null conditions would provide more information on whether or not there are new functions served by the truncated protein allele.

Due to our incomplete understanding of the exact nature of the function of the truncated protein isoform, a major caveat of our study is the potentially different mechanisms that may be involved in human patients with Shank3 mutations. Our genetic manipulation of the PDZ domain in the Fx/Fx mouse line is artificial and is highly unlikely to be found naturally in human patients. Even though some Shank3 mutations have been identified in the PDZ domain in human patients, it is unclear whether these human mutations would also produce this truncated alpha isoform. It is possible that if the human mutation disrupts splicing immediately before the PDZ domain that it may also lead to the same truncated protein mutant. However, due to the scarcity and technical challenges of human brain tissue analysis, we currently do not have direct biochemical evidence. To gain a comprehensive understanding of the relationship of each human mutation with the Shank3 protein isoform profile, one could take fibroblasts from each patient and use inducible pluripotent stem cell technology to convert the cells into neurons and then use western blot to

analyze Shank3 expression. Another approach is to take each human mutation and model them in transgenic animals to determine the impact of the mutation on the expression.

In the absence of evidence showing that this truncated protein isoform is expressed in human patients, it is possible that the mechanisms characterized in the Fx/Fx mice and TM rescue mice may differ from the mechanisms in human Shank3 patients. Thus, in addition to the usual limitations of extrapolating from mouse studies to humans, the presence of the truncated isoform in our Fx/Fx adds another layer of complication.

When I generated the Fx/Fx mice in 2011-2012, many aspects of the Shank3 gene structure and expression regulation had not yet been uncovered. In recent years, multiple studies from several labs reported new discoveries regarding the expression profile of some human mutations and the locations of intragenic promoters (Speed et al, 2015; Zhou et al, 2015; Wang et al, 2014; Jiang and Ehlers, 2013). Based on the newly available information, one could generate a Shank3 CKI mouse that is based on well-studied human point mutations using the fLEx cassette similar to the approach reported by Speed et al, 2015. Another strategy is to use the fLEx cassette to flank the entire Shank3 gene now that we have a more comprehensive understanding of the regulatory elements of Shank3. These alternative approaches would avoid the generation of artificial protein isoforms and more closely mimic the human pathology.

Nature of the New Synapses

One of the most intriguing questions stemming from our data is the nature of the new synapses after adult Shank3 expression. Our western blot data showed that in the striatum, the concentrations of the PSD scaffolding proteins and neurotransmitter receptors are increased significantly in the TM condition compared to the KO, with no differences between the WT and the TM conditions. Our electrophysiology recordings including the mEPSC and field recordings

in the striatum also demonstrated functional repair in the TM condition compared to the KO, with no differences between the WT and the TM conditions. However, when we quantified the dendritic spine density in the striatum in the TM, we found that the density is significantly increased not only compared to the KO, but also compared to the WT. If the new dendritic spines in the TM condition after Shank3 expression were identical to WT spines in both function and protein network as suggested by the electrophysiology and biochemical data, why did we not observe an increase in the protein concentration in the PSD and an increase in the electrophysiological functional recordings? How can we reconcile the significant increase in dendritic spine density in the TM condition compared to the WT condition with the biochemistry and electrophysiology data which suggest that there is no difference between the TM and the WT conditions? What do these data indicate about the nature of the new synapses in the TM condition as a whole?

One possibility is that after Shank3 expression in the TM condition, the previously defective synapses are not altered but that a new population of synapses is induced or stabilized. It is possible that the synaptic defects caused by Shank3 KO still remain in the TM condition, and that the expression of Shank3 led to the formation of new synapses that are fully functional. Because our biochemical and electrophysiological methods are performed on the dorsal striatum, our data only reflect the molecular composition and function of the striatal population without distinguishing between the old and the new synapses.

To determine whether the repair process after Shank3 expression in the adult only takes place in the new synapses and not in the previously defective synapses, one would have to conduct additional experiments. One approach is to use real-time imaging. One could culture neurons from the Fx/Fx striatum, identify a particular synapse with obvious synaptic defect such as low

Homer concentration in the PSD, use virus to deliver Cre into the cells, and then image the same synapse across time to determine whether or not Cre recombination causes the initially Homer deficient synapse to now increase in Homer labeling. If the results show that the previously defective synapse is unable to recruit Homer and other PSD proteins effectively in the same synapse, then this would strongly support the idea that the molecular process takes place through the induction of entirely new synapses. A major caveat to this strategy is that by using neuron culture, it is difficult to determine whether or not the results would apply to the adult brain. The data from this experiment can only provide information on whether Shank3 re-expression in Shank3 KO neurons can rescue the previously defective synapses, but does not provide us with any insights about whether the same process can be applied to the *in vivo* system after development. Another approach is to use immunohistochemistry to stain and quantify the Shank3-interacting partners in the synapse in the TM, KO, and WT conditions. By taking a comprehensive survey of the synapses in the brain slices and quantifying the signal from the PSD markers in each synapse in the TM condition, one could determine if there is a significant population of synapses with low PSD protein network concentrations even after Shank3 expression in adulthood. If the data show that there still remain many synapses with significantly lower PSD protein concentrations after tamoxifen treatment, similar to what is observed in the KO brain, then this would suggest that the defective synapses are not repaired after Shank3 expression. However, if the results show that all of the synapses have now repaired PSD protein concentrations, then this would indicate that Shank3 expression in adulthood can in fact amend the existing defective synapses.

Another possibility is that the protein network within each synapse in the TM condition after Shank3 expression may not be fully restored to WT level, but that at the population level, the total number of PSD proteins in the synapses and the cellular responses are rescued. A possible

scenario is that Shank3 expression in the adult brain causes the formation of many new synapses, much like during early development, when there is typically an overexuberance of synapse number that is then later pared down through synaptic pruning. However, unlike during development, the process of new synapse development may be less regulated in the adult brain due to the significantly different chemical and biological environment in the adult brain compared to the neonatal. Within the new synapses, the PSD proteins recruited to the synapse may be variable. Some may have fewer and some may have more. When I did the biochemical analysis on the WT, TM, KO conditions, I used the PSD fraction derived from the entire striatum. Thus the results show that the PSD protein concentrations may be rescued at the population level in the TM without providing information at the individual synapse level. To gain understanding of the impact on the individual synapses, one can conduct the immunohistochemistry experiments described above. Such an approach can elucidate the properties of molecular composition in individual synapses and potentially uncover subpopulations within the new synapses.

In addition, more comprehensive and detailed electrophysiological measurements can also help characterize more precise synaptic mechanisms. For our study, we recorded the field population spike in the striatum by stimulating the cortical afferents in the corpus callosum. However, the striatum receives many sources of input including the thalamus, substantia nigra, globus pallidus, and the cerebellum. It is possible that depending on the source of synaptic innervation, the synapses in the striatum respond differently to the impact of adult Shank3 expression. One can section the acute brain slices differently to preserve other circuit connections and/or stimulate afferents from other brain regions to dissect whether there are differences at the synaptic level in the striatum. We also collected data from mEPSC recordings in the striatum across the conditions. However, mEPSC responses are action potential independent and are not evoked. Thus, to gain more insights into the properties of the synapses after Shank3 expression,

one can perform spontaneous recordings to investigate cell activity in the presence of action potentials and evoked whole-cell recordings to investigate how the synapses respond after stimulation. Understanding the functional differences in the synapses through a more comprehensive study will allow us to gain insights into the fundamental properties of the new synapses after Shank3 restoration in the adult brain.

Toxicity of Tamoxifen in Developmental Studies

To enable earlier restoration of Shank3 during development, we used tamoxifen in P21 and P10 mice. However, as was shown by the rotarod data and the body weight differences, we observed significant health deficits as a result of the tamoxifen feeding in the WT mice. We do not understand why the tamoxifen affected the WT worse than it affected the TM mice. It is possible that because WT mice typically weigh more than the Fx/Fx mice, the WT mice therefore received more tamoxifen doses as a result of the body-weight-normalized dosing. Due to these health effects, it was difficult for us to determine whether the improvements in the TM condition compared to the KO were at the WT level.

An alternative method to characterize developmental restoration of Shank3 is to use systemic viral delivery of Cre. This route of AAV delivery of Cre recombination can cross the blood brain barrier and facilitate global expression of Shank3 in the Fx/Fx mice. This approach is potentially less toxic to the body, and may yield more straightforward results. However, a caveat is that systemic delivery of AAV is not nearly as efficient in the brain as tamoxifen oral gavage. If minimal behavioral rescue is observed post-viral injection, it could be due to the low viral infection rate in the brain.

Future Directions:

Circuit-Specific Dissection of the New Synapses in the Striatum

As mentioned above, the striatum receives inputs from many different brain regions. Due to our molecular, electrophysiological, and morphological evidence that there are increased synapse number in the striatum after Shank3 expression, it would be interesting to determine if there are any circuit-specific differences in these new synapses. For example, does one particular circuit confer more plasticity than others? Do the synapses in the distinct circuits respond to adult Shank3 expression differently? One could conduct fairly precise electrophysiology experiments to address these questions by using a combination of optogenetics, viral delivery, and patch-clamp recording. In the striatum in the TM condition, one could inject a rabies virus encoding the Cre protein which will then be taken up by the presynaptic terminals. A Cre-inducible Channelrholdopsin can then be delivered into the brain regions that give input to the striatum. Only the cells that have cre recombinase will then express Channelrholpsin. Using an optical fiber, one can then use it to activate the presynaptic cells and use electrophysiology to record from the striatum. This approach will allow for distinct activation of circuits inside the striatum, enabling the interrogation of synaptic responses to different afferents. Comparison of these responses across the WT, TM, and KO conditions can provide valuable information on how adult Shank3 expression affects the different circuits in the striatum. It is possible that synapses in certain circuits may display more improvement in function than others. Due to the abundance of cortically innervated synapses in the striatum, it is likely that given the rescued response in the field recordings in the striatum, the cortically innervated synapses have fully recovered evoked response.

Contributions of the striatal circuitry in behavioral phenotypes in the Shank3 KO

Shank3 is most highly expressed in the striatum and is the only member of the Shank family proteins to be expressed in this brain region. This unique expression pattern precludes the possibility of functional overlap with other Shank members in the striatum (Peca et al, 2011). In the Shank3B mutant and the Fx/Fx mice, we found many evidence from multiple levels of analysis that indicate significant striatal dysfunction. By isolating the striatal postsynaptic density from the mutant mice, we found that there was a significant reduction in the recruitment of multiple synaptic proteins that interact with Shank3 including SAPAP3, Homer, PSD-93, GluR2, NR2A, and NR2B in the knockouts compared to the wildtype controls (Peca et al, 2011). The number of dendritic spines in the striatum was also significantly reduced in the mutants. The change in the molecular composition as well as synaptic structure predicts an alteration in synaptic function. Analysis of the basal level of synaptic transmission, such as field cortico-striatal population spikes, miniature excitatory postsynaptic currents (mEPSCs), and the paired pulse ratio indeed indicated a defective basal synaptic transmission in the Shank3B mutants (Peca et al, 2011). This body of evidence suggesting a link between the striatal dysfunction and autistic-like phenotypes is consistent with the findings of many other studies. For example, it has been reported that cocaine challenge in the striatum can lead to repetitive behaviors in primates (Saka et al, 2004), and magnetic resonance imaging studies have found that increased volume of the right caudate and total putamen is positively correlated with repetitive behaviors in autistic-like patients (Hollander et al, 2005).

To specifically express Shank3 in the striatal circuit, one can cross the Shank3 conditional knock-in mouse with the Gng7-Cre mouse line. This mouse line has been

characterized by GenSAT and is reported to have Cre expression throughout the entire striatum (Gong et al, 2007) . The progeny from this breeding strategy should have specific Shank3 expression only in the striatum. Western blot and immunohistochemistry are needed to confirm that Shank3 expression is induced specifically in the striatal circuit. One will then perform a battery of behavioral tests to determine whether the circuit-specific Shank3 expression can rescue any of the behavioral deficits in the mutant mice including social interaction and repetitive behavior on the wildtype, Gng7-Cre$^{+/-}$, Shank3 Fx/Fx: Gng7-Cre$^{-/-}$, Shank3 Fx/Fx: Gng7-Cre$^{+/-}$. If the striatal circuit underlies the social defect in the Shank3 mutant mice, then I would expect that the Shank3 Fx/Fx: Gng7-Cre$^{+/-}$ mice will behave more closely to the wildtype controls in that they will choose to interact with other mice. If their behavior is closer to that of the Shank3 mutants, it would indicate that the expression of Shank3 in the striatal circuit is not sufficient to rescue the social interaction deficits, suggesting that other circuits are involved in normal social behavior. If the grooming behavior of Shank3 Fx/Fx: Gng7-Cre$^{+/+}$ mice is closer to that of the Shank3 mutant mice, then it will indicate that the striatal circuitry is not the sole contributor to repetitive grooming and that there are other neural circuits involved. In addition to the quantification of grooming behavior, one can also analyze the prevalence of skin lesions in these three groups of mice in adulthood. I expect to find that there will be significantly more skin lesions in the Shank3 Fx/Fx mice compared to the wildtype controls and the Shank3 Fx/Fx: Gng7-Cre$^{+/+}$.

Even though the Gng7-Cre line expresses Cre predominantly in the striatum, there are still some nonspecific sparse labeling in other brain regions including layer 5 in the cortex, CA1 and dentate granule cells of the hippocampus[38]. To ascertain that rescue in the striatum solely is sufficient for reversal of autistic-like behaviors, one can also use viral injections of Cre specifically in the striatum to eliminate expression in other regions. One can use commercially

available AAV-Cre-GFP viruses and AAV-GFP control viruses to stereotaxically inject bilaterally into the striatum of the Shank3 Fx/Fx mice. The accuracy and success of all viral injections can be confirmed by checking the GFP fluorescence and immunoblotting for Shank3 expression. Post-injection, the Shank3 Fx/Fx: GFP: Cre- and Shank3 Fx/Fx: GFP: Cre+ should be assayed with a battery of behavioral tests in adulthood. Specifically, I will focus on measuring the social interaction and grooming bouts.

Overlapping functions in the Shank Protein Family

Due to the structural and domain similarity between Shank1, Shank2, and Shank3, it is likely that they have overlapping functions. However, they have different expression patterns across the brain. An interesting question to address is whether Shank1, Shank2, and Shank3 serve similar or distinct functions. One approach is to use viral delivery of Shank2 or Shank1 into the striatum of Shank3 KO mice. Our previous characterizations showed that Shank3 is uniquely expressed in the striatum compared to Shank1 and Shank2. Thus, after injecting Shank1 or Shank2 into the striatum of a Shank3 KO mouse, one can use biochemistry, electrophysiology, and imaging to determine if the other Shank family proteins can improve the PSD molecular composition, neurotransmission, and morphological deficits incurred by the lack of Shank3. If there are improvements in any of these parameters, the results would indicate that there are some functional overlap between the different Shank proteins. One major caveat to such an approach is that both deletion and duplication of Shank proteins has been found to lead to behavioral phenotypes. Thus overexpression caused by viral delivery may confound the data interpretation. One can potentially overcome this technical barrier by using a promoter with very low activity in the virus carrying Shank1 or Shank2.

Conclusions:

In this work, I generated a novel Shank3 CKI mouse model using the fLEx strategy. To our knowledge, this is the first fLEx mouse model of autism. We demonstrated that this mouse model successfully recapitulates the KO phenotypes previously described in Shank3 mutants and enables efficient Shank3 expression in the adult brain.

Using this novel genetic model, we found that there is a certain degree of plasticity in the brain even long after development. The post-developmental restoration of Shank3 led to alterations in the PSD protein network, improvement in neurotransmission, and increase in the number of dendritic spines in the striatum. Even though the exact nature of the newly stabilized synapses remains to be further investigated, the changes observed along many dimensions in the adult brain supports the conclusion that there is not a strict developmental critical window for some aspects of the brain.

Behaviorally, we found that there is selective rescue in certain behaviors while others remained unaltered after Shank3 restoration. This phenomenon may be due to many different causes. One possibility is that certain circuits, maybe cell types, maybe brain regions, are more plastic than others. Many reports show that there is significant neurogenesis in different brain regions such as the hippocampus and the striatum. The birth of new neurons may then enhance the plasticity of these brain circuits. An exciting future direction is to investigate this underlying cause. Dissecting the mechanisms underlying the behavioral selectivity will provide valuable information on the fundamental properties of the Shank3 and adult brain plasiticty.

REFERENCES:

1. Abrahams Bs, Geschwind DH. 2008. Advances in autism genetics: on the threshold of a new neurobiology. *Nat Rev.Genet.* 9:341-55.
2. Altman J., Das GD. Autoradiographic and histological evidence of postnatal hippocampal neurogenesis in rats. . *J Comp Neurol.* 1965;124:319–335
3. Amaral, D. Geschwind, and G. Dawson, Eds., *Autism Spectrum Disorders*, 1st ed. Oxford University Press, 2011.
4. American Psychiatric Association. & American Psychiatric Association. Task Force on DSM-IV. *Diagnostic and statistical manual of mental disorders : DSM-IV-TR*, (American Psychiatric Association, Washington, DC, 2000.
5. Anderlid B.M et al. "FISH-mapping of a 100-kb terminal 22q13.3 deletion." Hum Genet. 110, 439-443.
6. Anney R et al. "A genome-wide scan for common alleles affecting risk for autism." Hum Mol Genet 2010, 19:4072-4082.
7. Asperger H. 1944. Die "autistischen Psychopathen" im Kindesalter. Arch Psychiatr. Nervenkrankh. 177; 76-137.
8. Baird G, Simonoff E, Pickles A, Chandler S, Loucas T, Meldrum D, Charman T. (2006) Prevalence of disorders of the autism spectrum in a population cohort of children in South Thames: the Special Needs and Autism Project (SNAP). *Lancet* 368:210-215.

9. Baron MK, Boeckers TM, Vaida B, Faham S, Gingery M, Sawaya MR, Salyer D, Gundelfinger ED, Bowie JU. (2006) An architectural framework that may lie at the core of the postsynaptic density. Science 311:531-5.

10. Batzoglou S, Pachter L, Mesirov JP, Berger B, Lander ES. "Human and mouse gene structure: comparative analysis and application to exon prediction." Genome Res. 2000 Jul; 10(7):950-958.

11. Berg JM and Geschwind DH. "Autism genetics: searching for specificity and convergence." Genome Biology 2012, 13:247.

12. Betancur C, Buxbaum JD. SHANK3 haploinsufficiency: a "common" but underdiagnosed highly penetrant monogenic cause of autism spectrum disorders. Mol Autism. 2013;4:17.

13. Boccuto L. et al. "Prevalance of SHANK3 variants in patients with different subtypes of autism spectrum disorders." Eur J Hum. Genet. 21, 310-316.

14. Boeckers TM, Segger-JuniusM, Iglauer P, Bockmann J, Gundelfinger ED, et al. 2004. Differential expression and dendritic transcript localization of Shank family members: identification of a dendritic targeting element in the 3_ untranslated region of Shank1 mRNA. Mol. Cell Neurosci. 26:182–90

15. Boeckers TM, Winter C, Smalla KH, Kreutz MR, Bockmann J, Seidenbecher C, Garner CC, Gundelfinger ED. (1999a) Proline-rich synapse-associated proteins ProSAP1 and ProSAP2 interact with synaptic proteins of the SAPAP/GKAP family. Biochem Biophys Res Commun. 264:247-52.

16. Bonaglia M.C." Identification of a recurrent breakpoint within the SHANK3 gene in the 22q13.3 deletion syndrome." J. Med. Genet. 43, 822-828.

17. Bozdagi et al, "Haploinsufficiency of the autism-associated Shank3 gene leads to deficits in synaptic function, social interaction, and social communication.," *Mol. Autism*, vol. 1, p. 15, 2010.

18. Bourdenx M, Dutheil N, Bezard E, and Dehay B. "Systemic gene delivery to the central nervous system using Adeno-associated virus." Front Mol Neurosci. 2014; 7:50.

19. Breitbart M, et al. Viral diversity and dynamics in an infant gut. Res. Microbiol. 2008; 159:367-73.

20. Bronson SL and Bale TL. "The placenta as a mediator of stress effects on neurodevelopmental reprogramming." Neuropsychopharmacology. 2015.

21. Carlisle HJ, Kennedy MB. Spine architecture and synaptic plasticity. Trends Neurosci. 2005. 28(4): 182-7. Review

22. Chakrabarty P, Rosario A, Cruz P, Siemienski, et al. "Capsid serotype and timing of injection determines AAV transduction in the neonatal mice brain." Plos One. 2013.

23. Chamberlain S.J., Lalande M. "Angelman Syndrome, a genomic imprinting disorder of the brain." Journal of Neuroscience. 2010.

24. Chandler et al, "Relevance of BAC transgene copy number in mice: Transgene copy number variation across multiple transgenic lines and correlations

with transgene integrity and expression," *Mamm. Genome*, vol. 18, pp. 693–708, 2007.

25. Chao et al, "Dysfunction in GABA signalling mediates autism-like stereotypies and Rett syndrome phenotypes.," *Nature*, vol. 468, pp. 263–269, 2010.

26. Christian SL et al. "Novel submicroscopic chromosomal abnorlaities detected in autism spectrum disorder." Biological Psychiatry 63:1111-17.

27. Chua JJE, Kindler S, Boyken J, Jahn R (2010). The architecture of an excitatory synapse. J Cell Sci 123, 819-823.

28. Clement et al, "Pathogenic SYNGAP1 mutations impair cognitive development by disrupting maturation of dendritic spine synapses," *Cell*, vol. 151, pp. 709–723, 2012.

29. Cooper et al. "A copy number variation morbidity map of developmental delay." Nature Genetics. 43:838-46.

30. D'Arcangelo G. "Reelin in the years: controlling neuronal migration and maturation in the mammalian brain." Advances in neuroscience. 2014.

31. Daigle TL, Wetsel WC, Caron MG. Opposite function of dopamine D1 and N-methyl-D-aspartate receptors in striatal endocannobinoid-mediated signaling. (2011). Eur J Neurosci. 34 (9): 1378-89.

32. De Angelis et al. "Fecal microbiota and metabolome of children with autism and pervasive developmental disorder not otherwise specified." Plos One. 2013.

33. Delmonte S, Balsters JH, McGrath J, Fitzgerald J, Brennan S, Fagan AJ, Gallagher L. (2012). Social and monetary reward processing in autism spectrum disorders. Mol Autism.

34. Devlin B, Scherer SW. 2012. Genetic architecture in autism spectrum disorder. *Curr Opin.Genet. Dev.* 22: 229-37.

35. De Zeeuw and Ten Brinke, "Motor learning and the cerebellum," *Cold Spring Harbor Perspectives in Biology.* 2015 Sep 1;7(9). Review.

36. Dhar SU, del Gaudio D, German JR, Peters SU, Ou Z, Bader PI, Berg JS, Blazo M., Brown CW, Graham BH, et al. 2010. 22q13.3 deletion syndrome: Clinical and molecular analysis using array CGH. Am J Med Genet A 152A: 573-581.

37. Dijikhuizen PA, Ghosh A. BDNF regulates primary dendrite in cortical neurons via the PI3-kinase and MAP kinase signaling pathways. J Neurobiol. 2005. 62(2):278-88.

38. Dolen et al, "Social reward requires coordinated activity of nucleus accumbens oxytocin and serotonin.," *Nature*, vol. 501, pp179-184, 2013.

39. Du, Y., Weed, S.A., Xiong, W.C., Marshall, T.D. & Parsons, J.T. (1998) Identification of a novel cortactin SH3 domain-binding protein and its localization to growth cones of cultured neurons. Mol Cell Biol 18, 5838-5851 (1998).

40. Durand CM, Betancur C, Boeckers TM, Bockmann J, Chaste P, Fauchereau F, Nygren G, Rastam M, Gillberg IC, Anckarsäter H, Sponheim E, Goubran-Botros H, Delorme R, Chabane N, Mouren-Simeoni MC, de Mas P,

Bieth E, Rogé B, Héron D, Burglen L, Gillberg C, Leboyer M, Bourgeron T. (2007) Mutations in the gene encoding the synaptic scaffolding protein SHANK3 are associated with autism spectrum disorders. *Nat Genet* 39, 25-27.

41. Ebert and Greenberg, "Activity-dependent neuronal signalling and autism spectrum disorder.," *Nature*, vol. 493, pp. 327–37, 2013.

42. Ehlers MD. (1999). Synapse structure: glutamate receptors connected by the shanks. Current Biol. 18; 9(22): R848-50.

43. Estes A, Shaw DW, Sparks BF, Friedman S, Giedd JN, Dawson G, Bryan M, Dager SR. Basal ganglia morphometry and repetitive behavior in young children with autism spectrum disorder. Autism Res. 3:212-220.

44. El-Fishawy and M. W. State, "The genetics of autism: key issues, recent findings, and clinical implications.," *Psychiatr. Clin. North Am.*, vol. 33, pp. 83–105, 2010.

45. Eriksson P.S. et al. "Neurogenesis in the adult human hippocampus." Nature Medicine. 1998; 4:1313-1317.

46. Farley MA et al. "Twenty-year outcome for indivdiuals with autism and average or near-average cognitive abilities. Autism Res. 2009;2:109-118.

47. Finegold SM, et al. Pyrosequencing study of fecal microflora of autistic and control children. Anaerobe. 2011; 16:444-53.

48. Fink CC, Bayer KU, Myers JW, Ferell JE Jr, Schulman H, and Meyer T. Selective regulation of neurite extension and synapse formation by the beta but not the alpha isoform of CaMKII. (2003). Neuron 39, 283-297.

49. Foust KD, Nurre E, Montgomery CL, Hernandez A, Chan CM, Kaspar BK. "Intravascular AAV9 preferentially targets neonatal neurons and adult astrocytes." *Nature Biotechnology* 27, 59-65 (2009).

50. Freimer N, Sabatti C. "The use of pedigree, sib-pair and association studies of common diseases for genetic mapping and epidemiology." Nature Genetics 2004, 36:1045-1051.

51. Freitag CM. 2007. The genetics of autistic disoders and its clinical relevance: a review of the literature. *Mol Psychiatry* 12:2-22.

52. Gaboriau-Routhiau V et al. "The key role of segmented filamentous bacteria in the coordinated maturation of gut helper T cell responses." Immunity. 2009; 31: 677-89.

53. Gage, F. "Structural Plasticity in the adult brain." Dialogues Clin Neurosci. 2004 Jun; 6(2): 135-141.

54. Ganz, ML. "The Lifetime Distribution of the incremental societal costs of autism." Arch Pediatr Adolesc Med. 2007; 161 (4):343-349.

55. Gauthier J, Spiegelman D, Piton A, Lafrenière RG, Laurent S, St-Onge J, Lapointe L, Hamdan FF, Cossette P, Mottron L, Fombonne E, Joober R, Marineau C, Drapeau P, Rouleau GA. (2009) Novel de novo SHANK3 mutation in autistic patients. *Am J Med Genet B Neuropsychiatr Genet* 150B, 421-424.

56. Gekas et al. "The placenta is a niche for hematopoetic stem cells." Dev Cell, 8 (2005), pp365-375.

57. Gilman SR et al. "Rare de novo variants associated with autism implicate a large functional network of genes involved in formation and function of synapses." Neuron 70:898-907.

58. Girirajan S et al. "A recurrent 16p12.1 microdeletion supports a two-hit model for severe developmental delay." Nature Genetics. 42-203-9.

59. Girirajan S et al. "Phenotypic heterogenetiy of genomic disorders and rare copy-number variants." New Engl. F Med. 367:1321-31.

60. Glessner JT et al. "Autism genome-wide copy number variation reveals ubiquitin and neuronal genes." Nature 459:569-73.

61. Goldman S., Nottebohm F. Neuronal production, migration and differentiation in a vocal nucleus of the adult female canary brain. . *Proc Natl Acad Sci USA.* 1983;80:2390–2394.

62. Gong S, Doughty M, Harbaugh CR, Cummins A, Hatten ME, Heintz N, Gerfen CR. (2007) Targeting Crerecombinase to specific neuron populations with bacterial artificial chromosome constructs. J Neurosci. 27:9817-23.

63. Gong X et al. "High proportion of 22q13 deletions andSHANK3 mutations in Chinese patients with intellectual disability." PLoS ONE 7, e34739.

64. Gross et al , "Serotonin1A receptor acts during development to establish normal anxiety-like behaviour in the adult.," *Nature*, vol. 416, pp. 396–400, 2002.

65. Guo, W. Yang, and C. G. Lobe, "A Cre recombinase transgene with mosaic, widespread tamoxifen-inducible action," *Genesis*, vol. 32, pp. 8–18, 2002.

66. Guy J, Gan J, Selfridge J, Cobb S, Bird A. Reversal of neurological defects in a mouse model of Rett syndrome. (2007). 315(5815): 1143-1147.

67. Hamdan FF, Gauthier J, Spiegelman D, Noreau A, Yang Y, Pellerin S, Dobrzeniecka S, Côté M, Perreau-Linck E, Perreault-Linck E, Carmant L, D'Anjou G, Fombonne E, Addington AM, Rapoport JL, Delisi LE, Krebs MO, Mouaffak F, Joober R, Mottron L, Drapeau P, Marineau C, Lafrenière RG, Lacaille JC, Rouleau GA, Michaud JL (Feb 2009). "Mutations in SYNGAP1 in autosomal nonsyndromic mental retardation". *The New England Journal of Medicine* **360** (6).

68. Han et al, "SHANK3 overexpression causes manic-like behaviour with unique pharmacogenetic properties.," *Nature*, vol. 503, pp. 72–7, 2013.

69. Hayashi MK, Tang C, Verpelli C, Narayanan R, Stearns MH, Xu RM, Li H, Sala C, Hayashi Y. (2009) The postsynaptic density proteins Homer and Shank form a polymeric network structure. Cell 137:159-71.

70. Hermonat P. L., Muzyczka N. (1984). Use of adeno-associated virus as a mammalian DNA cloning vector: transduction of neomycin resistance into mammalian tissue culture cells. *Proc. Natl. Acad. Sci. U.S.A.* 81 6466–6470

71. Hollander E, Anagnostou E, Chaplin W, Esposito K, Haznedar MM, Licalzi E, Wasserman S, Soorya L, Buchsbaum M. (2005) Striatal volume on magnetic resonance imaging and repetitive behaviors in autism. Biol Psychiatry 58, 226-232.

72. Howlin et al. "Adult outcome for children with autism." J Child Psychol Psychiatry 2004; 45:212-229.

73. Howlin et al. "Autism and developmental receptive language disorder – a followup comparison in early adult life. II: social, behavioral, and psychiatric outcomes. J child Psychol Psychiatry 2000: 41:561-578.

74. Huguet G, Ey E, Bourgerous T. 2013. "The genetic landscapes of autism spectrum disorders." Annu. Rev. Genomics Hum. Genet. 2013. 14:191-213.

75. Hyman S.L et al. "Environmental agents and autism: once and future associations." Intern Rev Res Ment Retard, 30 (2006), pp171-194.

76. Itsara A et al. "De novo rates and selection of large copy number variation." Genome Research. 20:1469-81.

77. Iyengar SK , Elston RC. The genetic basis of complex traits: rare variants or 'common gene, common disease'?" Methods Mol Biol 2007; 376:71-84.

78. Jacquemont ML et al. "Array-based comparative genomic hybridization identifies high frequency of cryptic chromosomal rearrangements in patients with syndromic autism spectrum disorders. J Med. Genet. 43: 843-49.

79. Jeffries AR, Curran S, Elmslie F, Sharma A, Wenger S, Hummel M, Powell J (2005) Molecular and phenotypic characterization of ring chromosome 22. Am J Med Genet A 137:139-147.

80. Jian L, Nagarajan L, De Klerk N, Ravine D, Bower C, Anderson A, Williamson S, Christodoulou J, Leonard H. (2006). "Predictors of seizure onset in Rett Syndrome." *The Journal of Pediatrics*. 149 (4):542-7.

81. Jiang YH and Ehlers M.D. "Modeling Autism by Shank gene mutations in mice." Neuron Review. 2013.

82. Kanner L. 1943. Autistic disturbances of affective contact. Nerv. Child 2:217-50.

83. Karayannis et al, "Cntnap4 differentially contributes to GABAergic and dopaminergic synaptic transmission.," *Nature*, 2014.

84. Kim JH, Liao D, Lau LF, Huganir RL (Apr 1998). "SynGAP: a synaptic RasGAP that associates with the PSD-95/SAP90 protein family". *Neuron* **20** (4): 683–91.

85. Kim et al, "GKAP, a novel synaptic protein that interacts with the guanylate kinase- like domain of the PSD-95/SAP90 family of channel clustering molecules," *J. Cell Biol.*, vol. 136, pp. 669–678, 1997.

86. Klei I et al. "Common genetic variants, acting additively, are a major source of risk for autism." Mol. Autism 3:9.

87. Klein JT, Platt ML. (2013). Social information signaling by neurons in primate striatum. Curr Bio. 8:691-6.

88. Koenig JE, et al. "Succession of microbial consortia in the developming infant gut microbiome." Proc Natl Acad Sci USA. 2011; 109 Suppl 1:4578-85.

89. Kong A et al. "Rate of de novo mutations and the importance of father's age to decrease risk." Nature 488:471-75.

90. Konur S, Ghosh A. Calcium signaling and the control of dendritic development. (2005). Neuron. 46(3):401-5. Review.

91. Kreienkamp, H.J. (2008) Scaffolding proteins at the postsynaptic density: shank as the architectural framework. Handb Exp Pharmacol, 365-380.

92. Kumar RA et al. "Recurrent 16p11.2 microdeletions in autism." Hum. Mol. Genet. 17:628-38.

93. Kumar RA, Christian SL. (2009) Genetics of autism spectrum disorders. Curr Neurol Neurosci Rep. 9:188-97.

94. Langen M, Schnack HG, Nederveen H, Bos D, Lahuis BE, de Jonge MV, van Engeland H, Durston S. (2009) Changes in the developmental trajectories of striatum in autism. Biol Psychiatry 66:327-33.

95. Leblond et al, "Meta-analysis of SHANK Mutations in Autism Spectrum Disorders: A Gradient of Severity in Cognitive Impairments.," *PLoS Genet.*, vol. 10, no. 9, p. e1004580, Sep. 2014.

96. Lee CC, Huang CC, Hsu KS. Insulin promotes dendritic spine and synapse formation by the PI3K/Akt/mTOR and Rac1 signaling pathways. (2011). Neuropharmacology. 61(4): 867-79.

97. Levy D et al. "Rare de novo and transmitted copy-number variation in autistic spectrum disordres." Neuron 2011. 70:886-897.

98. Lim S, Naisbitt S, Yoon J, Hwang JI, Suh PG, Sheng M, Kim E. (1999). Characterization of the Shank family of synaptic proteins. Multiple genes, alternative splicing, and differential expression in brain and development. J Biol. Chem. 274(41): 29510-8.

99. Limperopoulos et al. "Cerebellar injury in the premature infant is associated with impaired growth of specific cerebral regions. Pediatr. Res. 68. 145-150 (2010).

100. Limperopoulos et al. "Does cerebellar injury in premature infants contribute to the high prevalence of long-term cognitive, learning, and behavioral disability in survivors?" *Pediatrics.* 2007. Sep;120(3):584-93.

101. Lintas C, Persico AM. Autistic phenotypes and genetic testing: state-of-the-art for the clinical geneticist. J Med Genet 2009; 46:1-8.

102. Lipscombe D, Helton TD, Xu W. L-type calcium channels: the low down. (2004). J Neurophysiology. 92(5):2820-30. Review.

103. Lohmann C, Wong RO. Regulation of dendritic growth and plasticity by local and global calcium dynamics. (2005). Cell Calcium. 37(5): 403-409. Review.

104. Lord C, Shulman C, DiLavore P. "Regression and word loss in autistic spectrum disorders." J Child Psychol. Psychiatry 2004; 45:936-955.

105. Makalowski W, Zhang J, Boguski M S. Comparative analysis of 1196 orthologous mouse and human full-length mRNA and protein sequences. Genome Research. 1996;6:846–857.

106. Mao L, Wang JQ (2003). Group I metabotropic glutamate receptor-mediated calcium signaling and immediate early gene expression in cultured rat striatal neurons. Eur J Neurosci 17: 741-750.

107. Marshall C.R et al. "Structural variation of chromosomes in autism specrum disorders." AM. J Hum. Genet. 82, 477-488.

108. Mazmanian SK et al. An immunomodulatory molecule of symbiotic bacteria directs maturation of the host immune system." Cell. 2005; 122:107-18.

109. McLaughlin S. K., Collis P., Hermonat P. L., Muzyczka N. (1988). Adeno-associated virus general transduction vectors: analysis of proviral structures. *J. Virol.* 62 1963–1973

110. Miles, J. (2011). Autism spectrum disorders—A genetics review. Genetics in Medicine 13. 278-294.

111. Moessner R, Marshall CR, Sutcliffe JS, Skaug J, Pinto D, Vincent J, Zwaigenbaum L, Fernandez B, Roberts W, Szatmari P, Scherer SW. (2007) Contribution of SHANK3 mutations to autism spectrum disorder. *Am J Hum Genet* 81, 1289-1297.

112. Mulle JG et al. "The Gut Microbiome: A New Frontier in Autism Research." Current Psychiatry Rep (2013) 15:337.

113. Naisbitt S, Kim E, Tu JC, Xiao B, Sala C,Valtschanoff J, Weinberg RJ, Worley PF, Sheng M. (1999) Shank, a novel family of postsynaptic density proteins that binds to the NMDA receptor/PSD-95/GKAP complex and cortactin. Neuron 23: 569-82.

114. Nicholls, JG. (2001). From neuron to brain. Sinauer Associates.

115. Nordin V and Gillberg C. "The long-term course of autistic disorders: update on follow-up studies. Acta Psychiatr Scand 1998; 97:99-108.

116. Okamoto N et al. "22q13 microduplication in two patients with common clinical manifetations: a recognizable syndrome?" Am.J. Med. Genet. A. 143A, 2804-2809.

117. Ozonoff S et al. "A prospective study of the emergence of early behavioral signs of autism." J Am Acad Child Adolesc Psychiatry 2010; 49:256-266.

118. Parracho et al. Differences between the gut microflora of children with autistic specrum disorders and that of healthy children." J Med. Microbiol. 2005; 54; 987-91.

119. Patterson, PH. "Immune involvement in schizophrenia and autism: etiology, pathology and animal models." Behavioral Brain Research. 2009.

120. Peca J, Feliciano C, Ting JT, WangW, Wells MF, VenkatramanTY, LascolaCD, Fu Z and Feng G. (2011) *Shank3* mutant mice display autistic-like behaviours and striatal dysfunction. Nature, 472:437-42.

121. Person et al. "Known and possible roles of epigenetics in autism." Eds. Amaral, Dawson, and Geschwind. *Autism Spectrum Disorders*. P.737

122. Phelan K (2007). 22q13.3 Dletion Syndrome. In GeneReviews. R.A. Pagon, T.C. Bird. C.R. Dolan. And K.S.eds (Seattle, WA: Univresity of Seattle).

123. Phelan K and McDermid H.E. (2012). The 22q13.3 Deletion Syndrome (Phelan-McDermid Syndrome). Mol Syndromol. 2(3-5): 186-201.

124. Pinto D et al. "Functional impact of global rare copy number variation in autism spectrum disorders." Nature. 466:368-72.

125. Poirier and Schild. "The genotoxicity of tamoxifen: extent and consequences, Kona, Hawaii, January 23, 2003," Mutagenesis. 2003 July; 18(4): 395-9.

126. Proepper C, Johannsen S, Liebau S, Dahl J, Vaida B, Bockmann J, Kreutz MR, Gundelfinger ED, Boeckers TM. (2007). Abelson interacting protein 1(Abi-1) is essential for dendrite morphogenesis and synapse formation. EMBO J.5:1397-409.

127. Qiu A, Adler M, Crocetti D, Miller MI, Mostofsky SH. (2010). Basal ganglia shapes predict social, communication, and motor dysfunctions in boys with autism spectrum disorder. 6:539-551.

128. Qualmann B, Boeckers TM, Jeromin M, gundelfinger ED, Kessels MM. (2004) Linkage of the actin cytoskeleton to the postsynaptic density via direct interactions of Abp1 with the ProSAP/Shank family. J Neurosci 10: 2481-95.

129. Raisman G. Neuronal plasticity in the septal nuclei of the adult brain. . *Brain Res.* 1969;14:25–48.

130. Ramon Y., Cajal S. Degeneration and regeneration of the nervous system. May RM, trans. New York, NY: Hafner; 1928.

131. Reddy KS. Cytogenetic abnormalities and fragile-X syndrome in autism spectrum disorder. BMC Med Genet 2005;6:3.

132. Redmond L, Kashani AH, Ghosh A. Calcium regulation of dendritic growth via CaM kinase IV and CREB-mediated transcription. Neuron. 2002. 34(6): 999-1010.

133. Rex CS, Lin CY, Kramar EA, Chen LY, Gall CM, Lynch G. Brain-derived neurotrophic factor promotes long-term potentiation-related cytoskeletal changes in adult hippocampus. (2007). J J Neurosci. 27 (11): 3017-29.

134. Ribar TJ, Rodrigeuiz RM, Khiroug L, Wetsel WC, Augustine RJ, and Means AR. Cebrebellar defects in Ca2+/calcimodulin kinase IV-deficient mice. (2000). J Neurosci. 20, RC107.

135. Richardson PM., McGuiness UM., Aguya AJ. Axons from CNS neurons regenerate into PNS grafts. *Nature.* 1980;284:264–265

136. Ronesi JA, Collins KA, Hays SA, Tsai NP, Guo W, Birnbaum SG, Hu JH, Worley PF, Gibson JR, Huber KM. (2012). Nature Neuroscience. 15(3): 431-440.

137. Rosenberg RE, Law JK, Yenokyan G, McGready J, Kaumann WE, Law PA. (2009). Characteristics and concordance of autism spectrum disorders among 277 twin pairs. *Arch Pediatr Adolesc Med.* 163:907-914.

138. Rothwell et al. "Autism-associated neuroligin-3 mutations commonly impair striatal circuits to boost repetitive behaviors." *Cell*, 158, 198-212, 2014.

139. Roussignol G, Ango F, Romorini S, Tu JC, Sala C, Worley PF, Bockaert J, Fagni L. (2005) Shank expression is sufficient to induce functional dendritic spine synapses in aspiny neurons. J Neurosci 25, 3560-3570.

140. Samulski R. J., Berns K. I., Tan M., Muzyczka N. (1982). Cloning of adeno-associated virus into pBR322: rescue of intact virus from the recombinant plasmid in human cells. *Proc. Natl. Acad. Sci. U.S.A.* 79 2077–2081

141. S.S. Moy and J.J. Nadler. "Advances in behavioral genetics: mouse models of autism." Mol Psychiatry, 13 (2008), pp4-26.

142. Sahin M, Sur M. 2015. "Genes, circuits, and precision therapies for autism and related neurodevelopmental disorders." Science express reviews.

143. Saka E, Goodrich C, Harlan P, Madras BK, Grabiel AM: Repetitive behaviors in monkeys are linked to specific striatal activation patterns. J Neurosci 2004, 24: 7557-7565.

144. Sakai Y, Shaw CA, Dawson BC, Dugas DV, Al-Mohtaseb Z, Hill DE, Zoghbi HY. Sci Transl Med. (2011). 3(86):86ra49.

145. Sala C, Piëch V, Wilson NR, Passafaro M, Liu G, Sheng M. Regulation of dendritic spine morphology and synaptic function by Shank and Homer. (2001) Regulation of dendritic spine morphology and synaptic function by Shank and Homer. Neuron 31, 115-130.

146. Sanders SJ et al. "De novo mutations revealed by whole-exome sequencing are strongly associated with autism." Nature 2012, 485:237-241.

147. Sanders SJ et al. "Multiple recurrent de novo CNVs, including duplications of the 7q11.23 Williams syndrome region, are strongly associated with autism. Neuron 70:863-85.

148. Sato et al. "Shank1 mutations in males with autism spectrum disorder." Am. J Hum. Genet. 90:879-87.

149. Scannevin and Huganier (2000). Postsynaptic organization and regulation of excitatory synapses. Nature Reviews 1, 133-139.

150. Schaefer GB, Mendelsohn NJ. Clinical genetics evaluation in identifying the etiology of autism spectrum disorders. Genet Med 2008; 10:301-305.

151. Schanen N.C. "Epigenetics of autism spectrum disorders." *Hum Mol Genetics*. (2006).

152. Schmeisser MJ et al. "Autistic-like behaiors and hyperactivity in mice lacking ProSAP1/Shank2." Nature. 2012 Apr 29; 486 (7402):256-260.

153. Schnutgen F, Doerflinger N, Calleja C, Wendling O, Chambon P, Ghyselinck NB. (2003). Nature Biotechnology. 21 (5): 562-5.

154. Sebat J et al. "Strong association of de novo copy number mitations with autism." Science. 316:445-49.

155. Seltzer et al. "Trajectory of development in adolescents and adults with autism. Ment. Retard Dev Disabil Res Rv 2004; 10:234-247.

156. Sharma A, Hoeffer CA, Takayasu Y, Miyawaki T, McBride SM, Klann E, and Zukin RS. (2010). Dysregulation of mTOR Signaling in Fragile X Syndrome. 30 (2): 694-702.

157. Sheng and Kim, "The Shank family of scaffold proteins.," *J. Cell Sci.*, vol. 113 (Pt 1, pp. 1851–6, Jun. 2000.

158. Song Y et al. "Real-time PCR quantitiation of clostridia in feces of autistic children." Appl Environ Microbio. 2004; 70:6459-65.

159. Soorya L, Kolevzon A, Zweifach J, Lim T, Dobry Y, Schwartz L, et al. Prospective investigation of autism and genotype-phenotype correlations in 22q13 deletion syndrome and SHANK3 deficiency. Mol Autism. 2013;4:18.

160. Spooren W, Lindemann L, Ghosh A, Santarelli L. (2012). Synapse dysfunction in autism: a molecular approach to drug discovery in neurodevelopmental disorders. Trends in Pharmacological Sciences, 12: 669-684.

161. Stefanatos GA. "Regression in autistic spectrum disorders." Neuropsychol Rev 2008; 18:305-319.

162. Szatmari et al. "Mapping autism risk loci using genetic linkage and chromosomal rearrangements. Nat Genet. 39:319-28.

163. Takeuchi et al, "SAPAPs. A family of PSD-95/SAP90-associated proteins localized at postsynaptic density," *J. Biol. Chem.*, vol. 272, pp. 11943–11951, 1997.

164. Transmitter-evoked local calcium release stabilizes developing dendrites. (2002). Nature. 418 (6894):177-81.

165. Tu JC, Xiao B, Naisbitt S, Yuan JP, Petralia RS, Brakeman P, Doan A, Aakalu VK, Lanahan AA, Sheng M, Worley PF. (1999). Coupling of mGluR/Homer and PSD-95 complexes by the Shank family of postsynaptic density proteins. Neuron 3: 583-592.

166. Van Kerkhof LW, Damsteegt R, Trezza V, Voorn P, Vanderschuren LJ. (2013). Social Play behavior in adolescent rats is mediated by functional activity in medial prefrontal cortex and striatum. Neuropsychopharmacology.

167. Verpelli C, Dvoretskova E, Vicidomini C, Rossi F, Chiappalone M, Schoen M, Di Stefano B, Mantegazza R, Broccoli V, Boeckers TM, Dityatev A, Sala C. Importance of Shank3 protein in regulating metabotropic glutamate

receptor 5 (mGluR5) expression and signaling at synapses. (2011). J Biol. Chem. 286(40): 34839-50.

168. Voineagu I "Common expression studies in autism: moving from the genome to the transcriptome and beyond." Neurobio Dis 2012, 45:69-75.

169. Volkmar F et al. "Autism in infancy and early childhood". Ann Rv Psychol 2005; 56:315-336.

170. Vorstman et al. Identification of novel autism candidate regions through analysis of reported cytogenetic abnormalities associated with autism. Mol. Psychiatry 2006; 11:1, 18-28.

171. Waehler et al, "Engineering targeted viral vectors for gene therapy.," *Nat. Rev. Genet.*, vol. 8, pp. 573–587, 2007.

172. Wang X, Xu Q, Bey AL, Lee Y, Jiang YH. "Transcriptional and functional complexity of Shank3 provides a molecular framework to understand the phenotypic heterogeneity of SHANK3 causing autism and Shank3 mutant mice." *Mol. Autism.* 2014; 5:30.

173. Wang et al, "Synaptic dysfunction and abnormal behaviors in mice lacking major isoforms of Shank3," *Hum. Mol. Genet.*, vol. 20, pp. 3093–3108, 2011.

174. Wang et al. "Common genetic variants on 5p14.1 associate with autism spectrum disorders." Nature 2009, 459:528-533.

175. Wayman GA, Kaech S, Grant WF, Davare M, Impey S, Tokumitsu H, Nozaki N, Banker G, and Soderling TR. Regulation of axonal extension and

growth cone motility by calmodulin-dependent protein kinase I. (2004). J Neurosci. 24, 3786-2794.

176. Weinberg M.S., Samulski R.J., McCown T. J. (2013). Adeno-associated virus (AAV) gene therapy for neurological disease. *Neuropharmcology.*

177. Weiss LA et al. "A genome-wide linkage and association scan reveals novel loci for autism." Nature 2009. 461;802-808.

178. Welch, JM., Lu, J., Rodriguiz, RM., Trotta, NC., Peca, J., Ding, J-D., Feliciano, C., Chen, M., Adams, JP., Luo, J., Dudek, SM., Weinberg, RJ., Calakos, N., Wetsel, WC., and Feng, G. (2007) Cortico-striatal synaptic defects and OCD-like behaviors in SAPAP3 mutant mice. Nature 448:894-900.

179. Werner E, DawsonG. "Validation of the phenomenon of autistic regression using home videotapes." Arch Gen Psychiatry 2005; 62-889-895.

180. Wilson H.L. et al. "Interstitial 22q13 deletions: genes other than SHANK3 have major effects on cognitive and language development." Eur. J. Hum. Genet. 16, 1301-1310.

181. Wilson HL et al. Molecular characterization of the 22q13 deletion syndrome supports the role of hapinsufficiency of SHANK3/PROSAP2 in the major neurological symptoms. J. Med. Genet. 40, 575-584.

182. Wilson HL,Wong AC, Shaw SR, TseWY, Stapleton GA, PhelanMC, Hu S, Marshall J, McDermid HE. 2003. Molecular characterisation of the 22q13 deletion syndrome supports the role of haploinsufficiency of SHANK3 PROSAP2 in the major neurological symptoms. J Med Genet 40: 575–584.

183. Wong A.C. et al. "Molecular characterization of a 130-kb terminal microdeletion at 22q in a child with mild mental retardation." Am J Hum. Genet. 60, 113-120.

184. Wu GY, and Cline HT. Stabilization of dendritic arbor structure in vivo by CaMKII. (1998). Science. 279, 222-226.

185. Yang, M. *et al.* Reduced Excitatory Neurotransmission and Mild Autism-Relevant Phenotypes in Adolescent Shank3 Null Mutant Mice. *J. Neurosci.* **32,** 6525–6541 (2012).

186. Young P, Qiu L, Wang DQ, Zhao S, Gross J, Feng G. (2008). Nature Neuroscience. 11: 721-728).

187. Zhang H, Maximov A, Fu Y, Xu F, Tang TS, Tkatch T, Surmeier DJ, Bezprozvanny I. (2005) Association of CaV1.3 L-type calcium channels with Shank. J Neurosci. 25:1037-1049.

188. Zhao X et al. "A unified genetic theory for sporadic and inherited autism." Proc Natl Acad Sci USA 2007, 104:12831-12836.

189. Zoghbi HY, Bear MF. Synaptic Dysfunction in Neurodevelopmental Disorders Associated with Autism and Intellectual Disabilities. Cold Spring Harbor Perspectives in Biology. (2012).